JAERI-M
86-185

EVALUATION REPORT ON CCTF CORE-II REFLOOD TEST C2-3 (RUN 61)
—INVESTIGATION OF INITIAL DOWNCOMER WATER ACCUMULATION VELOCITY EFFECTS—

January 1987

Tsutomu OKUBO, Tadashi IGUCHI, Jun SUGIMOTO*
Hajime AKIMOTO, Kazuharu OKABE** and Yoshio MURAO

日本原子力研究所
Japan Atomic Energy Research Institute

JAERI-M レポートは，日本原子力研究所が不定期に公刊している研究報告書です。
入手の問合わせは，日本原子力研究所技術情報部情報資料課（〒319-11茨城県那珂郡東海村）あて，お申しこしください。なお，このほかに財団法人原子力弘済会資料センター（〒319-11 茨城県那珂郡東海村日本原子力研究所内）で複写による実費領布をおこなっております。

JAERI-M reports are issued irregularly.
Inquiries about availability of the reports should be addressed to Information Division Department of Technical Information, Japan Atomic Energy Research Institute, Tokai-mura, Naka-gun, Ibaraki-ken 319-11, Japan.

編集兼発行　日本原子力研究所
印　　刷　いばらき印刷㈱

Evaluation Report on CCTF Core-II Reflood Test C2-3 (Run 61)

—— Investigation of initial downcomer water accumulation velocity effects ——

Tsutomu OKUBO, Tadashi IGUCHI, Jun SUGIMOTO*,
Hajime AKIMOTO, Kazuharu OKABE** and Yoshio MURAO

Department of Reactor Safety Research,
Tokai Research Establishment
Japan Atomic Energy Research Institute

Tokai-mura, Naka-gun, Ibaraki-ken

(Received December 10, 1986)

This report presents the evaluation for the CCTF Core-II test C2-3 (Run 61), which was conducted on April 21, 1983. In this test, the effects of the downcomer water accumulation velocity in the initial period on the thermo-hydrodynamic behaviors during the reflood phase of a PWR-LOCA was investigated. This is because the higher downcomer water accumulation velocity in the initial period may result in the higher core flooding rate, and hence, promote the core cooling and increase the U-tube type oscillation. Since the downcomer flow area is larger than the PWR scaled value in the CCTF being expected to result in a lower downcomer water accumulation velocity than in the PWR during the initial period, it is important to investigate this effects in the CCTF in order to confirm that the CCTF test results are applicable to the PWR analyses without any difficulty on the scaling of downcomer flow area.

Comparing the data of the present test with those of the base case test, the following results are obtained:

The work was performed under contract with the Atomic Energy Bureau of Science and Technology Agency of Japan.

* Science and Technology Agency

** Mitsubishi Atomic Power Industry Inc.

(1) The time to fill the downcomer was about 8 s in the present test and was significantly shorter than that in the base case test (*i.e.* 16 s).

(2) The higher downcomer water accumulation velocity in the initial period is considered to result in the observed higher core flooding rate and the larger U-tube type oscillation in the initial period.

(3) The intact loop differential pressure, *i.e.* the steam binding, and the core differential pressure were also observed to increase rapidly. These are considered to reduce the core flooding rate rapidly.

(4) By 20 s the core flooding rates for the present test and the base case test were observed to become almost identical. The larger oscillation in the present test was also observed to be damped by 30 s.

(5) After 20 s the thermo-hydrodynamic behaviors in the system of both tests were observed to be almost identical, and the effects of the initial downcomer water accumulation velocity became unnoticeable.

(6) The core cooling behavior was observed to be almost identical in both tests through the whole transient including the initial period.

(7) Therefore, it is concluded that although the downcomer flow area of the CCTF is larger than the scaled value, with respect to this point, there is no problem for applying the CCTF test results to the PWR analyses.

Keywords: Reactor Safety, LOCA, ECCS, PWR, Reflood Experiment, Heat Transfer, Two-phase Flow, Downcomer

JAERI－M 86－185

大型再冠水円筒第2次炉心試験C2－3（Run 61）評価報告書
－初期ダウンカマ蓄水速度効果の検討－

日本原子力研究所東海研究所原子炉安全工学部
大久保　努・井口　　正・杉本　　純*
秋本　　肇・岡部　一治**・村尾　良夫

（1986年12月10日受理）

本報告書は，1983年4月21日に行われた円筒第2次炉心試験C2－3（Run 61）の評価を行ったものである。本試験は，PWR－LOCA時の再冠水過程に於ける熱水力挙動に及ぼす初期ダウンカマ蓄水速度の効果を検討する為に行われた。それは，これまでの試験結果から初期における高ダウンカマ蓄水速度は，高炉心冠水速度をもたらし，この為，炉心冷却の促進やU字管振動の増大をもたらす可能性があると考えられるからである。CCTFではダウンカマ流路面積がPWRの縮小値より大きく，そのため初期に於けるダウンカマ蓄水速度がPWRより小さくなると予想されるため，CCTFに於いてその効果を検討することはCCTF試験の結果をPWRの解析に適用する上でダウンカマ流路面積の縮尺に関して問題が無いことを確認するために重要である。

本試験のデータを基本試験のものと比較して，以下の結果が得られた。

(1) 本試験においてダウンカマを満水にする時間は約8秒であり，基準試験に対する値（16秒）に比べ著しく短かった。

(2) この初期における高ダウンカマ蓄水速度が初期において高炉心冠水速度および大U字管振動をもたらしたと考えられる。

(3) 健全ループの差圧即ちスティーム・バインディングおよび炉心差圧も迅速に増加した。これらにより，炉心冠水速度が迅速に減少し始めたと考えられる。

(4) 20秒までに，本試験および基準試験の炉心冠水速度はほぼ等しくなり，また，本試験でみられた大きな振動も30秒までに減衰した。

(5) 20秒以降の期間では，システムの熱力水挙動は，両試験でほぼ同じであり，初期のダウンカマ蓄水速度の効果は認められなくなった。

東海研究所：〒319－11　茨城県那珂郡東海村白方字白根2－4

本報告書は，電源開発促進対策特別会計法に基づき，科学技術庁からの受託によって行った研求の成果である。

＊　科学技術庁
＊＊　三菱原子力工業（株）

(6) 炉心の冷却挙動は，両試験の間で，全期間に渡ってほぼ同一であり，初期を含めて同一であった。

(7) 従って，CCTFのダウンカマ流路面積がPWRの縮小値より大きいにも係らず，この点に関しては，CCTFの試験結果をPWRの解析に適用する上で何ら問題が無いと結論される。

Contents

目　　次

Table List

Figure List

1. Introduction

A reflood test program[1] using large scale test facilities has been conducted at the Japan Atomic Energy Research Institute (JAERI). The facilities are the Cylindrical Core Test Facility (CCTF) and the Slab Core Test Facility (SCTF). This report presents the evaluation for the CCTF Core-II test, Test C2-3 (Run 61).

The CCTF is an experimental facility designed to model a full-height core section, four primary loops and their components of a pressurized water reactor (PWR). This facility is used to provide information on fluid behaviors in the core, downcomer and upper plenum including the steam and water carryover phenomena, and integral system effects during the refill and reflood phases of a hypothetical loss-of-coolant accident (LOCA) of a PWR.

The objectives of the test program using the CCTF are:

a. Demonstration of capability of emergency core cooling system (ECCS) during refill and reflood period.
b. Verification of reflood analysis codes.
c. Collection of information to improve the thermo-hydrodynamic models in the analysis codes, such as, (a) multi-dimensional core thermo-hydrodynamics including the radial power distribution effect, fall back effect and spatial oscillatory behavior, (b) flow behavior in the upper plenum and hot legs, (c) behavior of accumulated water at the bottom of the upper plenum including possible counter-current flow and sputtering effect, (d) hydrodynamic behavior of the injected ECC water and the water passing through the steam generator, (e) multi-dimensional thermo-hydrodynamic behavior in the hot annular downcomer, and (f) overall oscillatory behavior in the system.

As the first series of the CCTF tests, twenty-seven CCTF Core-I tests were conducted. This series of tests presented a lot of information[2] on the system thermo-hydrodynamic behavior as well as the core behavior during the refill and reflood phases of a LOCA in a PWR. The CCTF Core-I test series was initiated in March 1979 and terminated in April 1981. Subsequently, as the second series of the CCTF tests, the CCTF Core-II test series was initiated in March 1982. The special

purposes of the CCTF Core-II test program are to investigate the effects of alternative ECCS such as the combined and the downcomer injections as well as to extend the experimental range of Core-I test series.

Test C2-3 (Run 61) was conducted on April 21, 1983 in order to investigate the effects of initial downcomer water accumulation velocity on the thermo-hydrodynamic behaviors during the reflood phase of a PWR-LOCA. The downcomer flow area of the CCTF was designed to include the additional flow area of the barrel-baffle region as described in Section 2.1.1. Accordingly, the water accumulation velocity in the downcomer is expected to be lower than that in the reference PWR. The difference in the downcomer water accumulation velocity may result in the difference in the core flooding rate[3], and hence, the core cooling, the core water accumulation, the U-tube type oscillation and so forth. Therefore, the present test was conducted in order to clarify the items mentioned above.

In the present test, the ECC water was injected into the downcomer as well as the lower plenum and intact cold legs during the Acc period in order to increase the initial downcomer water accumulation velocity. The injection rate of the additional downcomer injection was determined to simulate the situation of the PWR as closely as possible.

In this report, the results of the present test are analyzed by being compared with those of the base case test[4]. The selected data of the present test are presented in Appendix B for better understanding of the test results.

2. Test Description

2.1 Test Facility

The CCTF Core-II was designed in consideration of the following objectives and criteria:

a. Design objectives

(1) The facility should provide the capability to reasonably simulate the flow conditions in the primary system of a PWR during the refill and reflood phases of a LOCA.

(2) The downcomer design should provide ECC water flow behavior throughout the test which is reasonably representative of that of the PWR downcomer.

b. Design criteria

(1) The reference reactors are the Trojan reactor in the USA and in certain aspects the Ohi reactor in Japan.

(2) The vertical dimensional and locations of system components are kept as close to those of the reference reactors as possible.

(3) The flow areas of the system components are scaled down in proportion to the scaling factor of core flow area.

(4) The facility is equipped with four loops which are composed of three intact loops and one broken loop.

(5) A 200% cold leg large break is simulated in the broken loop.

(6) The ECCS consists of two accumulator systems (Acc) and a low pressure coolant injection system (LPCI), and the injection locations are the upper plenum, the downcomer and the hot legs as well as the lower plenum and the cold legs.

(7) The maximum allowable pressure of the facility is 588 kPa (6 kg/cm^2 absolute).

(8) The maximum allowable temperature of the simulated fuel rods is 1173 K (900°C).

(9) The maximum allowable temperature of the components in the primary system except the simulated fuel rod assembly is 623 K (350°C).

(10) The reactor vessel contains approximately 2,000 electrically heated rods simulating the fuel rods.

(11) The design of upper plenum internals is based on that of a new Westinghouse 17×17 type fuel assembly.

(12) The flow resistance of each loop is adjusted by an orifice in the pump simulator.

(13) The containment system consists of two tanks.

A bird's-eye view of the CCTF is shown in Fig. 2.1. The scaled dimensions of the components are given in Table 2.1.

The differences in the design of the Core-II facility from the Core-I are:

(1) Axial and local peaking factors of heater rods

(2) Edge shape of grid spacers

(3) Upper plenum structures (upper plenum internals, plugging devices in end box region and a upper ring)

(4) Vent valves

(5) Alternative ECCS (downcomer injection and upper plenum injection)

(6) Instruments

2.1.1 Pressure Vessel and Internals

The pressure vessel is of a cylindrical type as shown in Figs. 2.2 and 2.3. The height is the same as the reference reactor pressure vessel. The radial direction is scaled down by the flow area scaling ratio of 1/21.44. The upper ring was newly installed in the Core-II facility for the installation of the upper plenum ECC water injection lines and the instruments. The upper plenum injection lines are shown in Figs. 2.4 and 2.5. The upper plenum injection is adopted in some 2-loop PWRs in Japan and the USA. Four vent valves and two donwcomer ECC water injection nozzles, which are called Core Flooding Nozze (CFN), are also newly equipped in the Core-II facility as shown in Figs. 2.2 and 2.3. Vent valves and CFNs are for the simulation of a Babcock & Wilcox (B & W) type PWR. Downcomer injection nozzles also exist in a couple of recent Japanese PWRs. The downcomer injection is also adopted in a couple of recent Japanese 2-loop PWRs without vent valves. The location of CFNs are shown in Fig. 2.6 in detail.

The cross section of the pressure vessel is shown in Fig. 2.3 and the dimensions are given in Fig. 2.7. The core consists of thirty-two 8×8 electrically heated rod bundles arranged in a cylindrical configuration

and simulates a Westinghouse 15×15 type fuel assemblies.

The downcomer is an annulus of 61.5 mm gap. In determining the gap size, the flow area of the core baffle region was added to that of the downcomer region. Thus, the core baffle flow area is included in the downcomer simulation and is not simulated separately in the vessel inserting stainless steel fillers to prevent fluid flow.

The vessel wall is constructed of carbon steel which is caldded with the 5 mm thick stainless steel plate. The wall is 90 mm thick to simulate the stored energy as reasonably as possible during ECC water injection.

The design of upper plenum internals is based on that of the new Westinghouse 17×17 type fuel assemblies instead of the old type simulated in the Core-I facility. The internals consists of ten control rod guide tubes, ten support columns and twelve open holes as shown in Fig. 2.8. The radius of each internals is scaled down by factor 8/15 from that of an actual reactor. They are illustrated in Fig. 2.9. Flow resistance baffles are inserted into the control rod guide tubes. The baffles consist of two kinds of baffle plates and a shaft. The baffle plates are shown in Fig. 2.10.

End boxes are attached beneath the UCSP. The structure for one heater rod bundle is shown in Fig. 2.11. Plugging devices are installed newly in the Core-II facility as shown in Figs. 2.11 and 2.12 to simulate the flow resistance more correctly.

2.1.2 Heater Rod Assembly

The heater rod assembly simulating the fuel assembly consists of thirty-two 8×8 array rod bundle. Each bundle consists of fifty-seven electrically heated rods and seven non-heated rods as shown in Fig. 2.13. The core is usually subdivided into three regions to achieve a desired radial power distribution. This is shown in Fig. 2.3. The high, medium and low power regions are named A, B and C regions, respectively. The local peaking factor of heated rods in a bundle is unity, that is, all heated rods in a bundle have the same power density in the Core-II facility.

A heater rod consists of a nichrome heating element, magnesium oxide (MgO) and boron nitride (BN) insulators, and Inconel-600 sheath. BN is used for only central part of the heated region and MgO for the

other part as shown in Fig. 2.14. The heated length and the outer diameter of the heater rods are 3.66 m and 10.7 mm, respectively, which are identical to the corresponding dimensions of reference PWR fuel rods. The sheath wall thickness is 1.0 mm and is thicker than the actual fuel cladding, because of the requirements for thermocouple installation. The heating element is a helical coil with a varying pitch to generate a 17-step chopped consine axial power profile as shown in Fig. 2.15. The peaking factor is 1.40, instead of 1.492 for a Core-I rod.

Non-heated rods are either stainless steel pipes or solid bars of 13.8 mm O.D. The pipes are utilized for installation of instruments such as superheated steam probes and thermocouples. The bars are used for supporting the assembly loads.

The heated rods and non-heated rods are held in radial position by grid spacers which are located at six elevations along the axial length as shown in Fig. 2.15. A grid spacer is a lattice structure composed of stainless steel plates of 0.4 mm and 0.8 mm thick and 40 mm high, whoes edges are sharpened in the Core-II. The rod pitch is 14.3 mm which is the same as that of the reference PWR.

The heater rods penetrate through the bottom plate of the vessel to facilite lead out of the power cables from the bottom of the vessel. The outer diameter of the rods in the lower plenum is reduced to 8.6 mm. Three-phase electric current is used for heating the heater rods and the electrical neutral point is at the top of the rods where they are interconnected to each other.

2.1.3 Primary Loops and ECCS

Primary loops consist of three intact loops and a broken loop. Each loop consists of hot leg and cold leg pipings, a steam generator simulator and a pump simulator. The 200 percent cold leg large break is simulated for the broken loop. The broken cold leg is connected to two containment tanks through blowdown valves. The primary loop arrangement is shown in Figs. 2.16 and 2.17.

The inner diameter of the piping is scaled down in proportion to the core flow area scaling. The length of each piping section is almost the same as the corresponding section of the reference PWR.

The steam generator simulators are of the U-tube and shell type as

shown in Fig. 2.18. The tube length is about 5 m shorter than in the reference PWR. The vertical hight of the steam generator simulators is also about 5 m lower than in the reference PWR. The primary coolant passes through the tube side and the secondary coolant is stagnant in the shell side. The steam generator simulators of two loops are housed in a single shell assembly which has two compartments, one simulator for each loop in one compartment. The wall thickness of the U-tube is 2.9 mm compared to 1.27 mm of the reference PWR, because of a higher pressure difference between the primary and secondary sides in the simulator.

The pump simulator consists of the casing and duct simulators and an orifice plate as shown in Fig. 2.19. The loop flow resistance is simulated with the orifice plate. Each orifice plate has a hole with diameter and thickness of 95 mm and 10 mm, respectively.

ECCS consists of two Accs and a LPCI. The injection points are at each hold leg, lower plenum, upper plenum and downcomer. The upper plenum and downcomer injection system was newly installed after Test C2-2 (Run 56) for the alternative ECCS tests. In the new injection system, two accumulator tanks are used for ECC water injection.

2.1.4 Instrumentation

The instrumentation is divided into two groups. One of them is JAERI-supplied instruments measuring the temperatures, absolute pressures, differential pressures, water levels and flow rates. Thermocouples measure the temperatures of the rod surface, fluid and structure. The absolute pressures are measured in the upper and lower plena, steam generator plena and containment tanks. The differential pressure measurements are carried out at many locations covering the whole system almost completely. In the ECC water supply tanks and the containment tank 1, the liquid levels are measured. The flow meters measure the ECC water flow rates. Furthermore, flow rates in the downcomer, loop seal pipings and the vent line from the containment tank 2 to the atmosphere are measured with drag disk flow meters, pitot tubes and a venturi tube, respectively. The total number of the JAERI-supplied instruments is 1338 channels as summarized in Table 2.2 and the signals from these instruments are recorded on a magnetic tape.

The other group of the instrumentation is the USNRC-supplied instruments. They are the advanced instrumentation for the two-phase flow measurement. The kinds and quantities of those are tabulated in Table 2.3. The total number is 540 channels.

2.2 Test Conditions and Procedures

2.2.1 Test Conditions

The summary of the test conditions are presented in Table 2.4. The distinctive feature of the present test is that the ECC water was injected into the downcomer as well as the lower plenum and intact cold legs to increase the Acc injection rate. Except the difference in injection location and rate, the other conditions were set equal to those in the base case test.

2.2.2 Test Procedures

In preparation for the test, the accumulator tanks, the LPCI tanks, the saturated water tank and the secondary sides of the steam generator simulators were filled with water which was purified with ion exchange resin. After all the components and instruments were inspected for mechanical and electrical leakages, the instruments were checked for zero points and sensitivity.

After these preparatory operation, the primary system was heated with the preheaters to its specified temperature (393 K) and pressurized to a specified pressure (200 kPa) by substituting steam for air in the system. The water in the accumulator tanks was electrically heated to its specified temperature (308 K) and pressurized with nitrogen gas to provide sufficient head to drive the injection flow required. The water in the LPCI tank was also heated to its specified temperature (308 K) and was circulated through the circulation line including the LPCI line so as to preheat the line to the same temperature as the water. The water in the saturated water tank was heated up near saturation temperature (393 K) of the expected primary system pressure (200 kPa). The water in the secondary side of each steam generator simulator was also heated and pressurized to the specified temperature (539 K) and pressure (5.3 MPa).

After establishing the initial conditions of the test, electric power for preheating was turned off and the lower plenum was filled to a specified level (0.9 m) directly from the saturated water tank. When the water level in the lower plenum reached the specified level and other initial conditions of the test were stabilized at allowable tolerance, electric power was applied to the heater rods in the core and the data recording was started. This is the initiation of the test, *i.e.* 0 s. The temperature rise of the rods were monitored by using a computer. At 85 s, Acc injection (0.105 m^3/s) into the lower plenum was initiated. The initiation time for ECC injection, *i.e.* 85 s, was scheduled to coincide with the timing when the clad temperature of 995 K was reached by four rods. This specified clad temperature (995 K) of the heater rods for initiation of coolant injection was predetermined by interpolation between the clad temperature (393 K) after preheating and the clad temperature (1073 K) assumed for the time of bottom of core recovery (BOCREC). Decay of power input to the rods was programmed to begin at the time of BOCREC. The specified power decay was obtained by normalizing the decay curve of the ANS standard $\times 1.2 + {}^{238}U$ capture $\times 1.1$ decay at 30 s after shutdown.

The BOCREC time was scheduled to be 94 s in this test. The downcomer injection (0.048 m^3/s) was initiated at 94 s using the new Acc. At 101 s, Acc injection location was switched from the lower plenum to three intact cold legs and the downcomer injection was terminated. Since the BOCREC was scheduled to occur at 94 s, some amount of steam generated in the core was expected to flow in the primary loops prior to switching of the Acc injection location. This procedure was for preventing an unrealistic condensation from occurring at the cold legs. At a specified time (23 s) after the initiation of Acc injection, the Acc injection mode was transferred to the LPCI injection mode. A specified LPCI injection rate (0.011 m^3/s) was maintained constantly until the ECC injection was turned off. The sequence of the ECC water injection of the present test is compared with that of the base case test in Fig. 2.20.

The generated steam and the entrained water flowed via broken and intact loops to the containment tank 2. The steam was then vented to the atmosphere to maintain the pressure in the containment tank constant at the specified initial pressure (200 KPa).

When all thermocouples on the surface of heater rods indicated quenching of the rods, the power supply to heater rods and the ECC water injection were turned off. After this the data recording was ended terminating the test.

The chronology of events is presented in Table 2.5.

Table 2.1 CCTF component scaled dimensions

COMPONENT		PWR	JAERI	RATIO
PRESSURE VESSEL				
VESSEL INSIDE DIAMETER	(mm)	4394 (173")	1084	
VESSEL THICKNESS	(mm)	216 (8 1/2")	90	
CORE BARREL OUTSIDE DIAMETER	(mm)	3874	961	
CORE BARREL INSIDE DIAMETER	(mm)	3760	929	
THERMAL SHIELD OUTSIDE DIAMETER	(mm)	4170		
THERMAL SHIELD INSIDE DIAMETER	(mm)	4030		
DOWNCOMER LENGTH	(mm)	4849	4849	1/1
DOWNCOMER GAP	(mm)	114.3	61.5	
DOWNCOMER (+ BUFFLE) FLOW AREA	(m^2)	4.23	0.197	1/21.44
LOWER PLENUM VOLUME	(m^3)	29.6	1.38	1/21.44
UPPER PLENUM VOLUME	(m^3)	43.6	2.04	1/21.44
FUEL (HEATER ROD) ASSEMBLY				
NUMBER OF BUNDLES	(—)	193	32	
ROD ARRAY	(—)	15 × 15	8 × 8	
ROD HEATED LENGTH	(mm)	3660	3660	1/1
ROD PITCH	(mm)	14.3	14.3	1/1
FUEL ROD OUTSIDE DIAMETER	(mm)	10.72	10.7	1/1
THIMBLE TUBE DLAMETER	(mm)	13.87	13.8	1/1
INSTRUMENT TUBE DIAMETER	(mm)	13.87	13.8	1/1
NUMBER OF HEATER RODS	(—)	39372	1824	1/21.58
NUMBER OF NON-HEATED RODS	(—)	4053	224	1/18.09
CORE FLOW AREA	(m^2)	5.29	0.25	1/21.2
CORE FLUID VOLUME	(m^3)	17.95	0.915	1/19.6
PRIMARY LOOP				
HOT LEG INSIDE DIAMETER	(mm)	736.6 (29")	155.2	1/4.75
HOT LEG FLOW AREA	(m^2)	0.426	0.019	1/22.54
HOT LEG LENGTH	(mm)	3940	3940	1/1
PUMP SUCTION INSIDE DIAMETER	(mm)	787.4 (31")	155.2	1/5.07
PUMP SUCTION FLOW AREA	(m^2)	0.487	0.019	1/25.77
PUMP SUCTION LENGTH	(mm)	7950	7950	1/1

Table 2.1 (Cont'd)

COMPONENT		PWR	JAERI	RATIO
COLD LEG INSIDE DIAMETER	(mm)	698.5 (27.5")	155.2	1/4.50
COLD LEG FLOW AREA	(m^2)	0.383	0.019	1/20.26
COLD LEG LENGTH	(mm)	5600	5600	1/1
STEAM GENERATOR SIMULATOR				
NUMBER OF TUBES	(—)	3388	158	1/21.44
TUBE LENGTH (AVERAGE)	(m)	20.5	15.2	1/1.35
TUBE OUTSIDE DIAMETER	(mm)	22.225 (0.875")	25.4	
TUBE INSIDE DIAMETER	(mm)	19.7 (0.05")	19.6	1/1
TUBE WALL THICKNESS	(mm)	1.27	2.9	
HEAT TRANSFER AREA	(m^2)	4784 (51500 ft^2)	192	1/24.92
TUBE FLOW AREA	(m^2)	1.03	0.048	1/21.44
INLET PLENUM VOLUME	(m^3)	4.25	0.198	1/21.44
OUTLET PLENUM VOLUME	(m^3)	4.25	0.198	1/21.44
PRIMARY SIDE VOLUME	(m^3)	30.50 (1077 ft^3)	1.2	1/25.41
SECONDARY SIDE VOLUME	(m^3)	157.33 (5556 ft^3)	2.5	1/62.93
CONTAINMENT TANK - I	(m^3)		30	
CONTAINMENT TANK - II	(m^3)		50	
STORAGE TANK	(m^3)		25	
ACC. TANK	(m^3)		5	
SATURATED WATER TANK	(m^3)		3.5	
ELEVATION				
BOTTOM OF HEATED REGION IN CORE	(mm)	0	0	
TOP OF HEATED REGION IN CORE	(mm)	3660	3660	0
TOP OF DOWNCOMER	(mm)	4849	4849	0
BOTTOM OF DOWNCOMER	(mm)	0	0	0
CENTERLINE OF COLD LEG	(mm)	5198	4927	- 271
BOTTOM OF COLD LEG (INSIDE)	(mm)	4849	4849	0
CENTERLINE OF LOOP SEAL LOWER END	(mm)	2056	2047	- 9
BOTTOM OF LOOP SEAL LOWER END	(mm)	1662	1959	+ 297

Table 2.1 (Cont'd)

COMPONENT		PWR	JAERI	RATIO
CENTER OF HOT LEG	(mm)	5198	4927	－ 271
BOTTOM OF HOT LEG (INSIDE)	(mm)	4830	4849	＋ 19
BOTTOM OF UPPER CORE PLATE	(mm)	3957	3957	0
TOP OF LOWER CORE PLATE	(mm)	－ 108	－ 50	＋ 58
BOTTOM OF TUBE SHEET OF STEAM GENERATOR SIMULATOR	(mm)	7308	7307	－ 1
LOWER END OF STEAM GENERATOR SIMULATOR PLENUM	(mm)	5713	5712	－ 1
TOP OF TUBES OF STEAM GENERATOR SIMULATOR (avg)	(mm)	17952.7	14820	

Table 2.2 List of items measured with JAERI-supplied instruments

Item	Number of channels
Rod surface temperature	673
Core fluid temperature	40
Core barrel wall temperature	10
UP fluid temperature	120
UP wall temperature	36
DC fluid temperature	20
DC wall temperature	40
LP fluid temperature	8
LP wall temperature	4
SG primary side fluid temperature	24
SG secondary side fluid temperature	66
Primary loop piping fluid temperature	94
Primary loop piping wall temperature	4
Water supply tank fluid temperature	12
Core differential pressure	28
DC differential pressure	20
UP differential pressure	8
LP differential pressure	1
SG primary side differential pressure	8
Primary loop differential pressure	52
Pressure	15
Water level	7
Flow rate	39
Electric power	9
Total	1338

Note

UP : Upper plenum, DC : Downcomer

LP : Lower plenum, SG : Steam generator

Table 2.3 List of USNRC-provided instruments

Instrument	Number of sets	Number of sensors
DC FDG	18	162
DC VOP	1	1
DC drag disk	4	8
Core velocimeter	4	4
Core flag probe	12	24
Core LLD	6	96
LP LLD	3	15
End box turbine meter	8	8
UP turbine meter	4	4
UP FDG	11	110
UP film probe	2	4
UP prong probe	2	4
UP VOP	1	1
VV turbine meter	2	2
VV string probe	2	2
HL film probe	2	4
HL VOP	1	1
Reference probe	1	1
Spool piece	8	89
Total	92	540

Note

DC : Downcomer, FDG: Fluid distribution grid,
VOP: Video optical probe, LLD: Liquid level detector,
LP : Lower plenum, UP : Upper plenum,
VV : Vent valve

Table 2.4 Summary of test conditions

1. Test type: Initial downcomer water accumulation velocity effects test
2. Test No.: C2-3 (Run 61)
3. Test date: April 21, 1983
4. Power: Total; 9.35 MW, Average linear; 1.40 kW/m
5. Radial power distribution:

   A B C

   1.91 : 1.68 : 1.07 kW/m
6. Pressure (MPa):

   Upper plenum ; 0.26

   Containment ; 0.21
7. Temperature (K):

   Downcomer wall; 467, Vessel internals; 395

   Primary piping; 396, Lower plenum liquid; 395

   ECC liquid; 309, Steam generator secondary; 540
8. ECC injection type:: Cold leg injection
9. Pump K-factor: 15
10. ECC injection rates and duration:

    Acc; 89×10^{-3} m^3/s from 104.0 to 111.0 s (at half maximum)

    LPCI; 11×10^{-3} m^3/s from 112.0 to 1008.0 s

    New Acc; 48×10^{-3} m^3/s from 94.0 to 104.0 s

    ECC injection to lower plenum; from 85.0 to 101.5 s
11. Initial water level in lower plenum: 0.80 m
12. Power decay: ANS × 1.2 + Actinide × 1.1 (30 s after scram)
13. Peak clad temperature at BOCREC: 1078 K

Table 2.5 Chronology of events for test

Event	Time (s)
Test initiated (Heater rods power on) (Data recording initiated)	0.0
Accumulator injection initiated	85.0
Power decay initiated (Downcomer injection initiated)	94.0
Bottom of core recovery (BOCREC)	94.5
Accumulator injection switched from lower plenum to cold legs	101.5
LPCI injection initiated	112.0
All heater rods quenched	633.0
Power off	1008.0
LPCI injection ended	1008.0
Test ended (Data recording ended)	1038.0

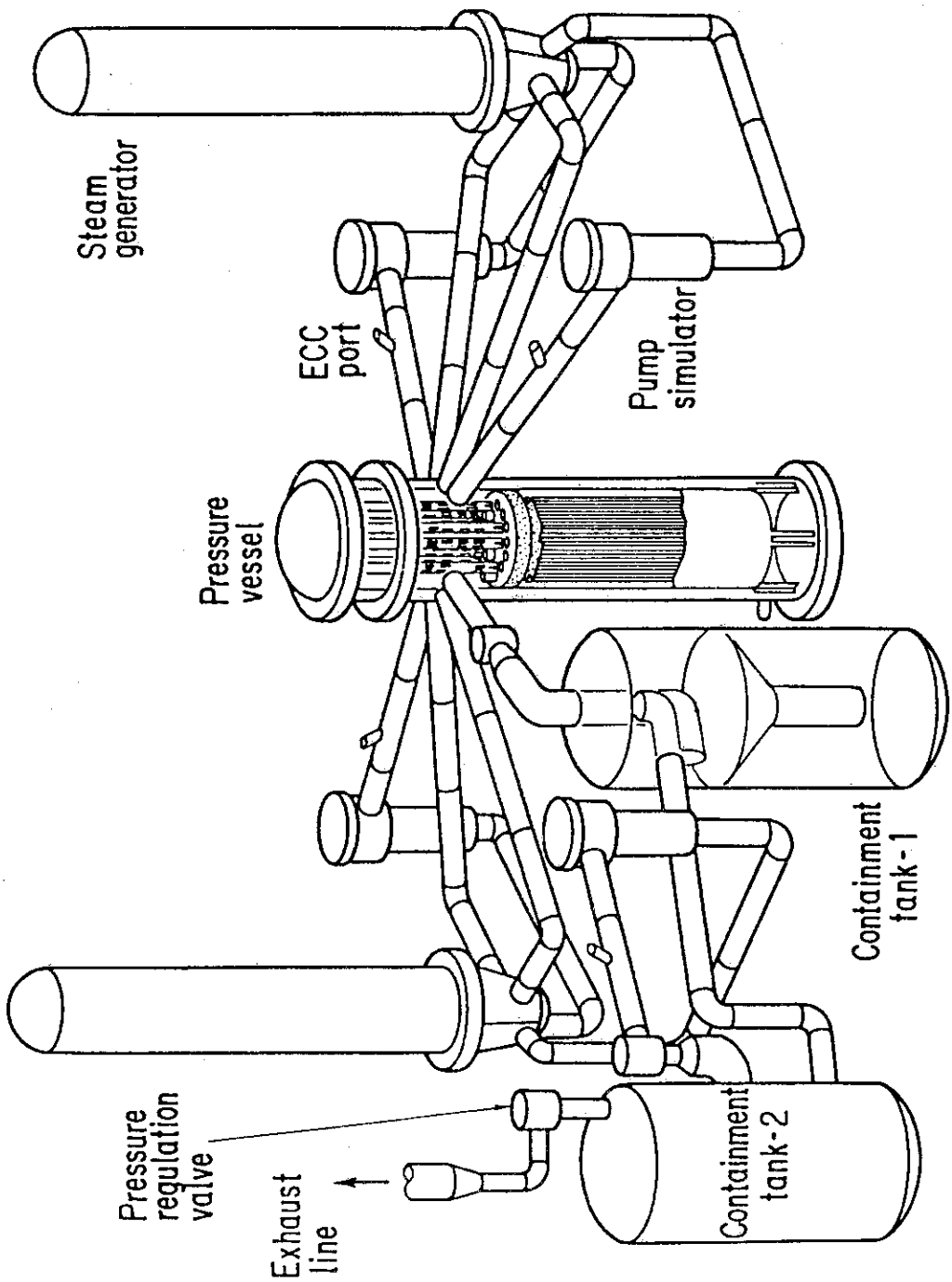

Fig. 2.1 Bird's-eye view of CCTF

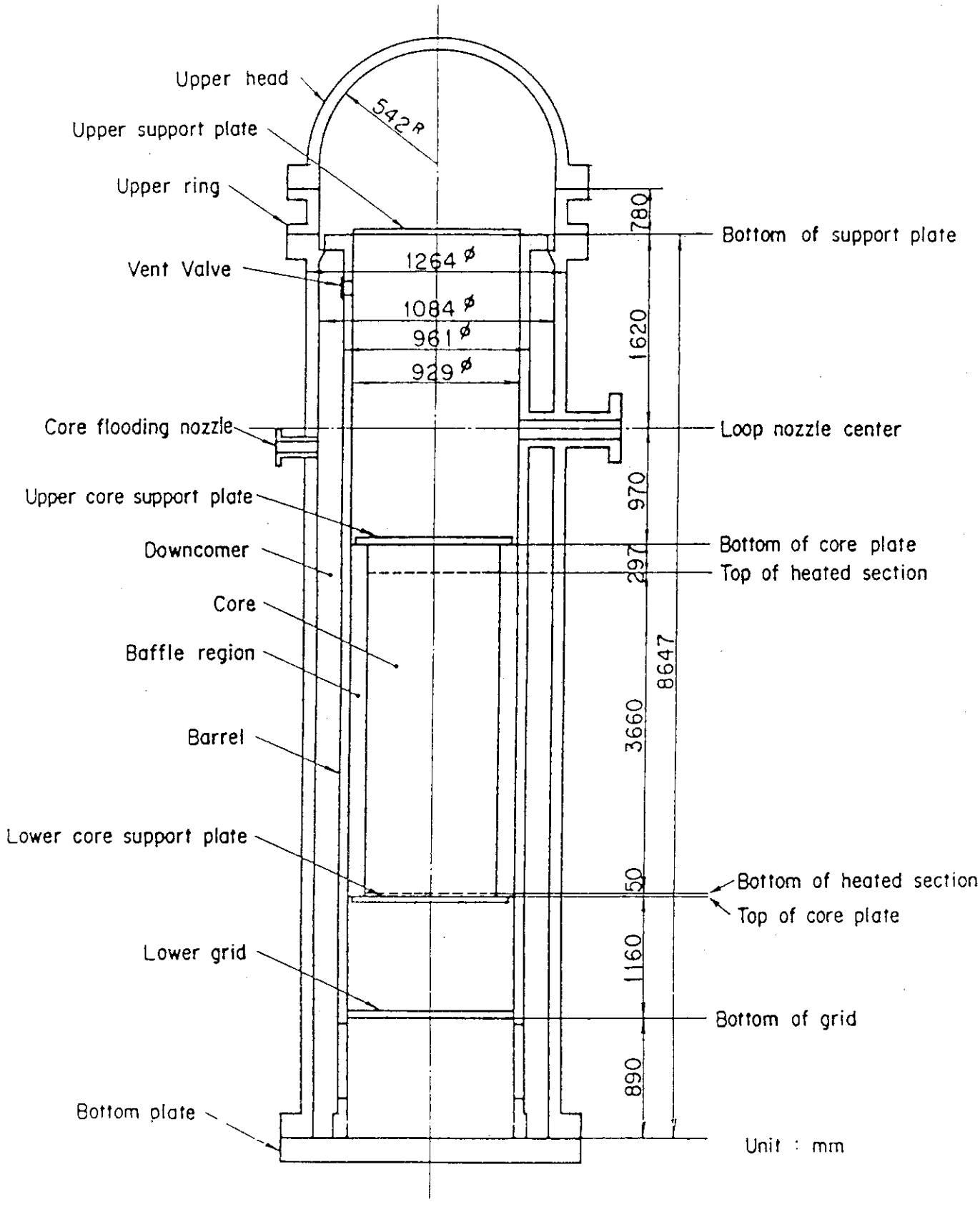

Fig. 2.2 CCTF Core-II pressure vessel

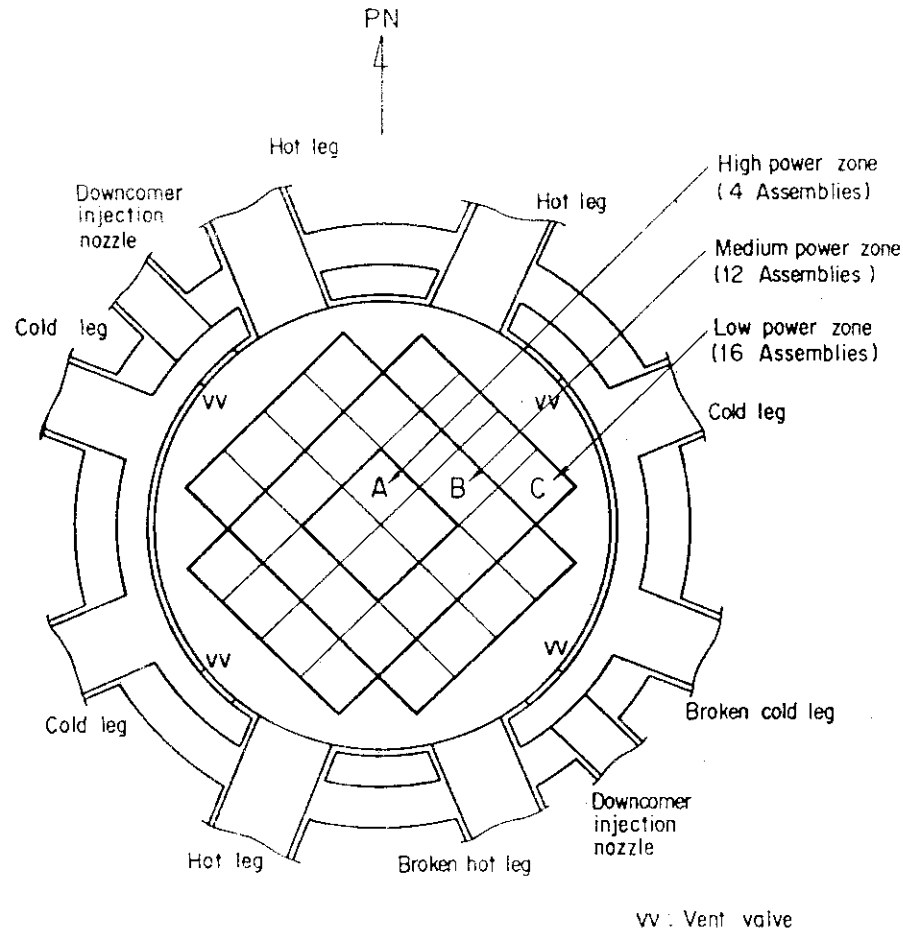

Fig. 2.3 Cross section of CCTR Core-II pressure vessel

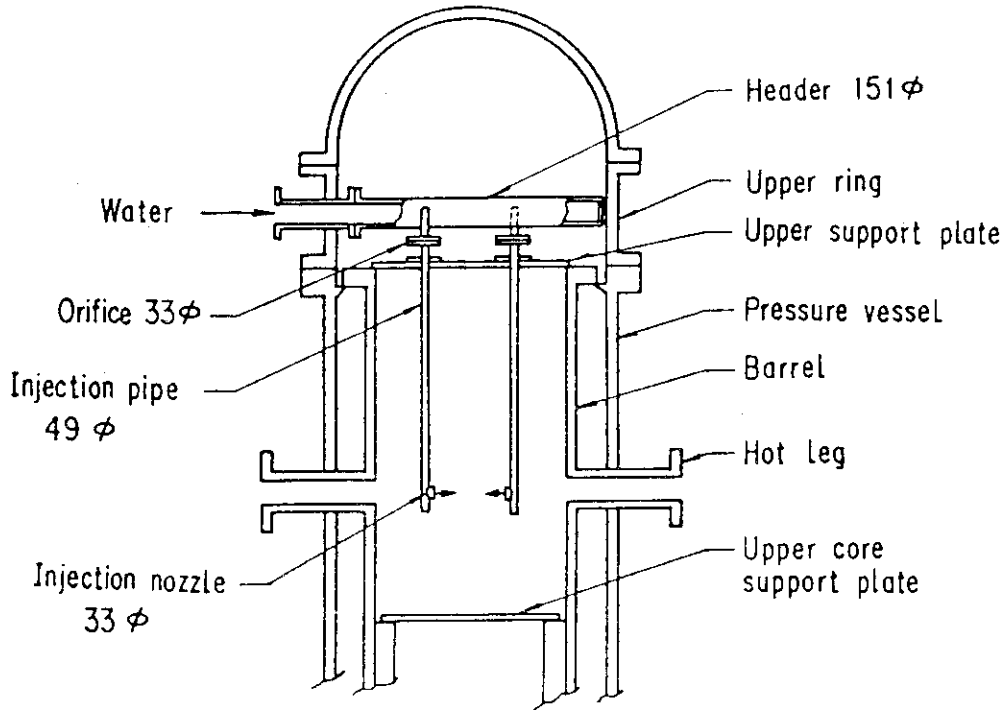

Fig. 2.4 Configuration of upper plenum injection pipe

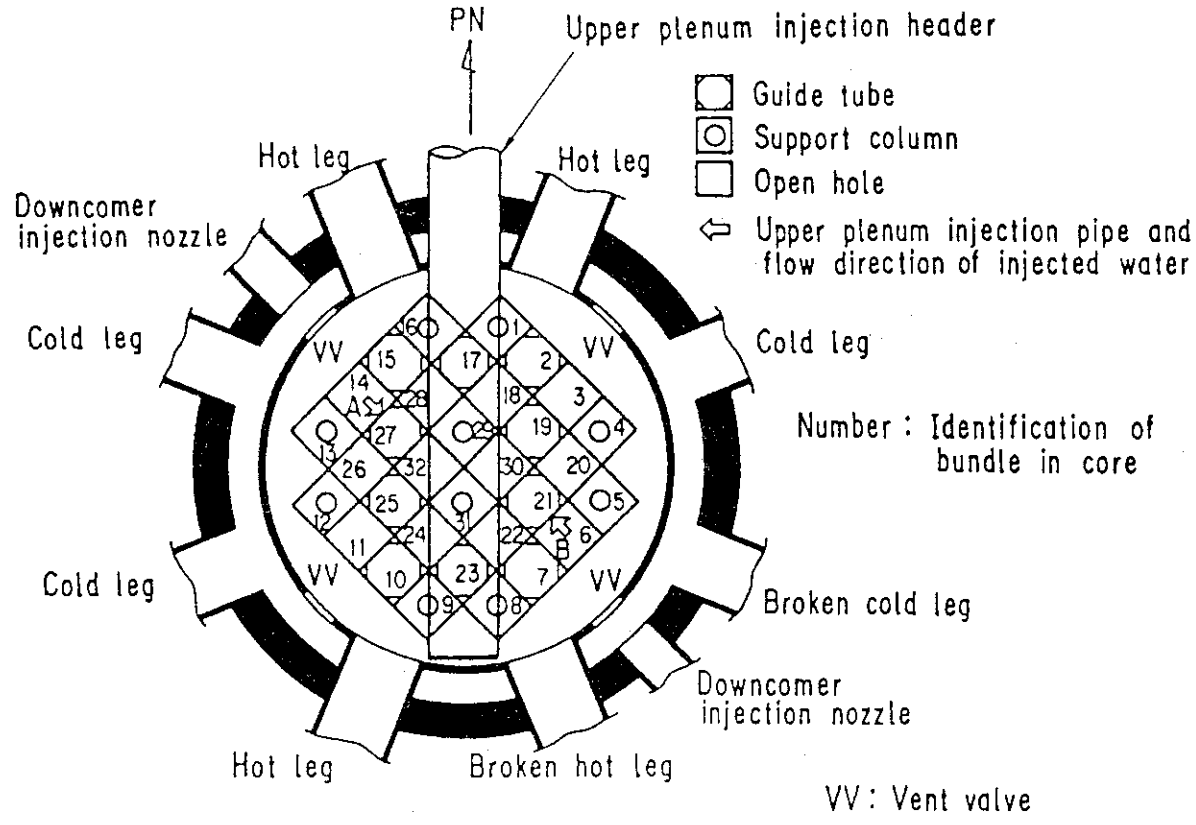

Fig. 2.5 Arrangement and location of upper plenum injection pipe

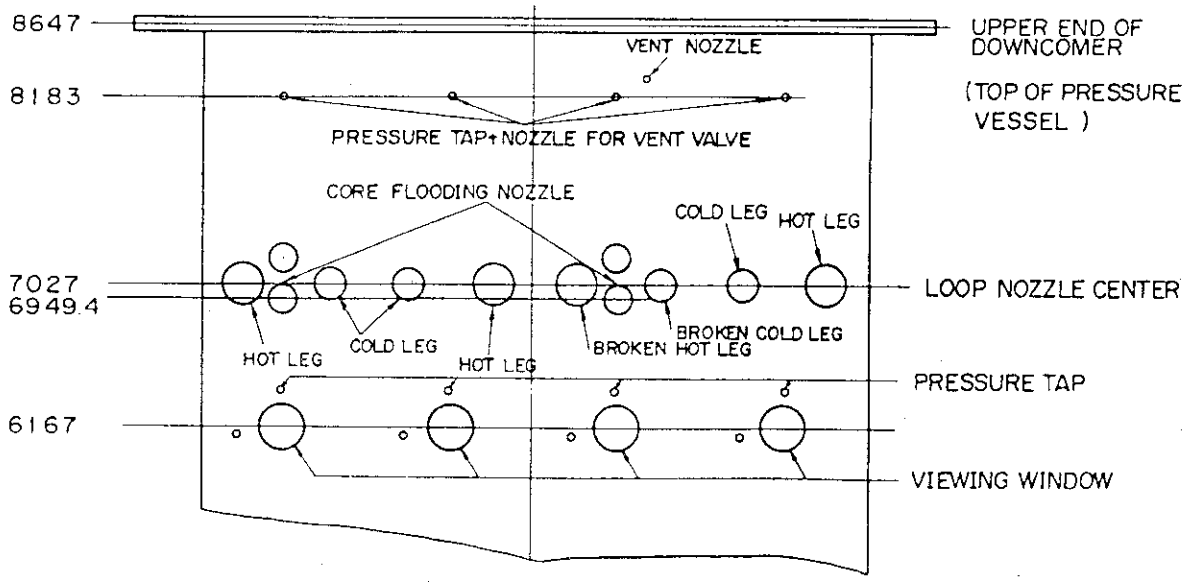

Fig. 2.6 Location of Core Flooding Nozzles

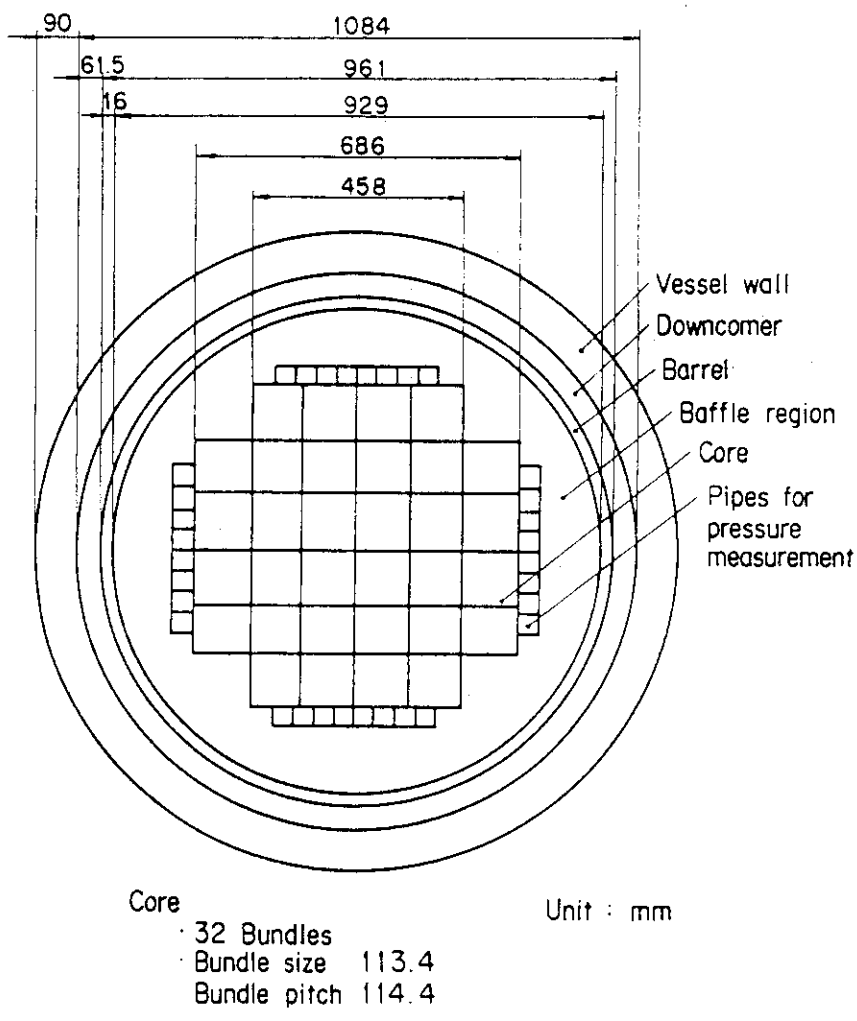

Fig. 2.7 Dimension of CCTF Core-II pressure vessel cross section

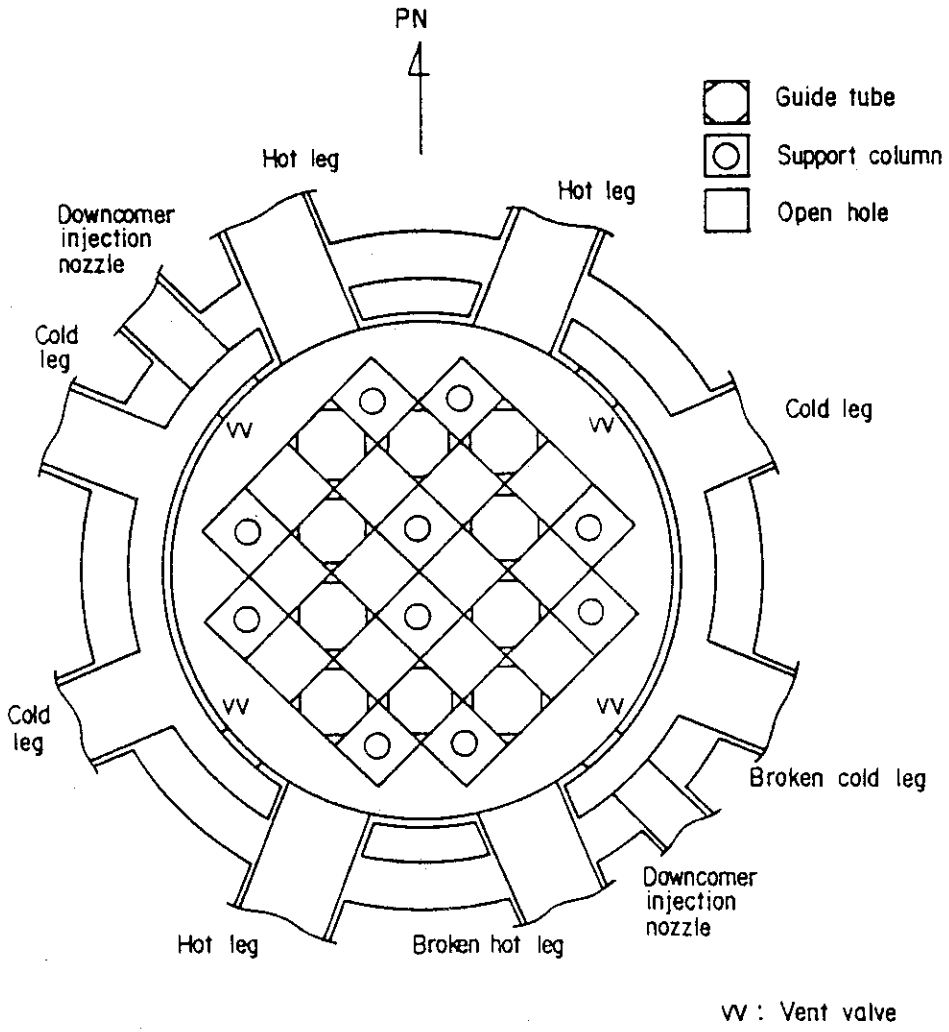

Fig. 2.8 Arrangement of upper plenum internals

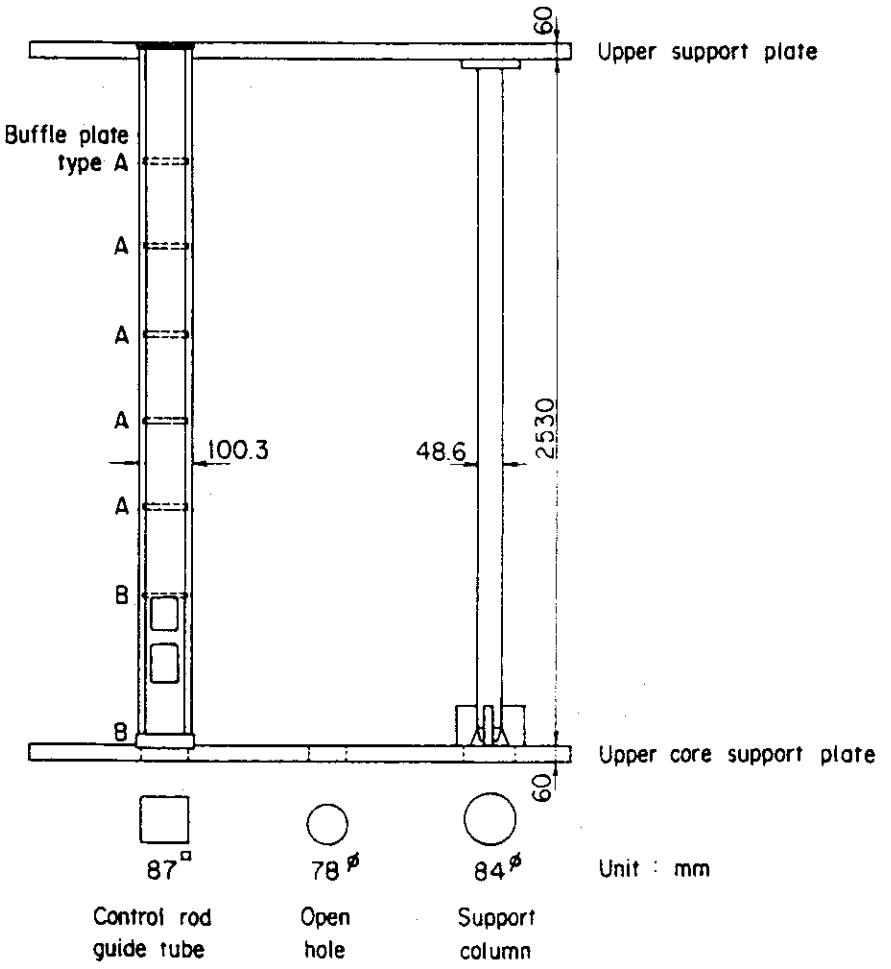

Fig. 2.9 Upper plenum internals

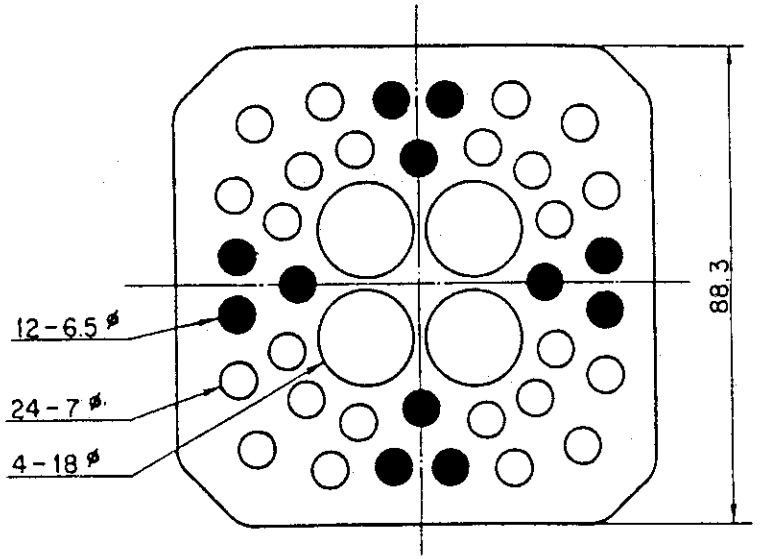

Type A

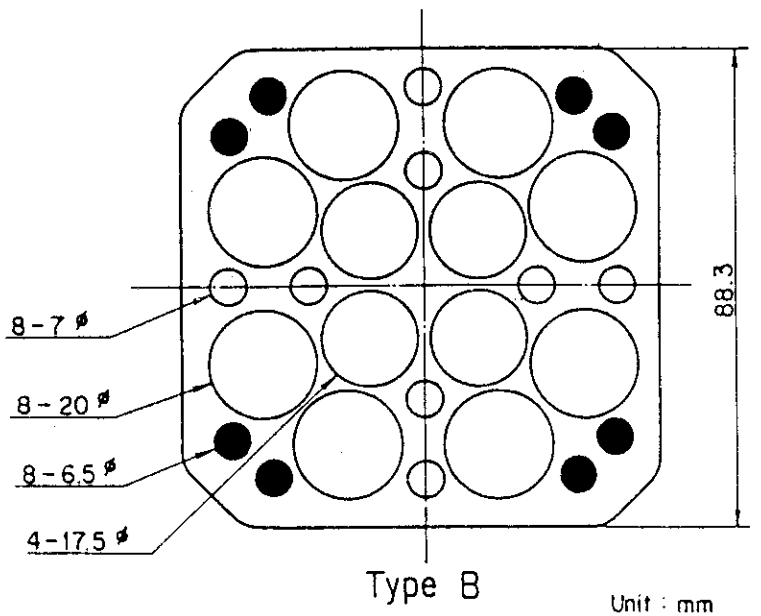

Type B

Unit : mm

Fig. 2.10 Buffle plates in control rod guide tube

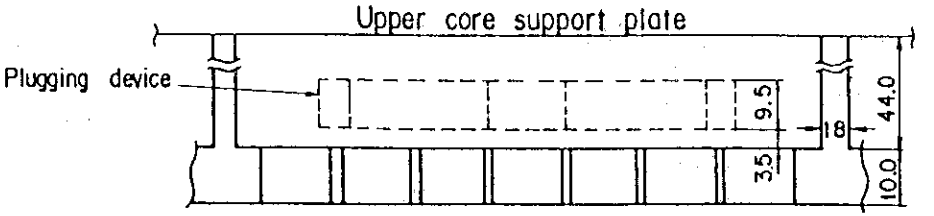

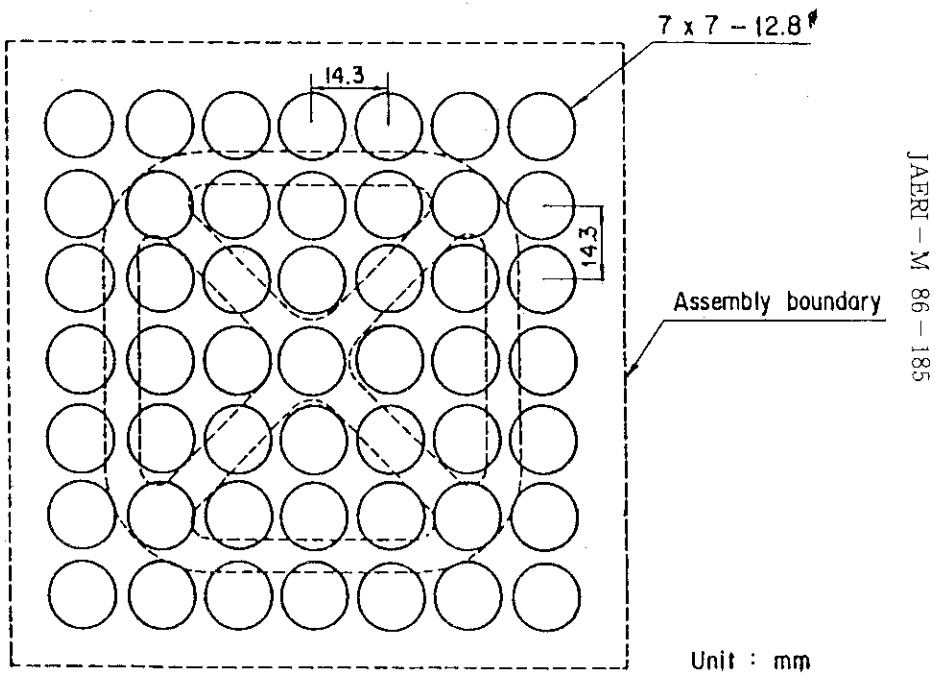

Unit : mm

Fig. 2.11 End box

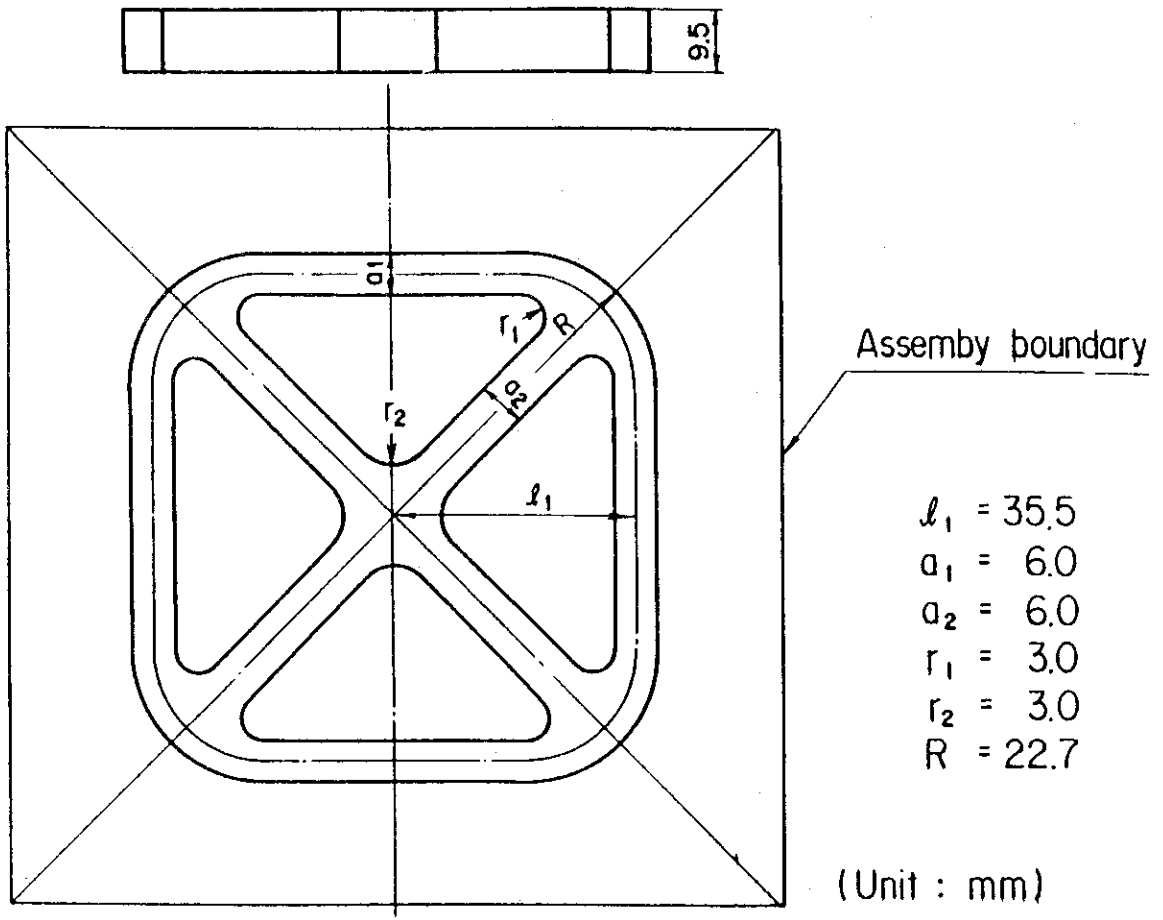

Fig. 2.12 Dimensions of plugging device

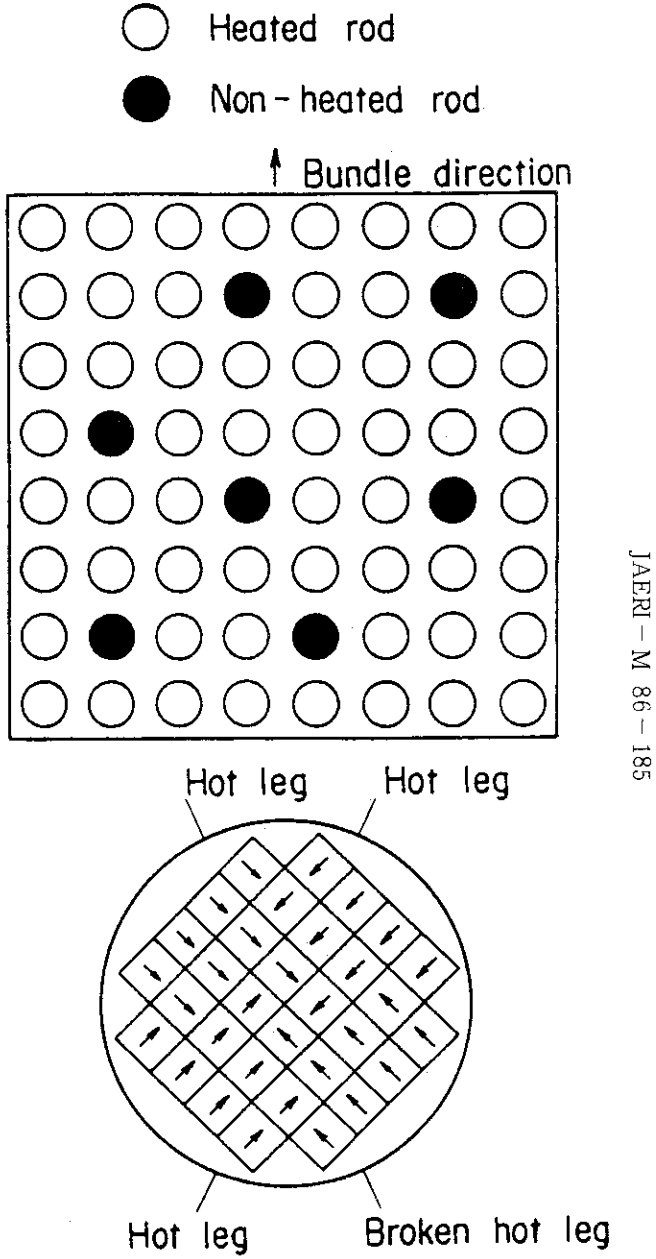

Fig. 2.13 Arrangement of non-heated rods and bundle direction

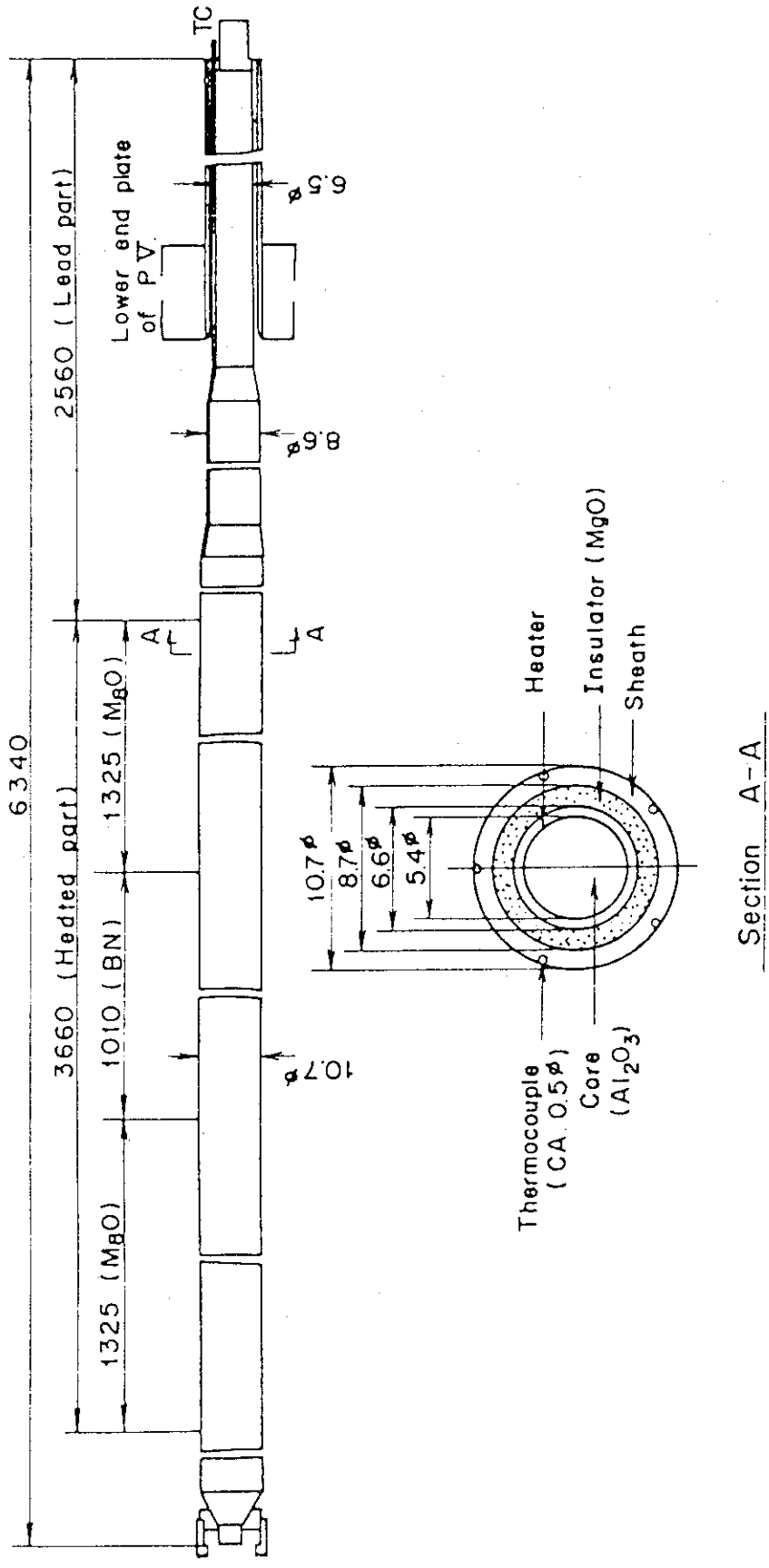

Fig. 2.14 Heater rod

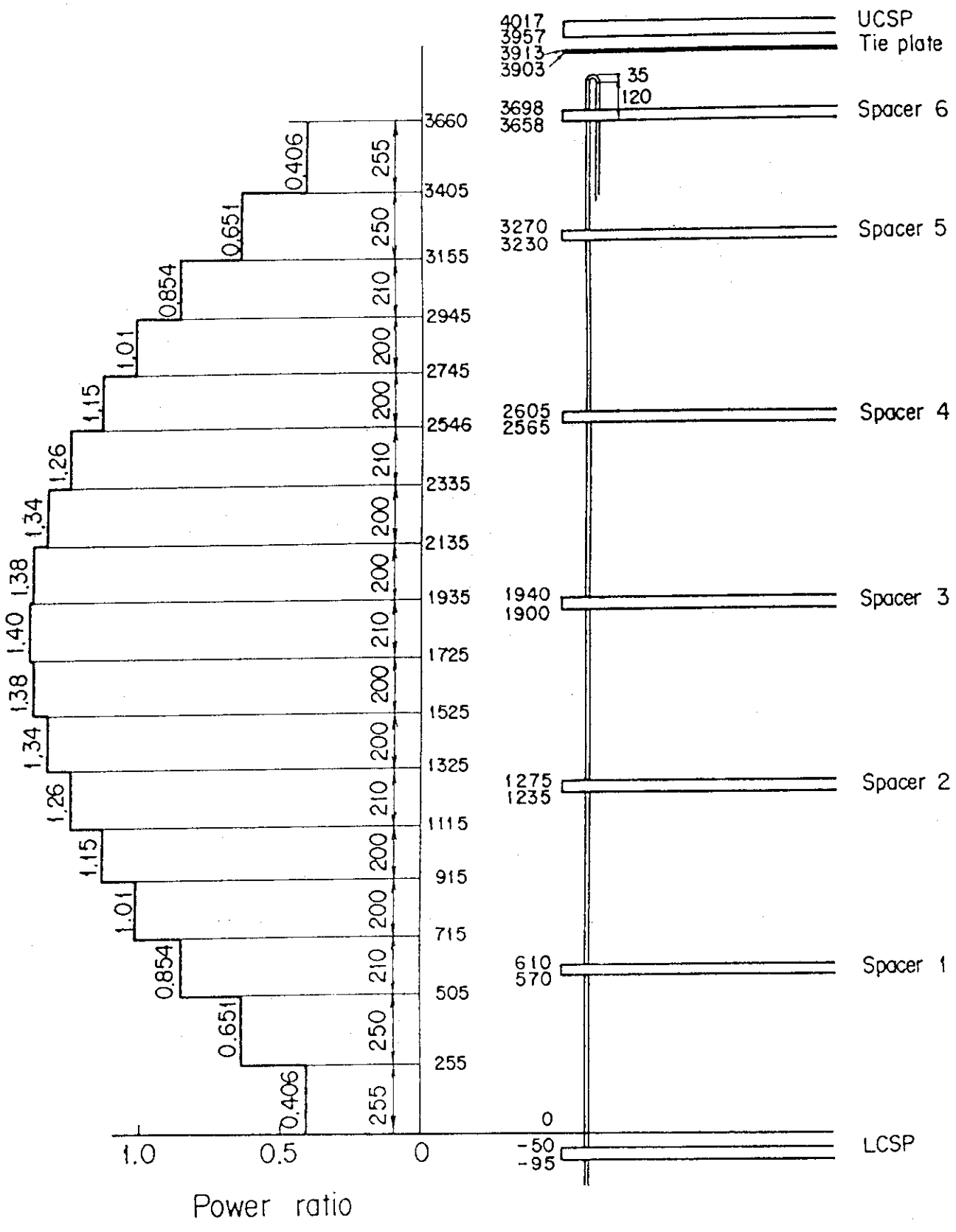

Fig. 2.15 Axial power profile of CCTF Core-II heater rod

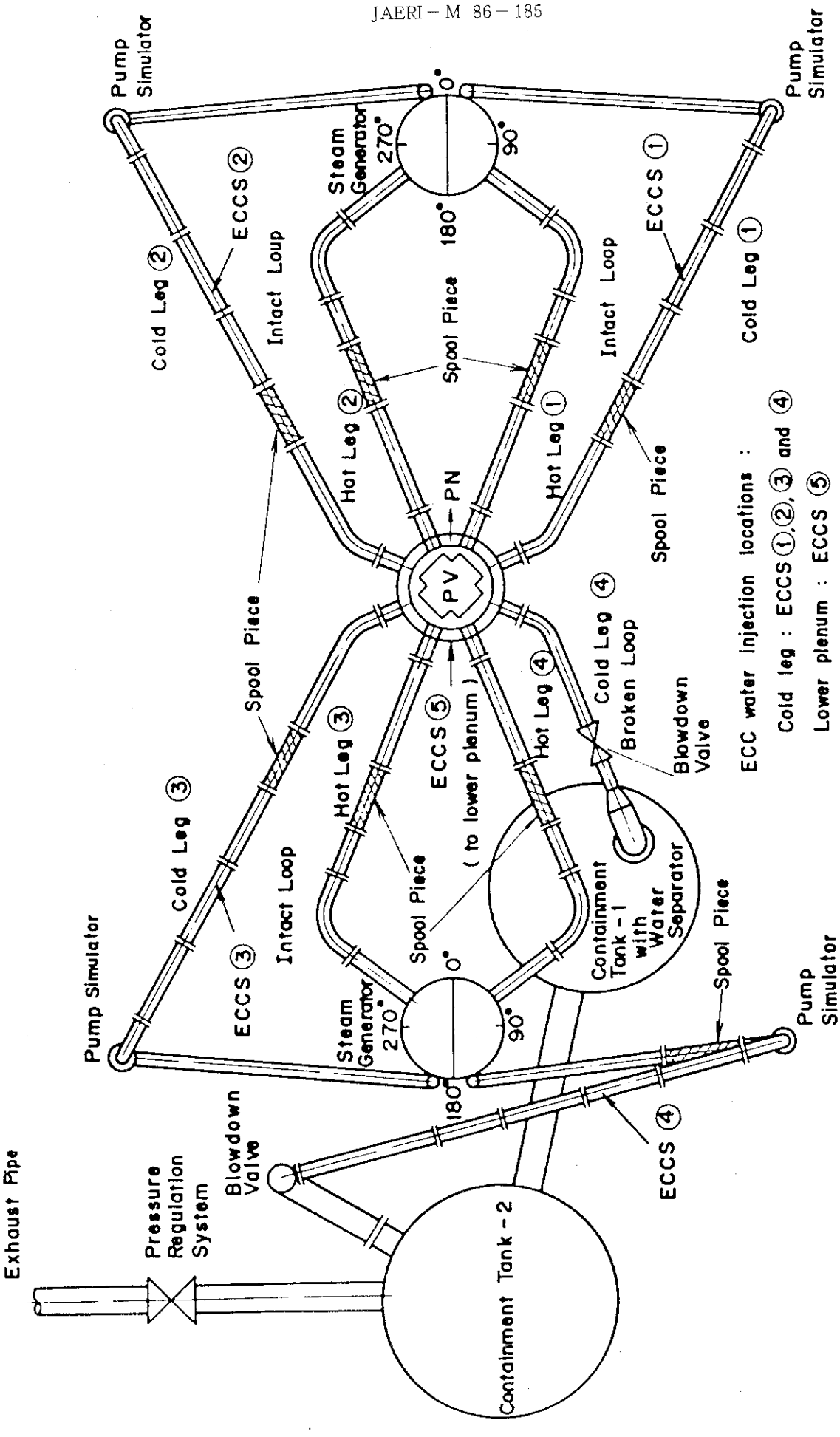

Fig. 2.16 Top view of primary loop pipings

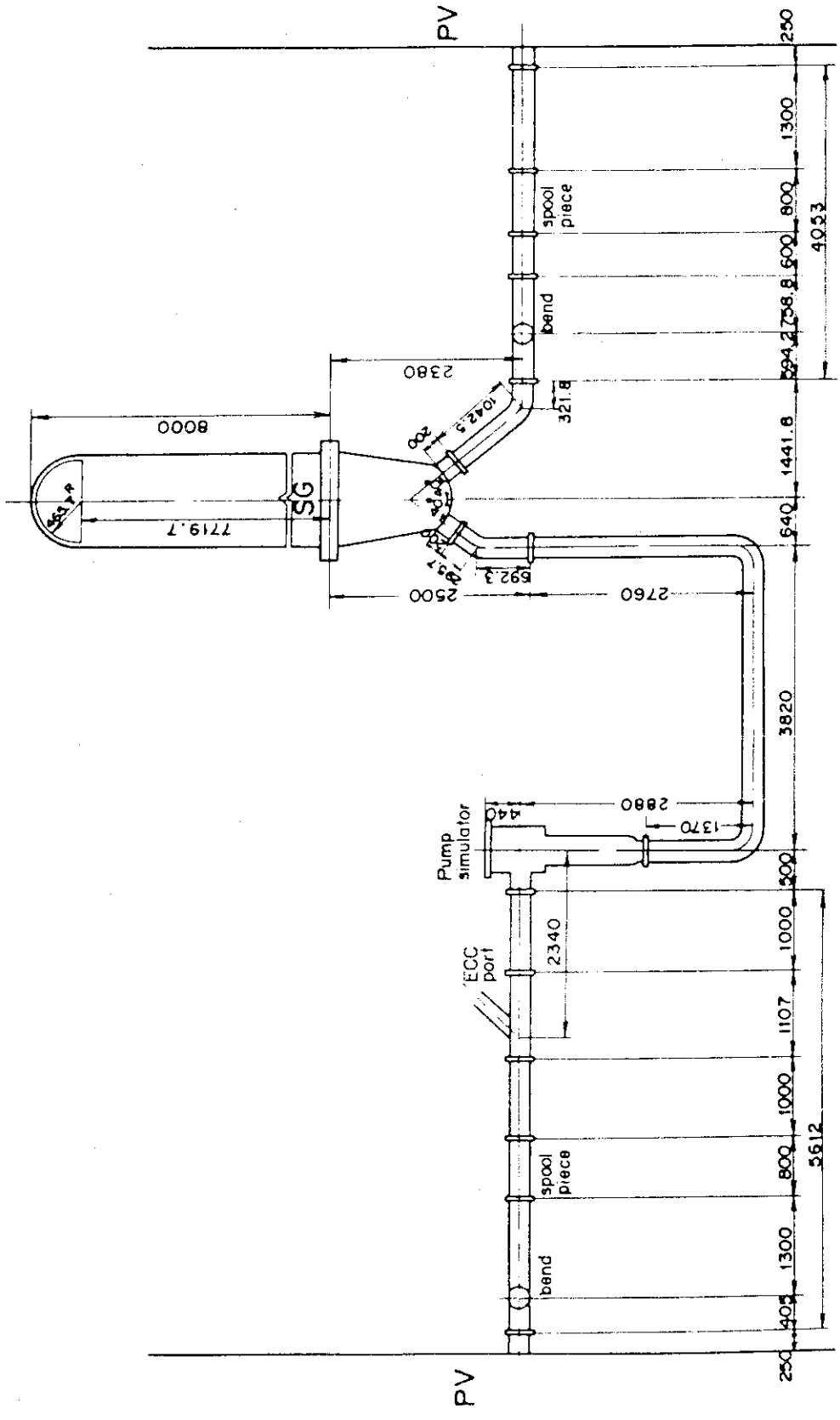

Fig. 2.17 Dimensions of primary loop

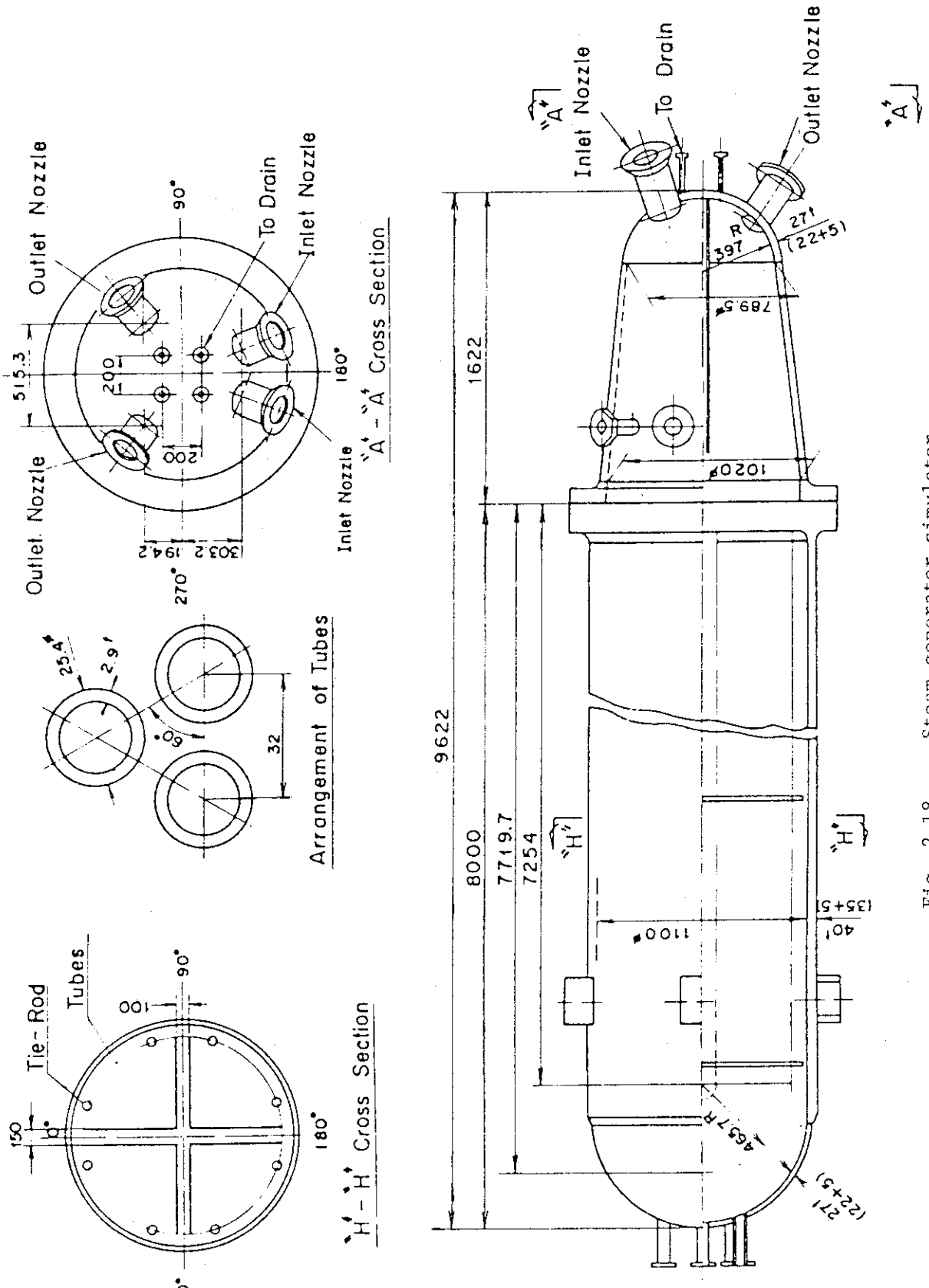

Fig. 2.18 Steam generator simulator

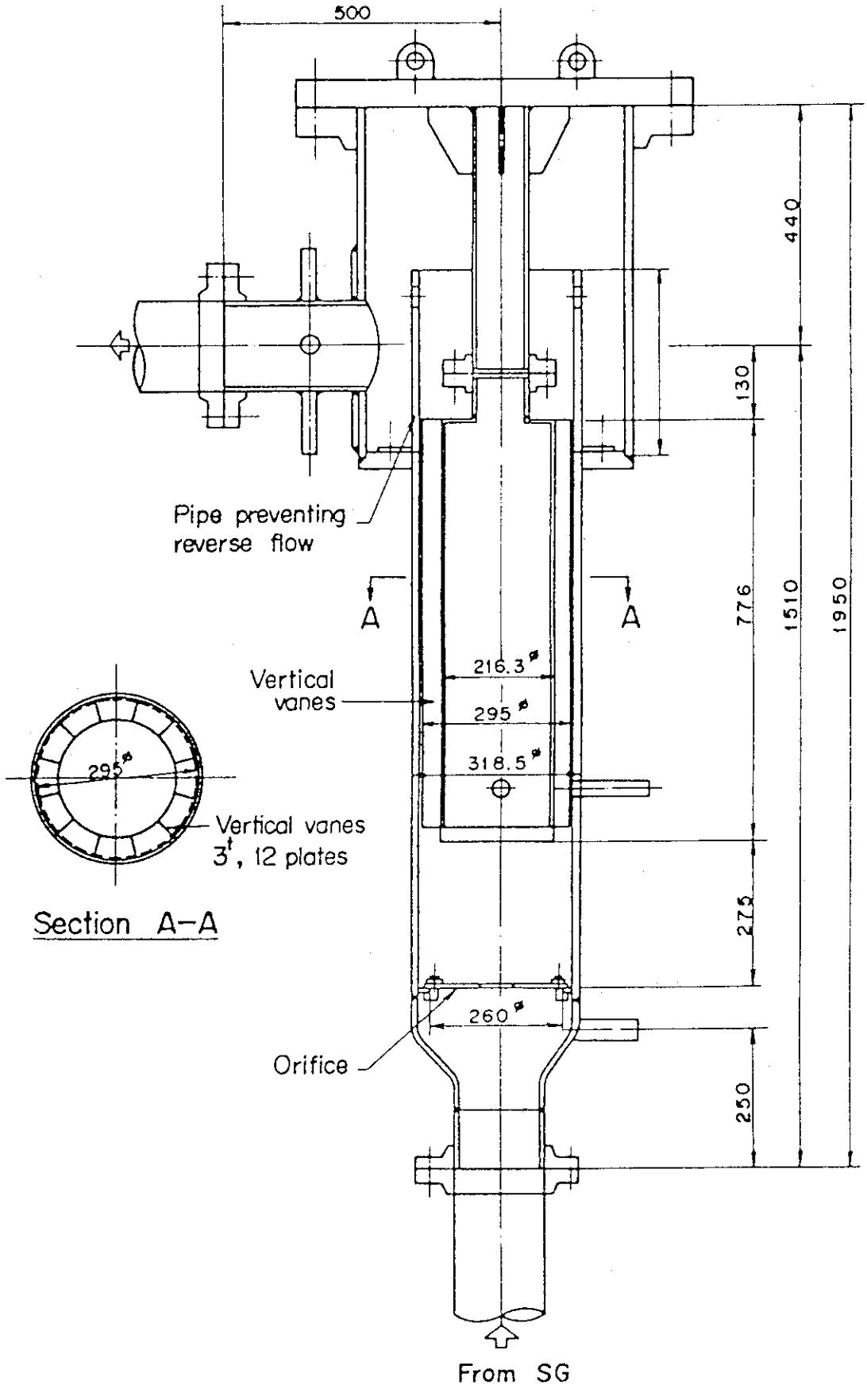

Fig. 2.19 Pump simulator

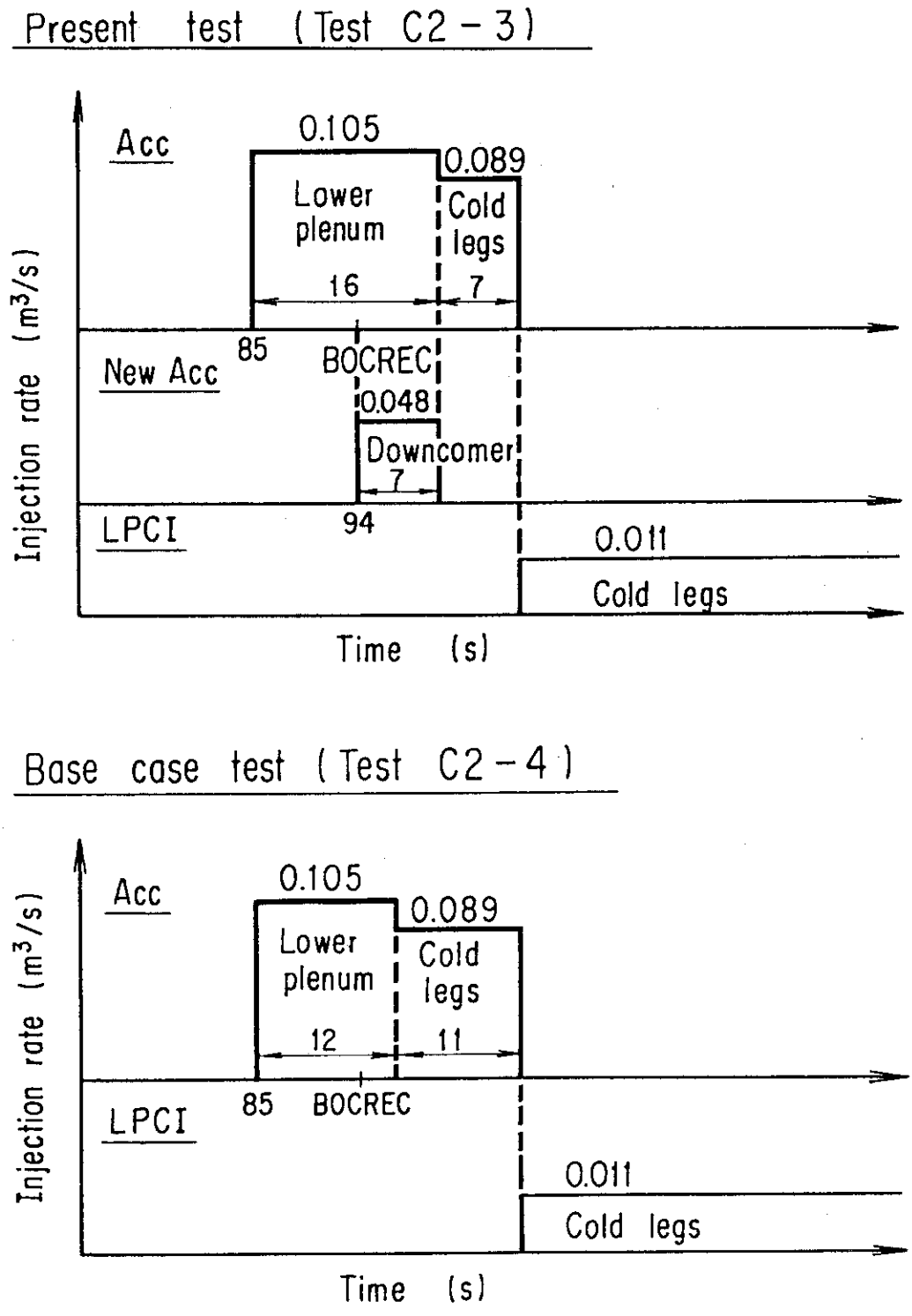

Fig. 2.20 Schematic of ECC water injection sequence

3. Discussion on Initial Downcomer Water Accumulation Velocity

3.1 Investigation of Time of Fill Downcomer

The time to fill the downcomer is about 10 s in the safety evaluation for the reference PWR[5] and is about 8 s in the recent safety evaluation for a Japanese 4-loop PWR[6]. However, in the base case test[4] of the CCTF, it took about 16 s to fill the downcomer as shown in Fig. 3.1 and the average water accumulation velocity is evaluated to be 0.3 m/s.

The main reason for the difference in the time to fill the downcomer between the CCTF test and the safety evaluations is considered to be the larger flow area of the CCTF than the scaled value as mentioned in Section 1. The flow areas of the downcomer, barrel-baffle region and core are compared in Table 3.1 among the reference PWR, CCTF and SCTF. The downcomer flow area of the CCTF is

$$\frac{0.197}{0.115} = 1.71 \tag{1}$$

times larger than the scaled value.

Since the Acc injection rate (from cold legs) in the base case test is set to 0.0892 m^3/s as shown in Fig. 2.20, it is evaluated to take

$$\frac{0.115 \times 4.849}{0.0892} = 6.25 \text{ s} \tag{2}$$

to fill the scaled downcomer. The length of downcomer is 4.849 m as presented in Table 2.1. Until the downcomer is filled, the core and barrel-baffle region are also filled partly. Assuming 0.5 m of the core and barrel-baffle region are filled based on the safety evaluation for the reference PWR[5], it is evaluated to take additionally

$$\frac{(0.247 + 0.082) \times 0.5}{0.0892} = 1.84 \text{ s} \tag{3}$$

Adding this value (3) to the value (2), the total time to fill the scaled downcomer is evaluated to be

$$6.25 + 1.84 = 8.09 \text{ s} \tag{4}$$

and this means the water accumulation velocity is 0.6 m/s. The value (4) is close to the values of safety evaluations presented above. Therefore, in order to simulate the initial water accumualtion velocity in the downcomer of the PWR with the CCTF, the Acc injection rate is suggested to be increased up to

$$1.71 \times 0.0892 = 0.153 \ m^3/s \qquad (5)$$

based on the value (1) to compensate the largeness of the CCTF downcomer.

3.2 Review of CCTF and SCTF Tests Results

Since the measured Acc injection rate was 0.091 m^3/s in the CCTF base case test[4], the time to fill the downcomer is evaluated to be

$$\frac{0.197 \times 4.849}{0.091} = 10.5 \ s \qquad (6)$$

As shown in Fig. 3.1, it took 16 s to fill the downcomer in this test and by this time 0.9 m of the core was filled. Accordingly, it is evaluated to take

$$\frac{0.260 \times 0.9}{0.091} = 2.6 \ s \qquad (7)$$

additionally, and hence, the total time becomes

$$10.5 + 2.6 = 13.1 \ s \qquad (8)$$

This estimated value (8) is larger than that for the scaled PWR, *i.e.* (4), by 5 s and this difference is attributed to the largeness of the CCTF downcomer. However, the value (8) is not equal to and is smaller than the experimental value, *i.e.* 16 s. The reason for this difference will be discussed later.

In the SCTF, the downcomer flow area is simulated almost satisfactory, and hence, the time to fill the downcomer is expected to be almost the same as that for the scaled PWR, *i.e.* value (4). However, it took 17 s to fill the downcomer in Test S1-14 (Run 520)[7] as shown in Fig. 3.2. Since the Acc injection rate in the test was 0.089 m^3/s, the time to fill the downcomer is evaluated to be (the length of downcomer is 4.777 m)

$$\frac{0.121 \times 4.777}{0.089} = 6.5 \ s \qquad (9)$$

and the additional time to fill the core and the barrel-baffle region is evaluated to be

$$\frac{(0.35 + 0.10) \times 1.3}{0.089} = 6.6 \text{ s} \quad (10)$$

assuming 1.3 m of these regions above the bottom of the heated section is filled based on the data shown in Fig. 3.2. Accordingly, the total time is evaluated to be

$$6.5 + 6.6 = 13.1 \text{ s} \quad (11)$$

However, the value (11) is not equal to and is smaller than the experimental value, *i.e.* 17 s, as also observed in the CCTF base case test. The reason for these difference is investigated in the following.

In both the CCTF and SCTF tests, the evaluated times to fill the downcomer were shorter than the experimental values by 3 to 4 s. This difference is attributed to the time delay of the Acc water delivery from the cold leg ECC injection ports to the downcomer due to the water accumulation in the cold leg pipings when the injection location was switched from the lower plenum to the intact cold legs. The flow area and the piping length between the ECC ports and the downcomer are 0.0189 m^2 and 4.022 m, respectively, in the CCTF and 0.0697 m^2 and 3.3 m, respectively, in the SCTF. Therefore, it is evaluated to take

$$3 \times 0.0189 \times 4.022 \times \frac{1}{0.091} = 2.5 \text{ s} \quad (12)$$

and

$$0.0697 \times 3.30 \times \frac{1}{0.089} = 2.6 \text{ s} \quad (13)$$

to fill the cold leg piping for the CCTF and the SCTF, respectively. These values (12) and (13) are close to the difference mentioned above.

The data of the downcomer water level shown in Figs. 3.1 and 3.2 show the decrease in the water accumulation rate between about 6 s to 10 s. This decrease is considered to suggest the water accumulation in the cold leg pipings. The Acc injections into cold legs were initiated at 3 and 4 s for the CCTF and SCTF tests, respectively.

In the CCTF and SCTF tests, the intact cold legs were empty at the initiation of the reflood phase, whereas they are considered to be filled with the ECC water during the LOCA. This difference induced the delay of the Acc water delivery of about 3 s in the CCTF and SCTF tests.

Therefore, in order to simulate the initial downcomer water accumulation rate correctly with the CCTF, this delay should be prevented from occurring.

3.3 Determination of ECC Water Injection Sequence

Based on the investigation presented in Section 3.1, the Acc injection rate was determined to be 0.153 m^3/s (see (5)). In order to eliminate the delay of the ECC water described in Section 3.2, this injection was determined to be conducted with the downcomer injection line as well as the lower plenum injection line because the maximum injection rate for the lower plenum injection line is about 0.1 m^3/s.

The duration of this injection (0.153 m^3/s) was determined to be 7 s and is shorter than the evaluated value of 8 s (see (4)), taking account that the injection rate does not decrease to zero momentarily.

The temperature of the ECC water of the lower plenum injection was determined to be 308 K, which is the same as in the base case test. The temperature of the ECC water of the downcomer injection was determined to be 393 K, *i.e.* the saturation temperature for 0.2 MPa, to prevent the unrealistic condensation, which is expected to occur when the subcooled ECC water is injected at the top of the downcomer in the very initiation period of the reflood phase. This saturation temperature was also expected to reduce the excess subcooling of the ECC water injected from the lower plenum. During the LOCA, the ECC water injected into the cold legs are considered to be heated up to some extent due to the condensation of the steam flowing there and the heat release from the structure, and hence, the water temperature of the ECC water flowing into the downcomer is expected to be higher than that at the time of injection into cold legs.

There are two downcomer injection ports in the CCTF as shown in Figs. 2.3 and 2.6. In the present test, only one of them, which is located at the opposite side of the broken loop, was determined to be used.

Table 3.1 Comparison of flow areas

	Reference PWR		CCTF	SCTF
	Actual	Scaled		
Downcomer	2.47	0.115	0.197	0.121
Barrel-baffle region	1.76	0.082	———	0.100
Core	5.29	0.247	0.250 (0.260)*	0.259 (0.350)*

Note: (1) Unit is m^2.

(2) Scaling ratio is 1 : 21.44.

(3) Value with symbol * was obtained by measured water filling curve (level vs. volume).

(4) Length of downcomer is 4.849 m, but 4.777 m in SCTF (bottom is defined to be the same as that of core).

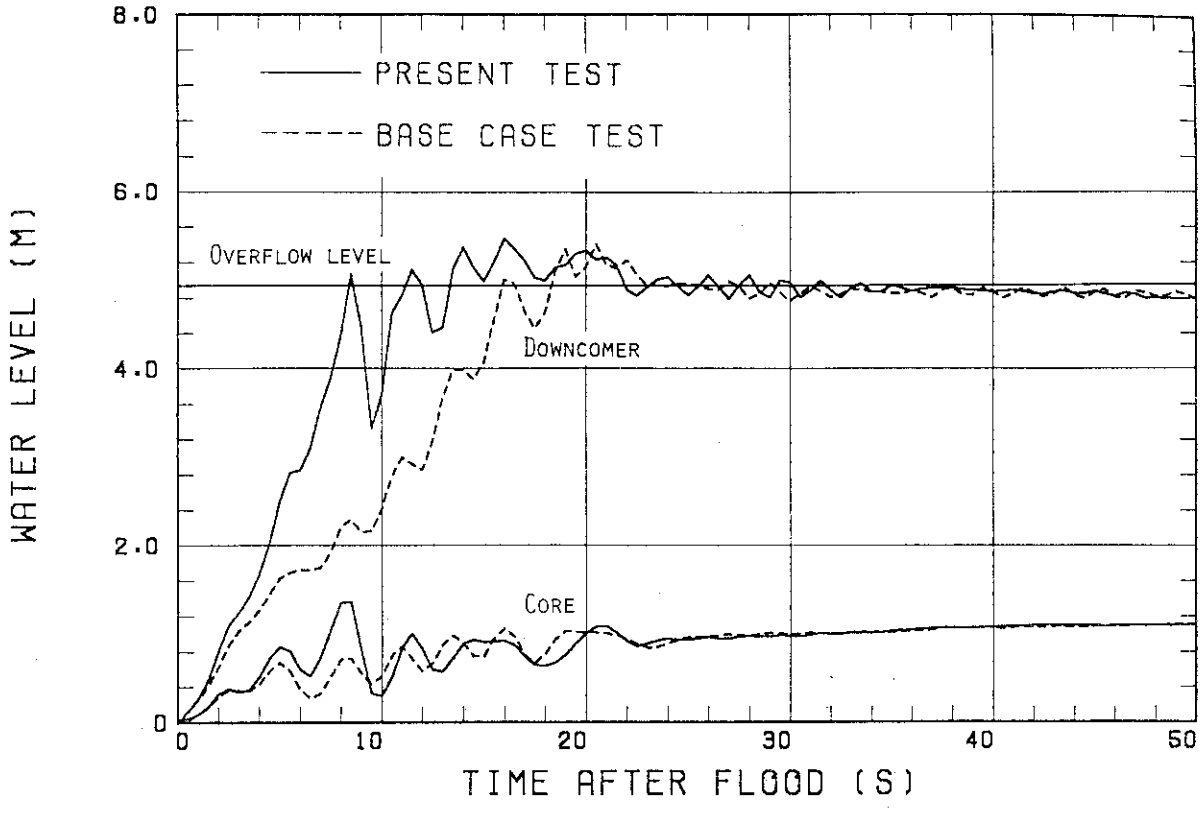

Fig. 3.1 Downcomer and core water level of CCTF tests

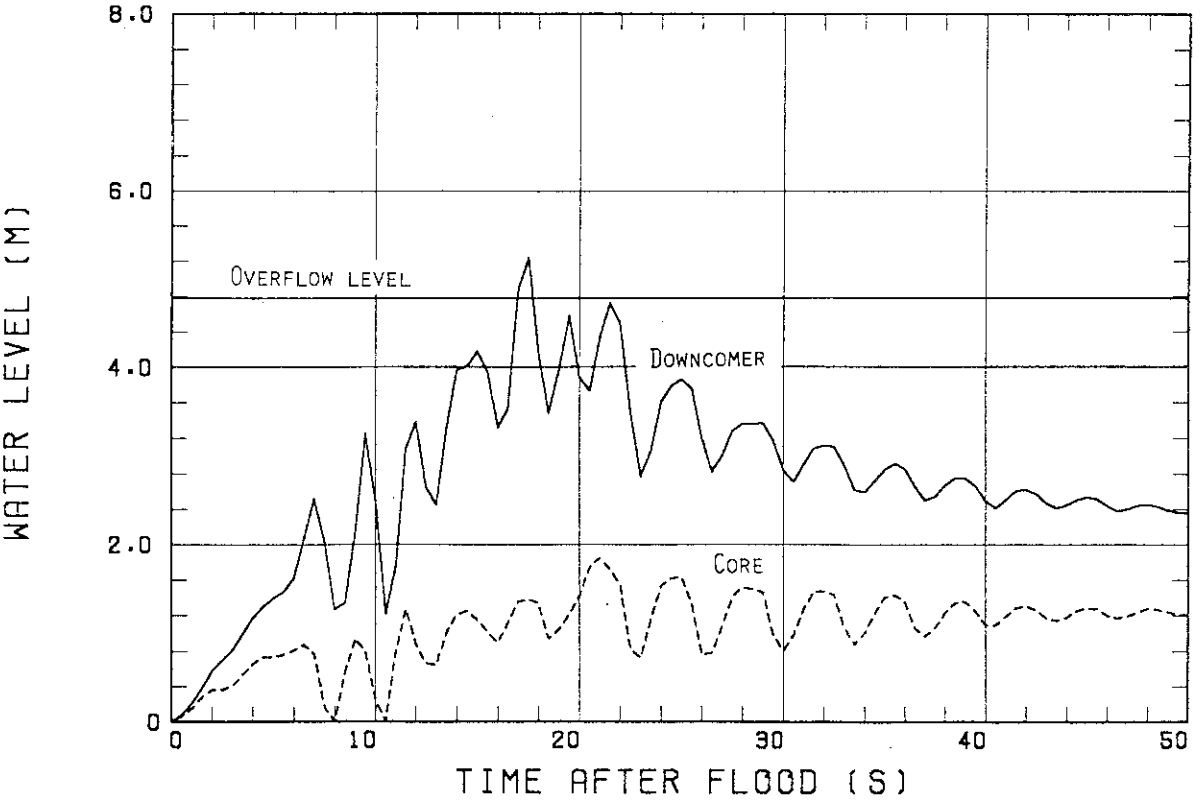

Fig. 3.2 Downcomer and core water level of SCTF Test S1-14

4. Results and Discussion

4.1 System Behavior

4.1.1 Downcomer Differential Pressure

The downcomer differential pressure of the present test is compared with that of the base case test in Fig. 4.1. In order to see the data in the initial period in detail, the data plots for the time period of 0 to 100 s are presented in Fig. 4.2. This figure shows that the water accumulation in the downcomer is much rapider in the present test. Although the time to fill the downcomer is 16 s in the base case test, it is 8 s in the present test and the corresponding water accumulation velocity is evaluated to be 0.6 m/s. That value is almost the same as the estimated value (4) in Section 3.1, and hence, the water accumulation in the downcomer of the present test is considered to simulate the situation in a PWR well.

Figure 4.2 also shows that the oscillation of the downcomer differential pressure of the present test in the initial period is larger in the amplitude. This result is reasonable because the rapider water accumulation in the downcomer is expected to cause the larger U-tube type oscillation due to the higher core flooding rate in the initial period. Figure 4.3(a) shows the comparison of the core flooding rates, which were obtained by the mass balance calculation, and supports above discussion indicating the evaluated core flooding rate is higher in the initial period in the present test than in the base case test. The period of the U-tube type oscillation is about 3 s for both tests.

The important points Fig. 4.2 shows are that the differential pressures are almost identical after 20 to about 90 s and the U-tube type oscillations become very small after 30 s in both tests. These results suggest that the difference in the downcomer water accumulation velocity causes the difference in the downcomer differential pressure only in the very initial period and within a short time (about 25 s for those two tests) after the downcomer is filled the difference becomes unnoticeable.

Although Fig. 4.1 shows some difference in the downcomer differential pressure from 90 to 310 s, this difference is considered not to be attributed to the difference in the water accumulation velocity in the initial period but to the other phenomena described in the following

because the differential pressures for both the tests are almost identical from 20 to 90 s. The decreases in the downcomer differential pressure after about 20 s in Fig. 4.1 are considered to be caused by the boiling of the downcomer water due to the heat release of the downcomer outside wall[8], which was superheated initially, as well as the bypass of the water to the break due to the steam flow from the intact cold legs.

According to the results presented in reference 8, the smaller downcomer water subcooling tends to result in the rapider decrease in the downcomer differential pressure. This explains the rapider decrease in the downcomer differential pressure for the present test because the fluid temperatures in the downcomer were generally higher before 100 s in the present test as shown in Figs. 4.4(a) through (d).

The water mass flow rates bypassing the downcomer to the break are compared in Fig. 4.5. They were obtained from the liquid level data in the containment tank 1 shown in Fig. 4.6 by performing time differentiation. Figure 4.5 indicates that the bypass becomes small after 120 to 180 s in the present test and this seems to be the reason for increasing in the downcomer differential pressure in that period shown in Fig. 4.1. The decrease of water bypass above seems to be caused by the increase of containment tank pressure shown later in Fig. 4.14.

4.1.2 Core and Upper Plenum Differential Pressures

The core differential pressures are compared in Figs. 4.7 and 4.8. In the initial period before 12 s, the core differential pressure is larger in the present test on the average as shown in Fig. 4.8. Also, in this period, the U-tube type oscillation is larger in the magnitude for the present test and this is the same tendency as observed for the downcomer differential pressure. The periods of the oscillation are almost identical between those two tests.

From about 150 to 280 s, the core differential pressure for the present test is larger than in the base case test (Fig. 4.7). This difference is mainly caused by the difference in the section between 0.61 and 1.22 m elevations as shown in Figs. 4.9(a) through (f). The reason for this difference has not been clarified yet. As described in Section 4.1.1, the downcomer differential pressure for the present test is also larger for almost the same time period (Fig. 4.1). The evaluated core flooding rates are, however, almost identical on the average during that

period as shown in Fig. 4.3. Figure 4.3(b) shows the time-integrals of core flooding rates.

As recognized from Figs. 4.9(c) through (f), there is the same trend in the comparisons of differential pressures in the sections above 1.22 m elevation. That is, the data for the present test are slightly smaller from 25 to 85 s, whereas they are slightly larger from 150 to 280 s. Although the reason for this trend has not been clarified yet, this trend seems to influence the core cooling as described in Section 4.2 later.

The upper plenum differential pressures are compared in Fig. 4.10. In general, they are almost identical as also observed for the differential pressures in the core (Figs. 4.9(c) through (f)). In detail, the data for the present test become slightly smaller after 25 s but become slightly larger by 220 s. This trend is similar to that observed for the core differential pressured described above.

4.1.3 Thermo-hydrodynamic Behaviors in Other Parts of Primary System

The intact loop differential pressures are compared in Figs. 4.11 and 4.12. The latter is the detailed plot to investigate the behavior in the initial period. This figure shows that the differential pressure for the present test increases much rapider than for the base case test. It takes only 8 s to reach the maximum value in the present test, whereas 16 s in the base case test. These timings are the same as those for filling the downcomer (Section 4.1.1). Therefore, it is found that the intact loop differential pressure, which represents the steam binding, also increases rapidly corresponding to the rapid increase in the downcomer differential pressure.

The downcomer differential pressure acts as the driving force for core flooding and the core and intact loop differential pressures act as the negative feed-back for it[3]. Therefore, the rapider increase in the downcomer differential pressure for the present test is expected to induce the higher core flooding rate in the very initial period, but soon after that the rapider increases in the core and intact loop differential pressures are expected to reduce the core flooding rate achieving the balance with the downcomer differential pressure[3]. Figure 4.3(a) supports this discussion. Therefore, the discussion presented in reference 3 is confirmed to be valid even in the much higher Acc injection rate case than concerned in the reference.

Figure 4.3(a) shows an interesting phenomenon. That is, the evaluated core flooding rate for the present test is lower between 7.5 and 20 s than for the base case test. This is explained as in the following. In the present test the downcomer differential pressure increased rapidly and so did the intact loop and core differential pressures. Since the downcomer differential pressure reached the overflow level value in a short time and could not increase any more, the driving force for core flooding became small soon. On the other hand, in the base case test, the downcomer differential pressure increased more slowly than in the present test and so did the intact loop and core differential pressures. Therefore, the decrease in the core flooding rate was slower, and hence, the core flooding rate between 7.5 and 20 s became higher than that for the present test.

At 20 s, the downcomer differential pressures become almost identical. At 90 s, they start to differ from each other. However, the average values are almost identical in the two tests. Comparing Fig. 4.11 with Fig. 4.1, the tendency for the behavior of the intact loop differential pressures can be recognized to be the same as that of the downcomer differential pressures.

Figure 4.13 shows the broken loop differential pressures. At about 115 and 420 s, the data for the present test decreases significantly. These decreases seem to be caused by the increases in the containment tank pressure shown in Fig. 4.14. These are caused by the trouble of the pressure regulation system in the present test. The upper plenum pressures are compared in Fig. 4.15. In the initial period, the value for the present test is significantly larger than for the base case test. This seems to be caused by the larger steam generation in the present test due to its higher core flooding rate in the initial period.

The fluid temperatures and subcoolings at the core inlet are compared in Figs. 4.16 and 4.17, respectively. Although there are some differences between the two tests, the magnitude of differences are 10 K at most. These differences seem to be caused by the difference in the amount of the subcooled Acc water injected into the lower plenum. The amount of the Acc water injected into the lower plenum was about 30 percent larger in the present test than in the base case test and this difference seems to cause the fluid temperature in the lower plenum to be lower in the present test, although the saturated water was injected

into the downcomer. Figure 4.18 shows the fluid temperatures in the lower plenum and these data support the discussion above.

The lower fluid temperature in the present test due to the larger amount of the subcooled Acc water injected is also observed in the downcomer at 2.423 m elevation as shown in Fig. 4.4(a). In this figure, however, the fluid temperature becomes higher than in the base case test after 20 till 110 s. This increase is attributed to the saturated Acc water injected into the top of the downcomer (6.9494 m) in the present test and the higher downcomer fluid temperatures presented in Figs. 4.4(b) through (d) are also caused by this saturated Acc water.

4.2 Core Cooling Behavior

Quench envelopes are compared in Fig. 4.19. It is the comparison of the average quench times of each power region. Figures 4.20(a) and (b) show the mean values (lines) and standard deviations (symbols) for the present test and the base case test, respectively. Figure 4.19 indicates that although, in detail, the quench time of the present test is slightly shorter, the quench times are almost identical in both tests.

Figures 4.21(a) through (c) show the rod surface temperatures at four elevations in A, B and C regions, respectively. The rod surface temperatures for the present test are not higher than those of the base case test at 1.015 and 1.83 m elevations in every power region. On the other hand, at 2.44 and 3.05 m elevations, the temperatures for the present test are slightly higher than for the base case test before they turnaround, and then become slightly lower after they turnaround. Figure 4.22 shows the rod surface temperatures at the upper part of the core above 3 m elevation in A region. These data indicate the same tendency as observed at 2.44 m elevation. However, these differences in the rod surface temperatures are relatively small, and hence, they can be said to be almost identical.

Figure 4.23 shows the comparison of the heat transfer coefficient at four elevations in the higher power region, corresponding to Fig. 4.21(a). Comparing these data with the core differential pressure data, it is recognized that a consistent relation exists between them. In order to confirm this, the heat transfer coefficients at 2.44 m elevation and the core differential pressures in the section between 1.83 and 2.44 m elevations are compared in Fig. 4.24. When the core differential

pressure for the present test is larger than for the base case test, the heat transfer coefficient for the present test is also larger, and vice versa. However, the differences in the heat transfer coefficient between the two tests are relatively small, and hence, they can be said to be almost identical.

4.3 Investigation of Effects of Initial Downcomer Water Accumulation Velocity on Reflooding Behavior

The higher downcomer water accumulation velocity during the initial period in the present test shown in Fig. 4.2 is considered to result in the higher core flooding rate in the initial period as shown in Fig. 4.3(a). The U-tube type oscillation between the core and the downcomer was larger in the magnitude during the initial period and the thermo-hydrodynamic behaviors in the primary system also showed the larger oscillation during the initial period in the present test.

The evaluated core flooding rate, however, started to decrease earlier and became smaller than in the base case test at 7.5 s (Fig. 4.3(a)). This decrease in the core flooding rate is considered to result from the rapid increases in the intact loop and core differential pressures (Figs. 4.12 and 4.8, respectively), because they tend to reduce the core flooding rate. That is, the downcomer differential pressure acts as the driving force for core flooding, whereas the intact loop, core and upper plenum differential pressures act as the negative feed-back for it[3]. The contribution of the upper plenum differential pressure is usually much smaller than the others.

The results of the present test indicate that when the downcomer differential pressure increases rapidly, the intact loop differential pressure and the core differential pressure also increase rapidly, and hence, reduce the core flooding rate rapidly. The important point is the intact loop differential pressure, which represents the steam binding effects, increases rapidly being able to follow promptly the increase in the downcomer differential pressure. By this reason, the core flooding rate for the present test is considered to become almost identical to that for the base case test by 20 s.

After 20 s, the thermo-hydrodynamic behaviors in the primary system were almost identical as shown in the previous sections. Also, the oscillations became small by 30 s. Therefore, the effects of the

initial downcomer water accumulation velocity was unnoticeable after about 30 s.

The core cooling behavior was observed to be almost identical in both tests through the whole transient including the initial period. Therefore, the effects of the initial downcomer water accumulation velocity on the core cooling was not observed between those two tests. The reason for this is as follows. Although the difference in the core flooding rate was observed in the initial period, the duration when the core flooding rates differed was very short, *i.e.* 20 s. Furthermore, from 0 to 7.5 s, the core flooding rate for the present test was larger, whereas from 7.5 to 20 s that for the present test was smaller which seems to cancel the difference from 0 to 7.5 s.

Therefore, it is concluded that although the downcomer flow area of the CCTF is larger than the scaled value of the reference PWR, this difference does not make any significant difference in the reflooding behavior, and hence, with respect to this point there is no problem for applying the CCTF test results to the PWR analyses.

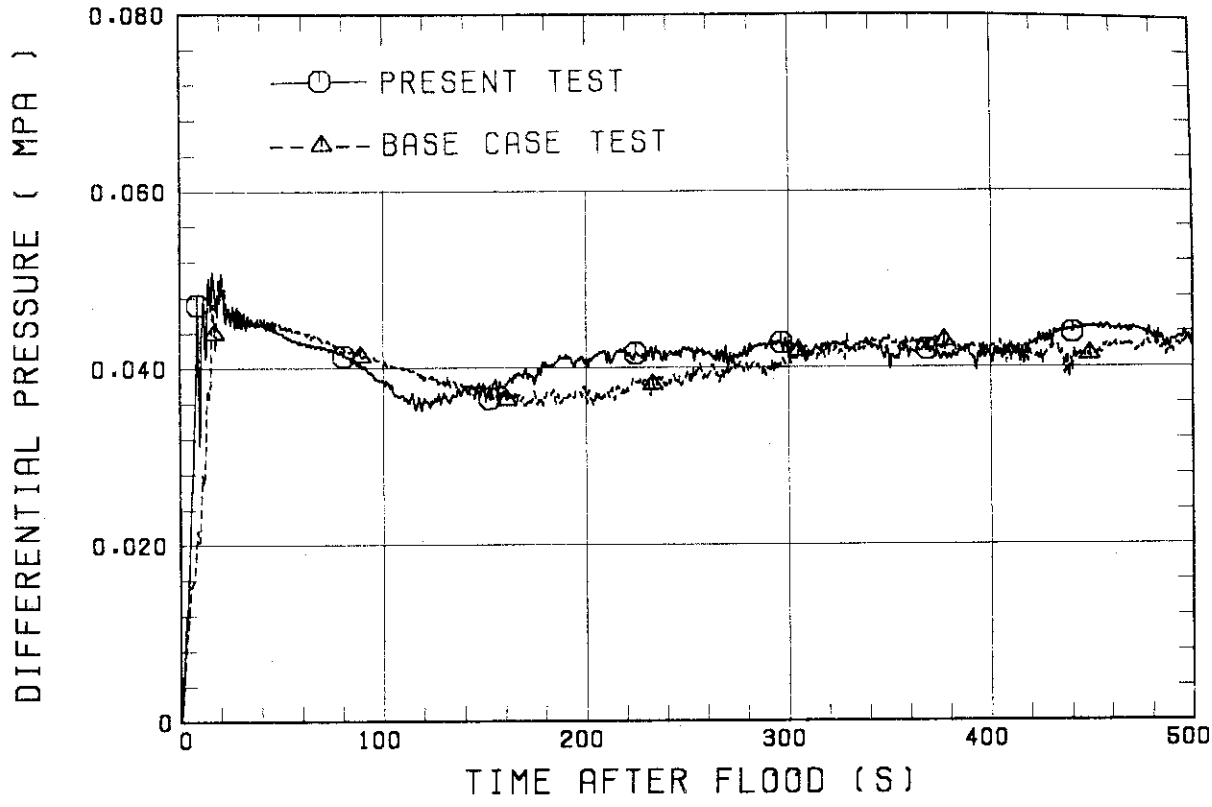

Fig. 4.1 Downcomer differential pressures

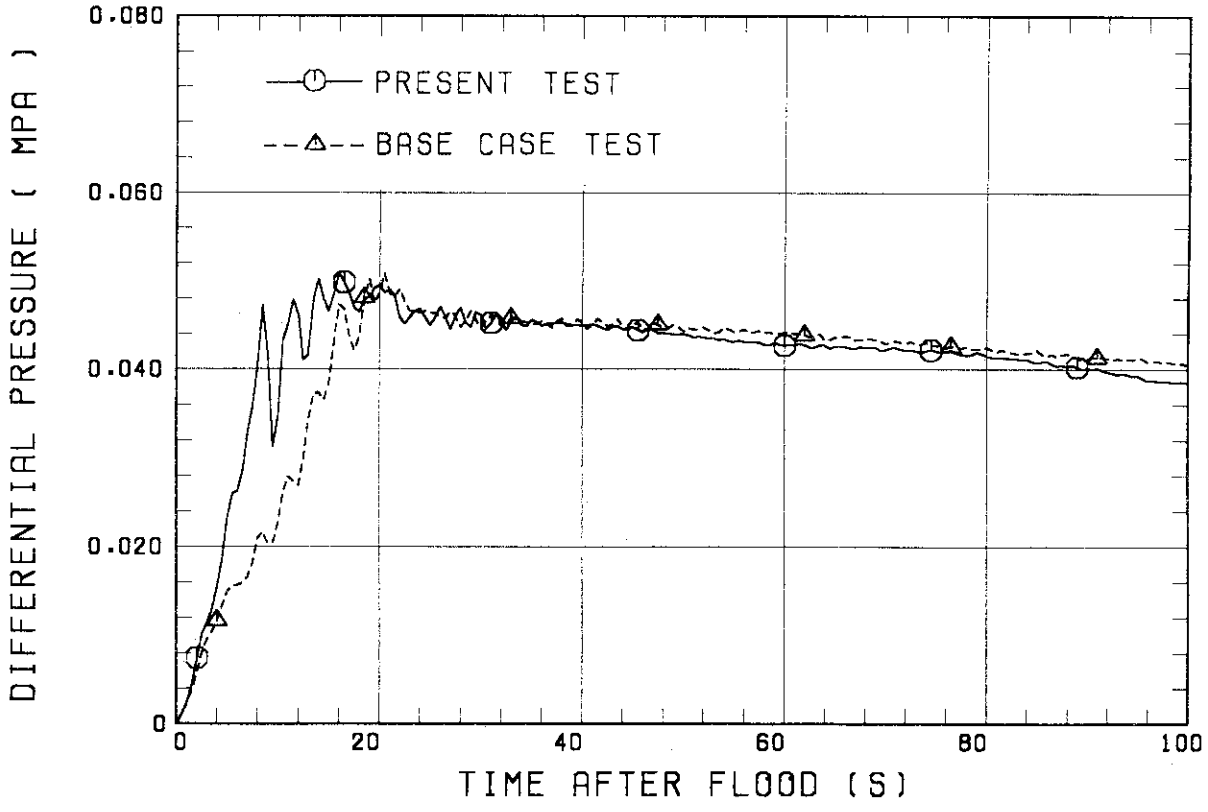

Fig. 4.2 Downcomer differential pressures (0 - 100 s)

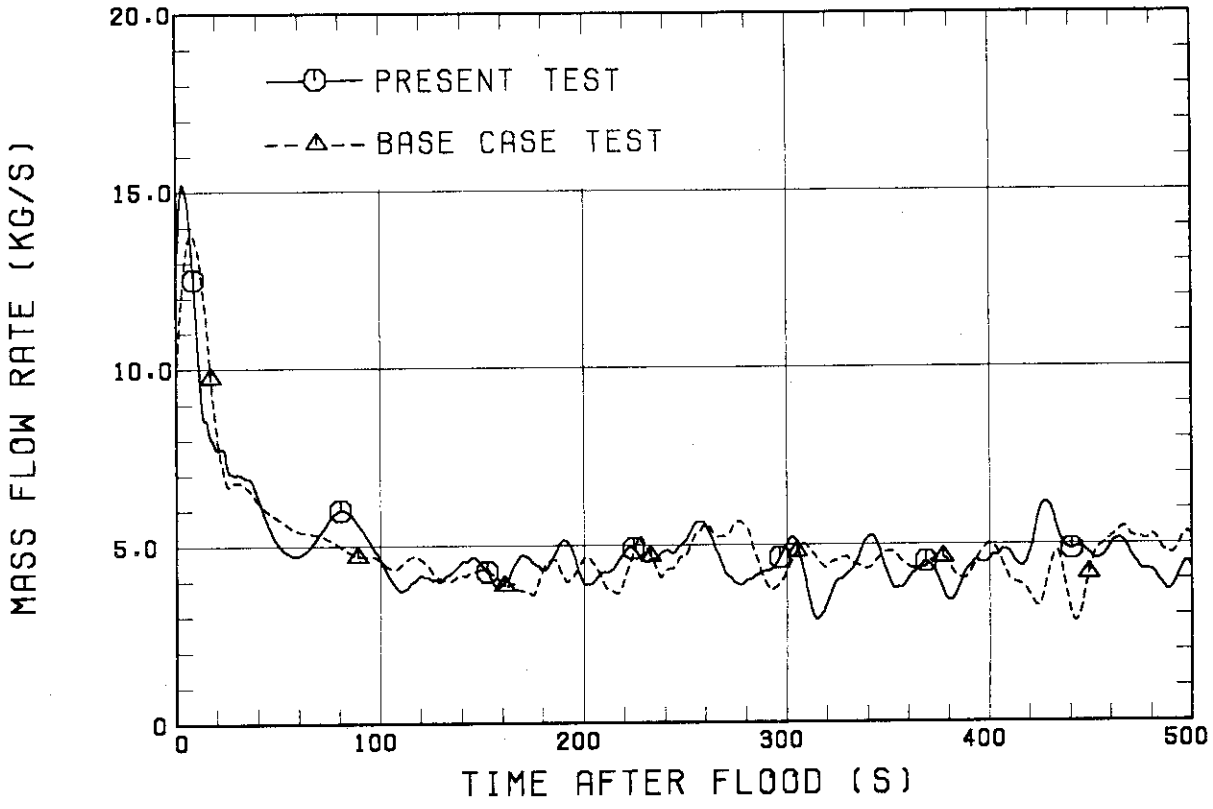

Fig. 4.3(a) Core flooding rates

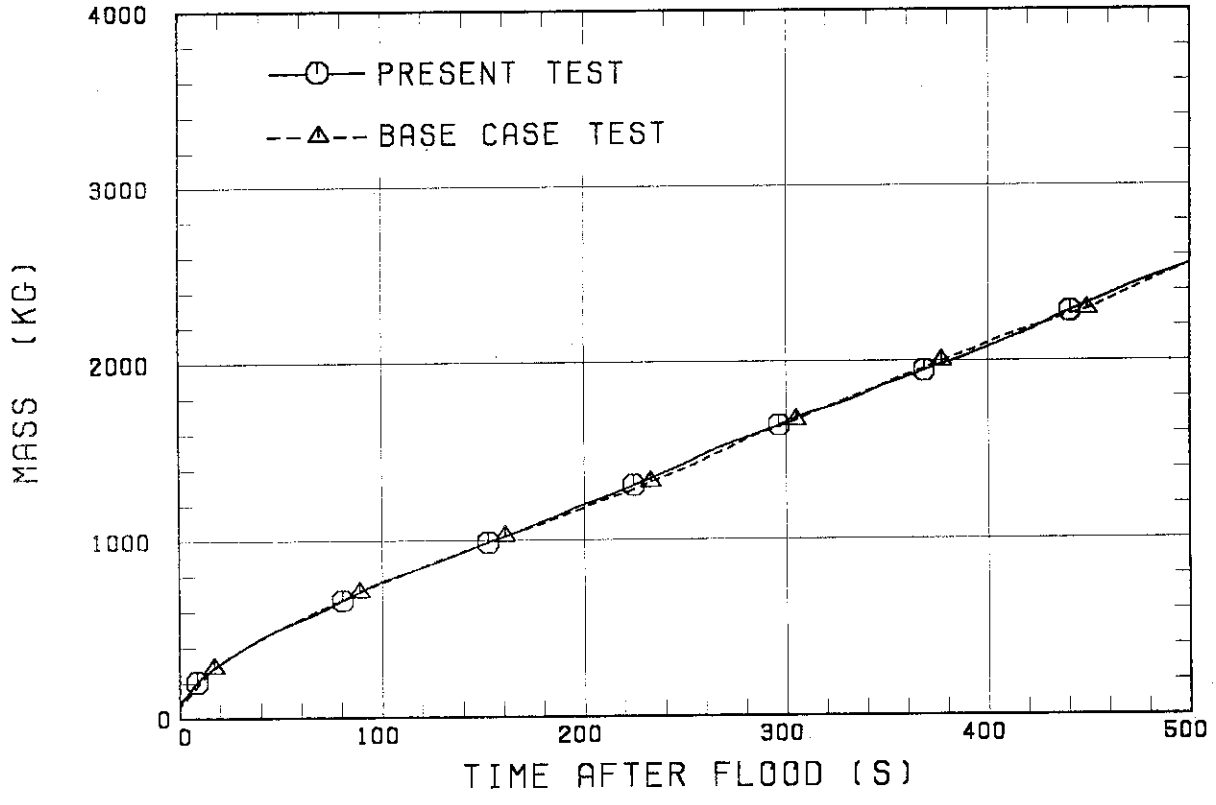

Fig. 4.3(b) Time-integrations of core flooding rate

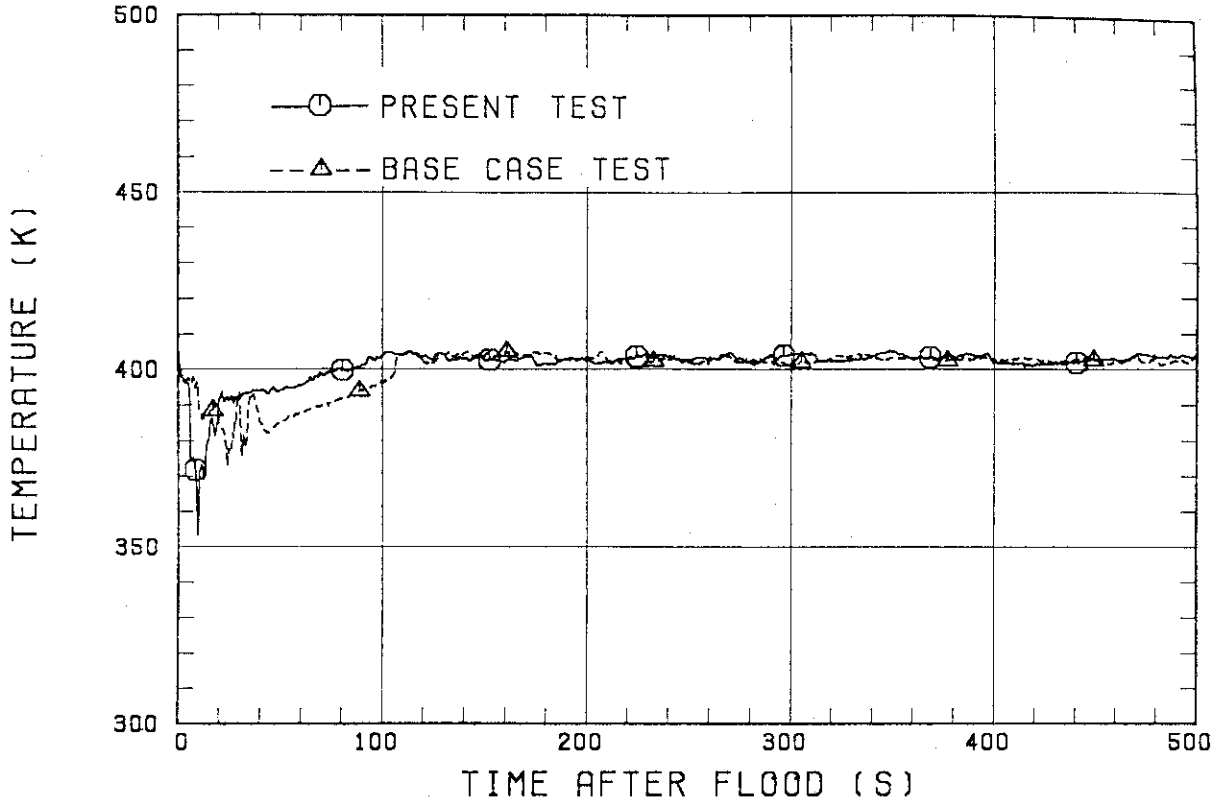

Fig. 4.4(a) Downcomer fluid temperatures at 2.423 m

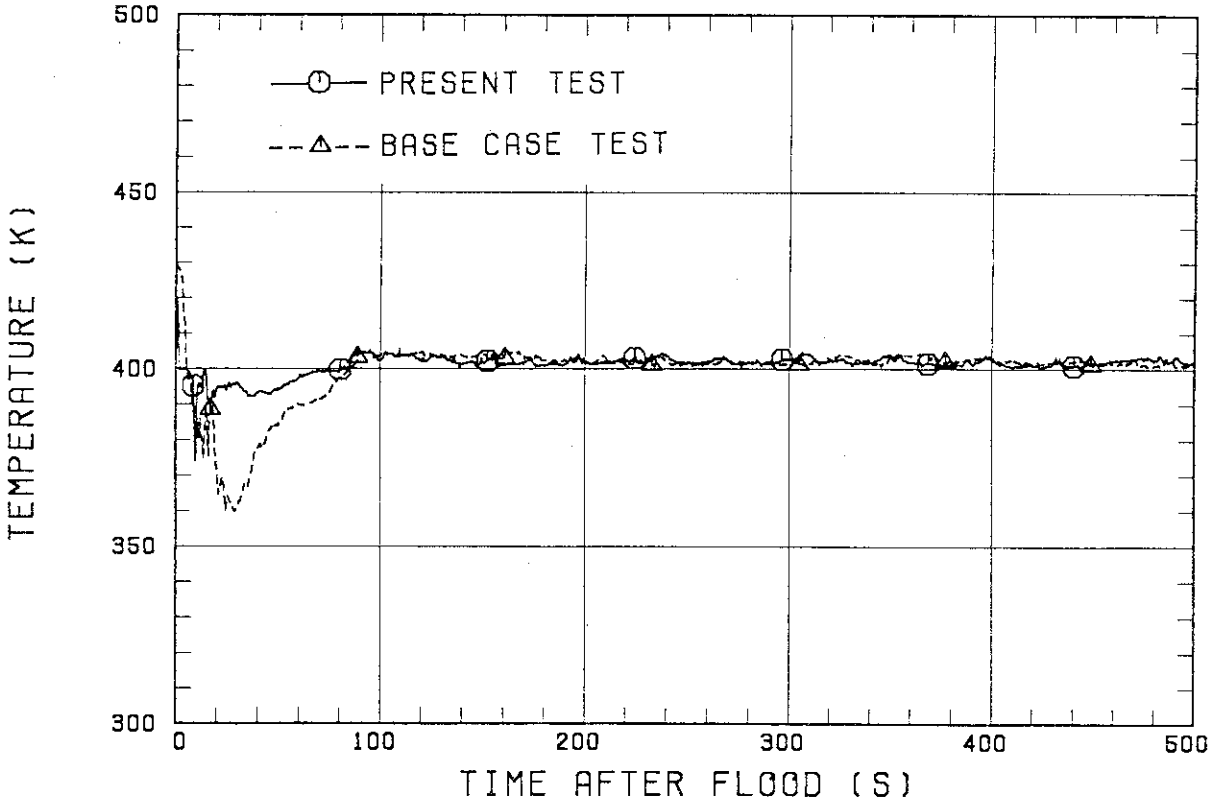

Fig. 4.4(b) Downcomer fluid temperatures at 3.863 m

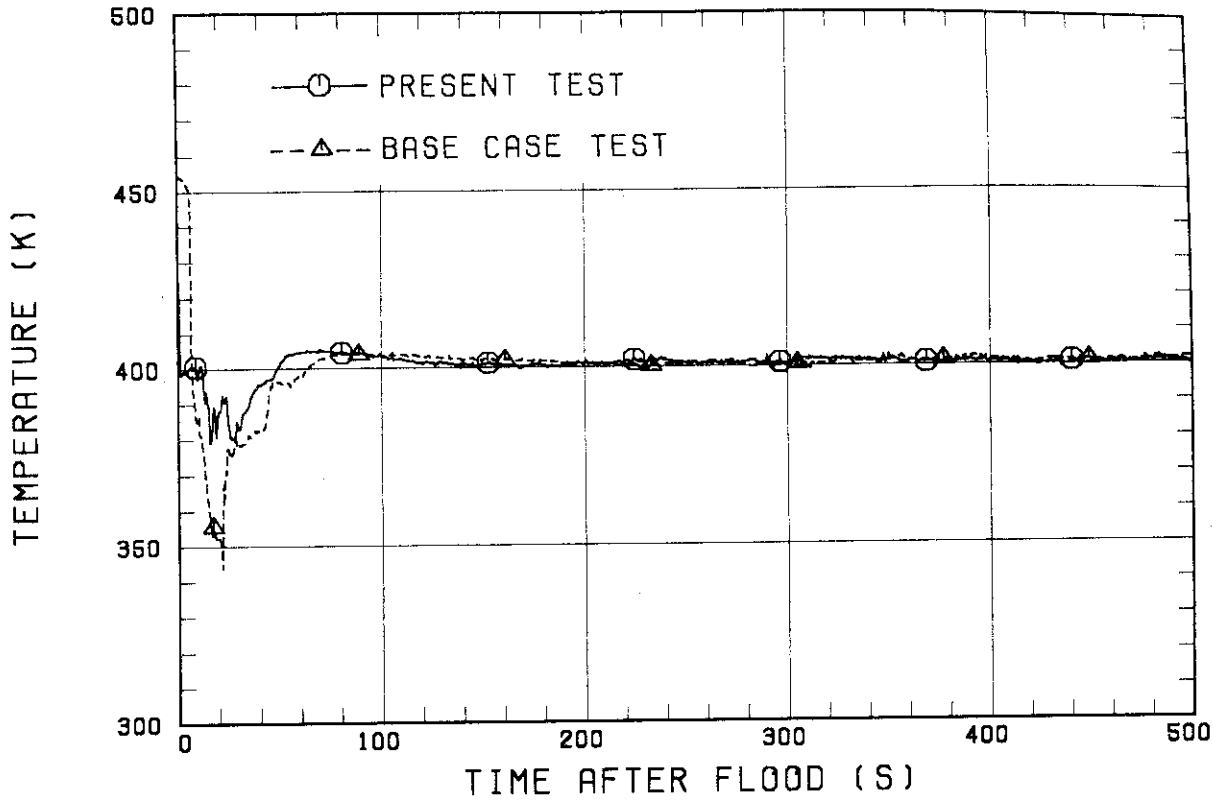

Fig. 4.4(c) Downcomer fluid temperatures at 5.303 m

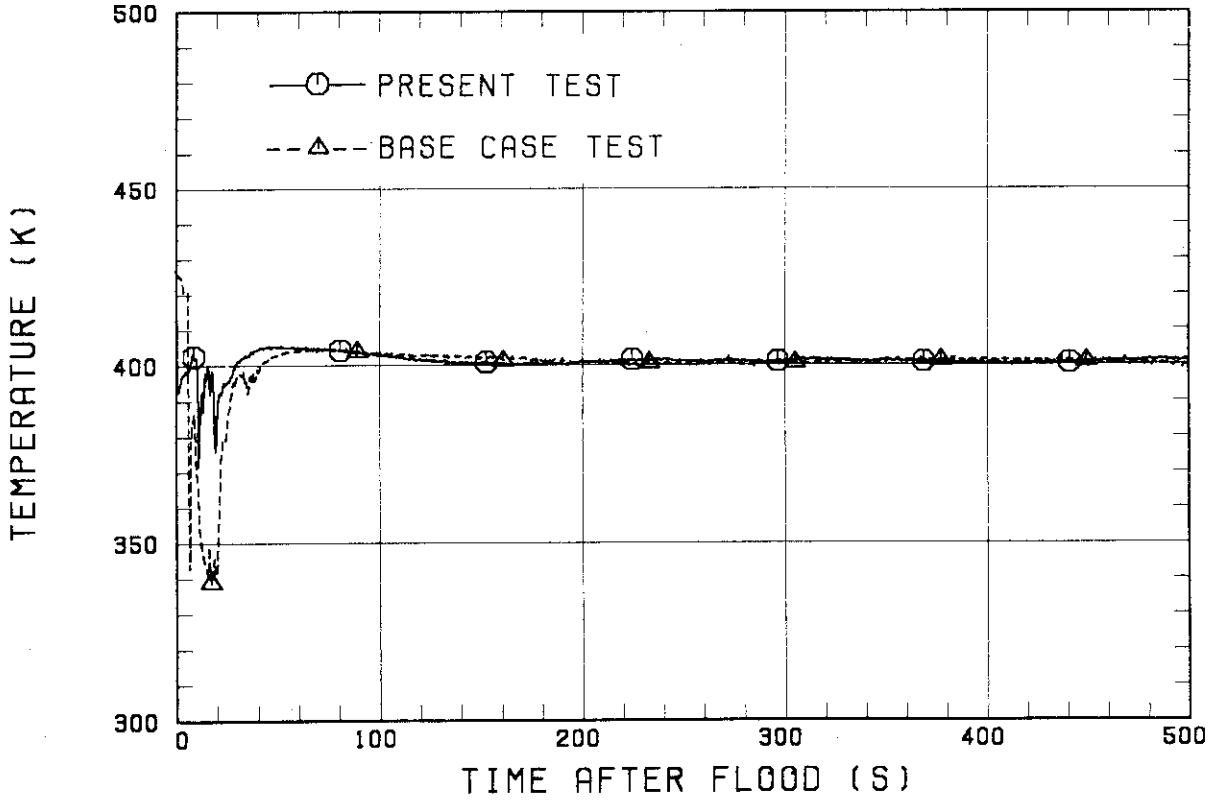

Fig. 4.4(d) Downcomer fluid temperatures at 6.743 m

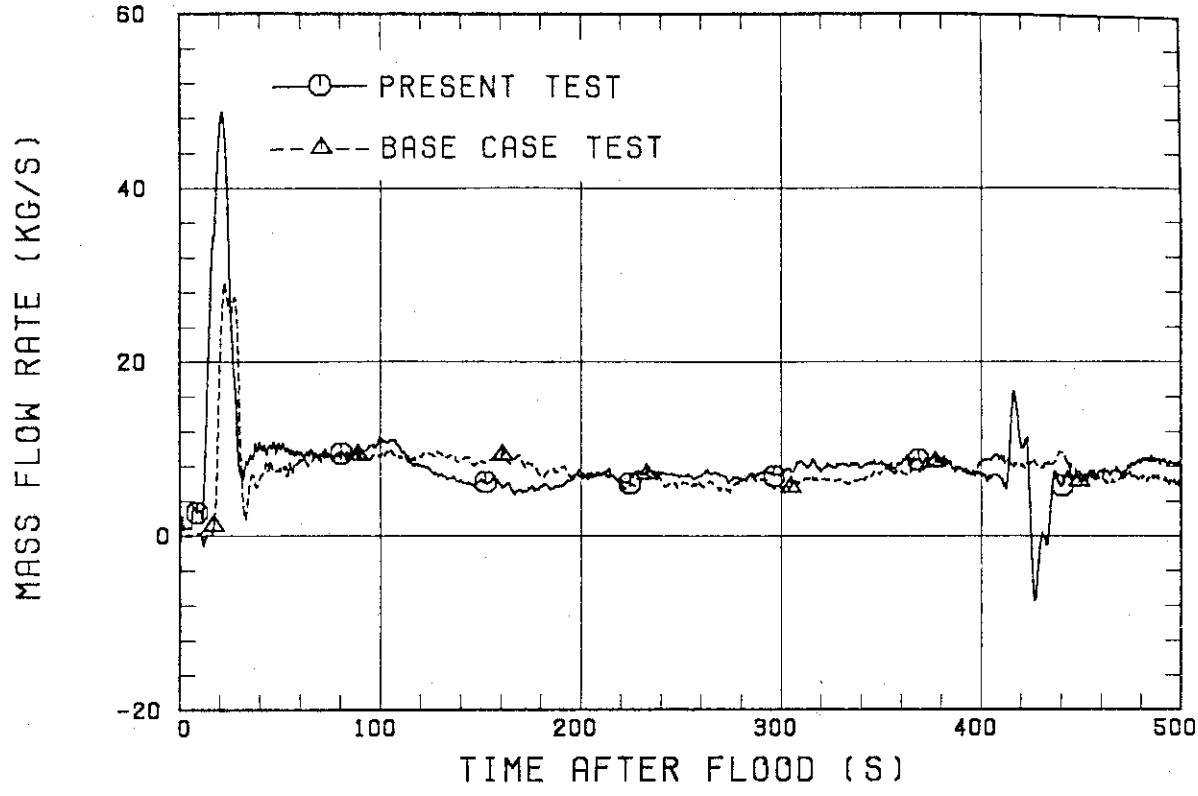

Fig. 4.5 Water accumulation rates in Containment tank 1

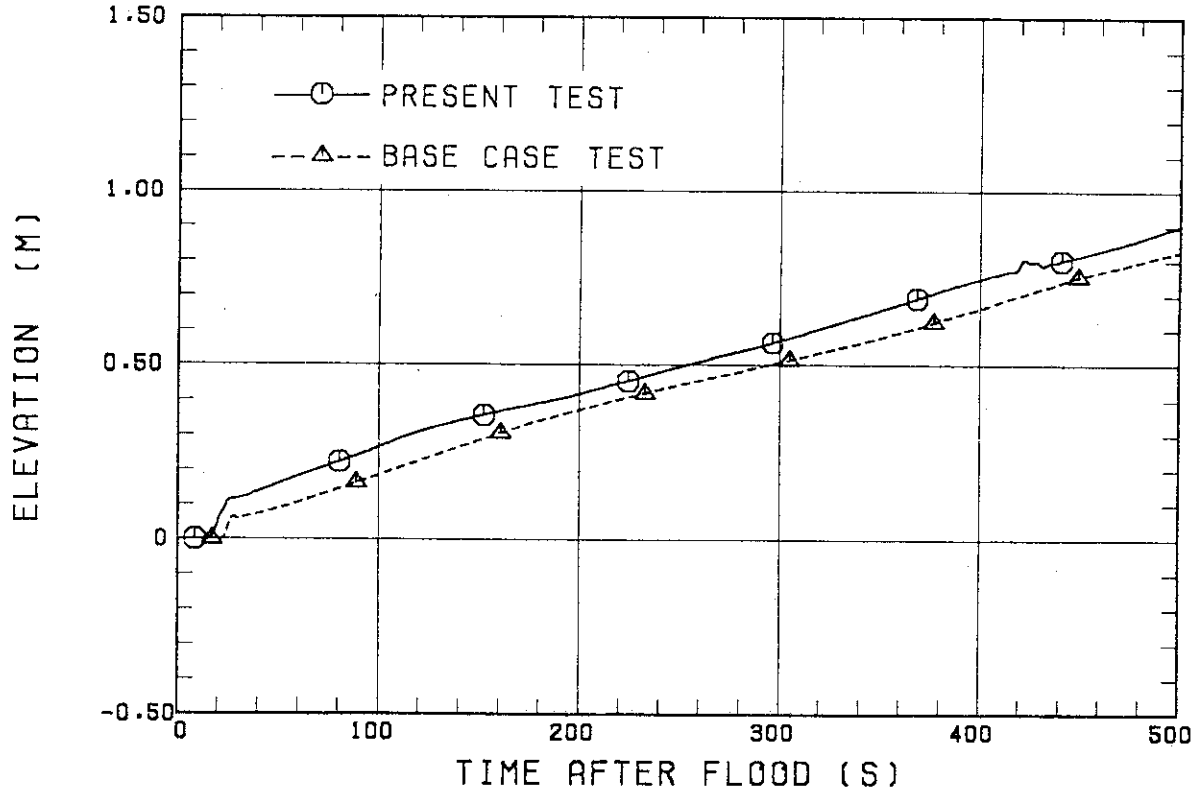

Fig. 4.6 Water levels in Containment tank 1

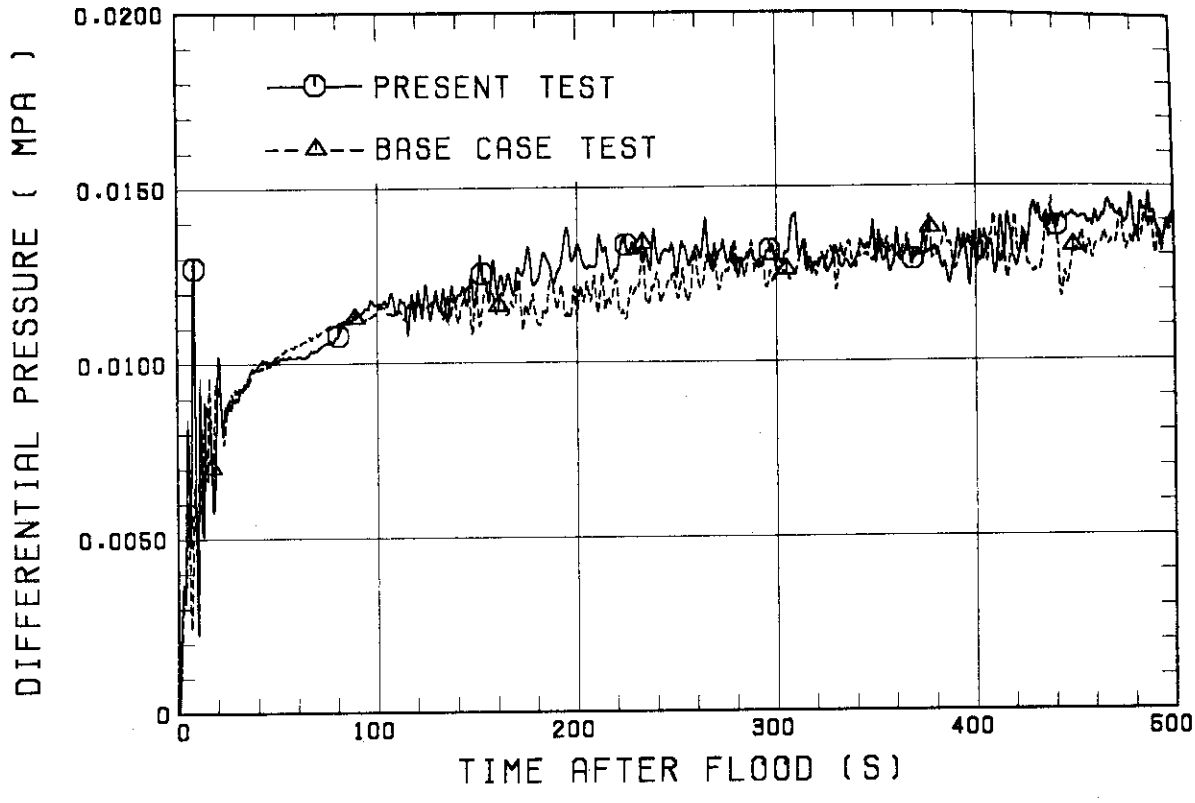

Fig. 4.7 Core differential pressures

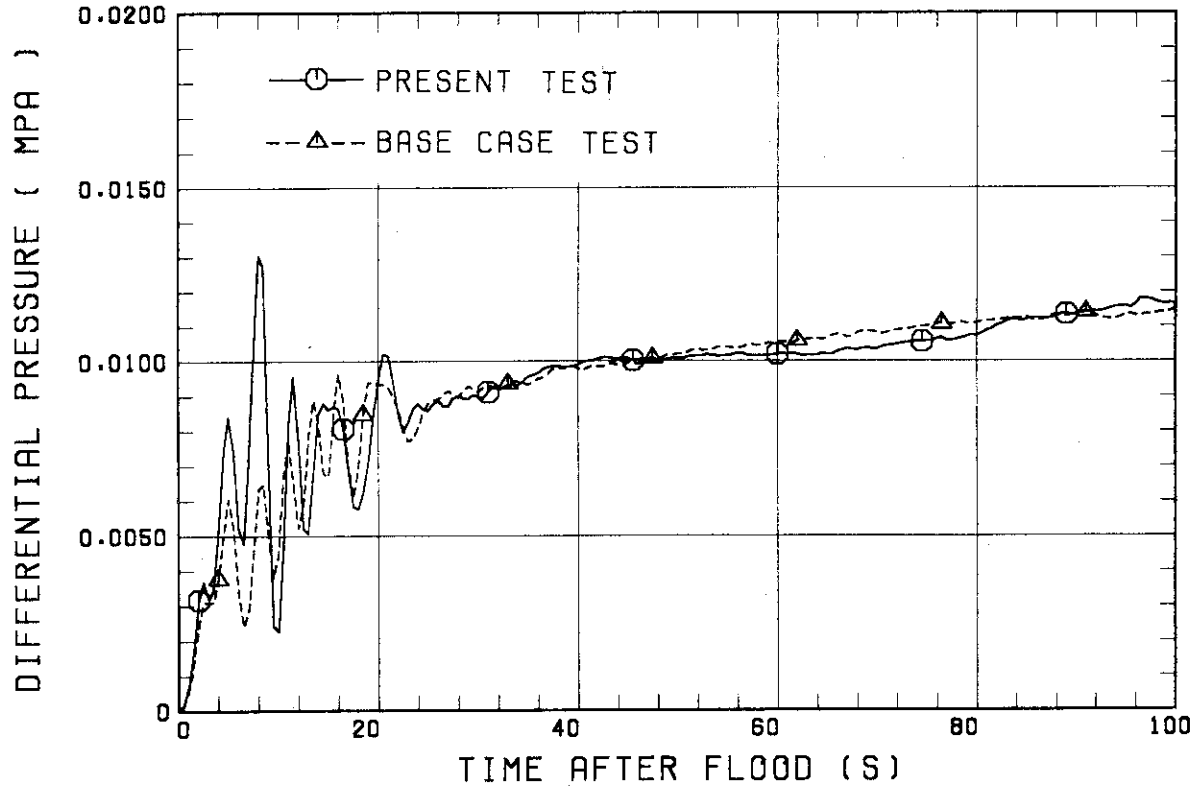

Fig. 4.8 Core differential pressures (0 - 100 s)

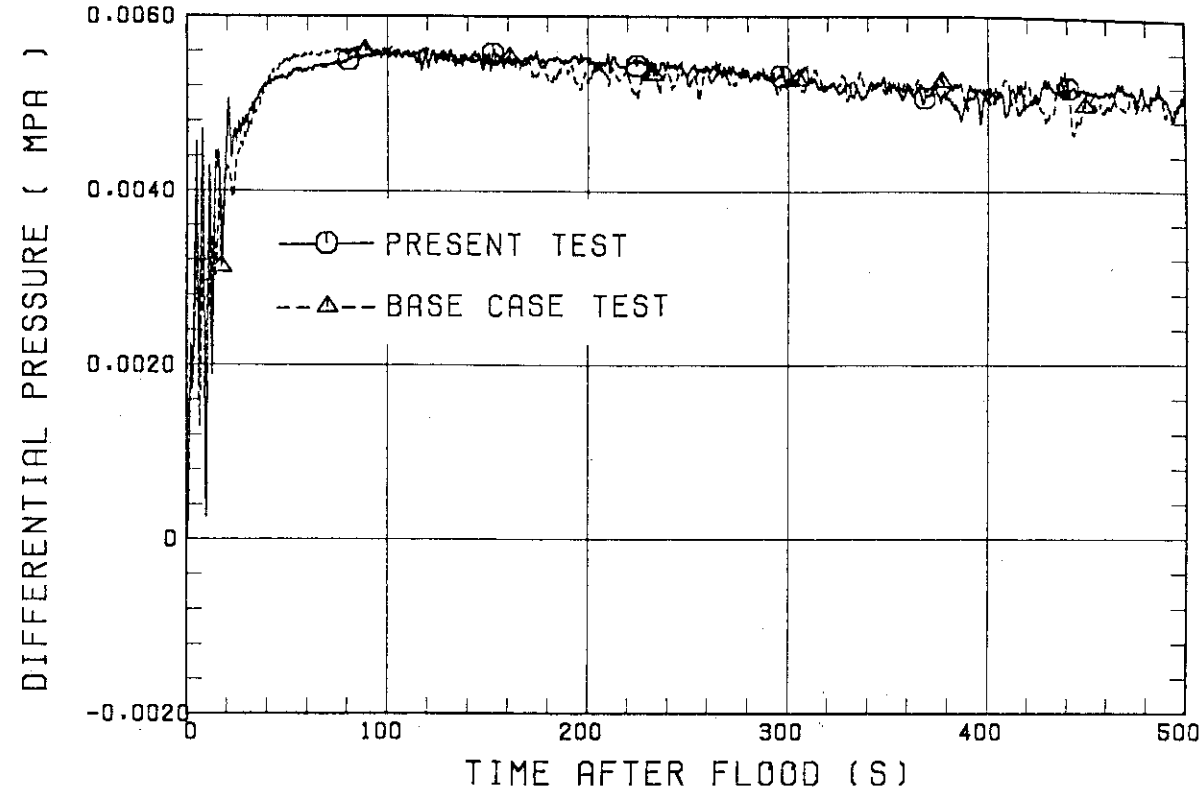

Fig. 4.9(a) Core sectional differential pressures between 0 and 0.61 m elevations

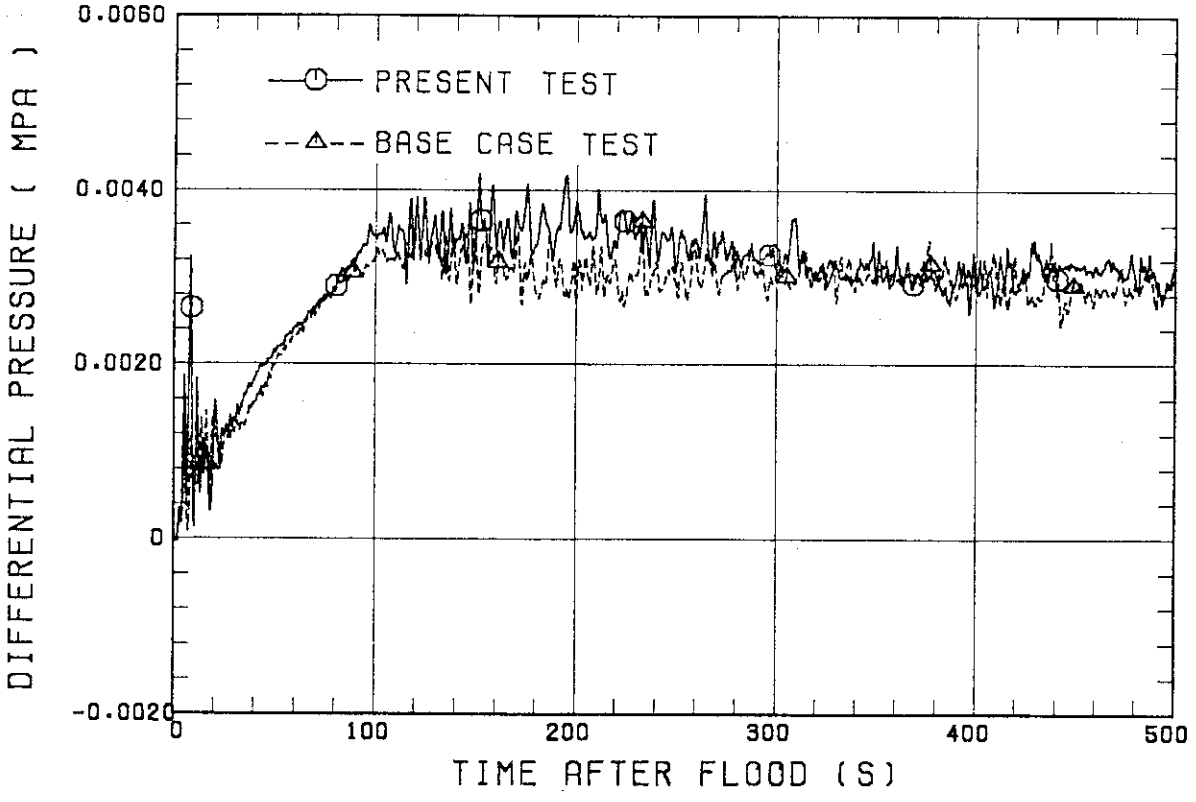

Fig. 4.9(b) Core sectional differential pressures between 0.61 and 1.22 m elevations

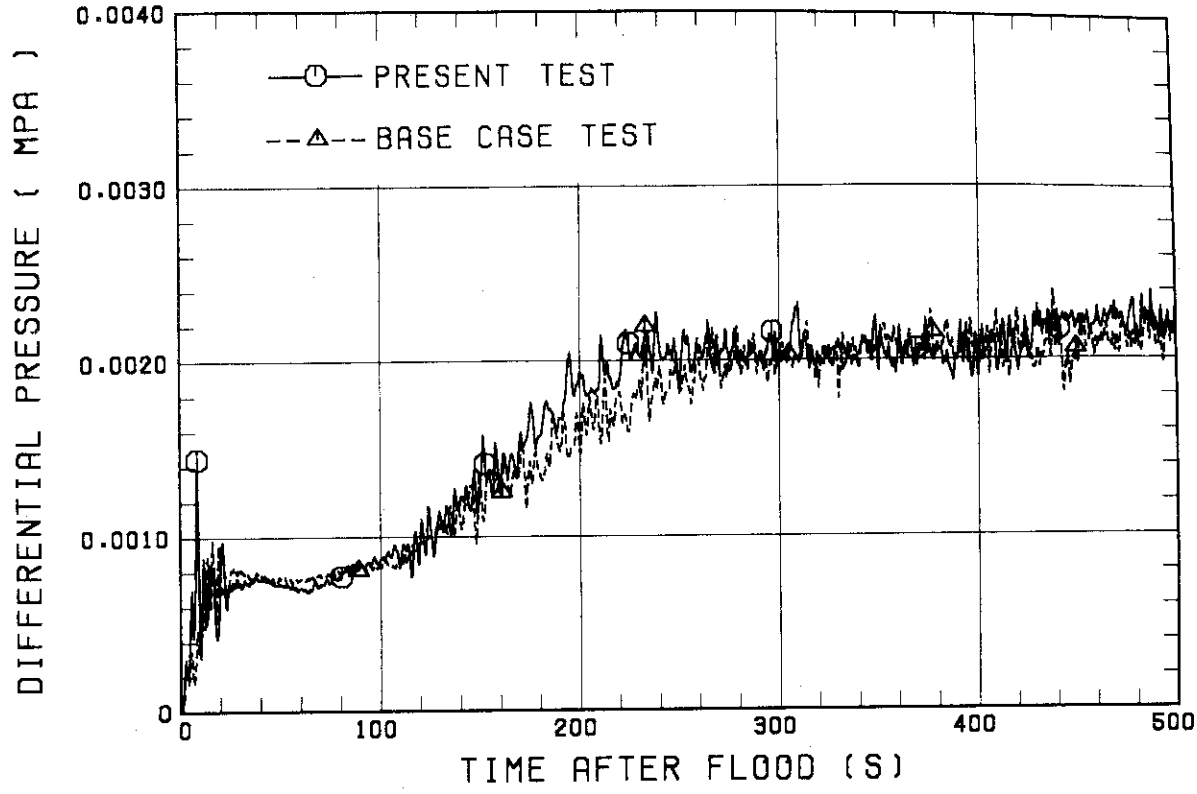

Fig. 4.9(c) Core sectional differential pressures between 1.22 and 1.83 m elevations

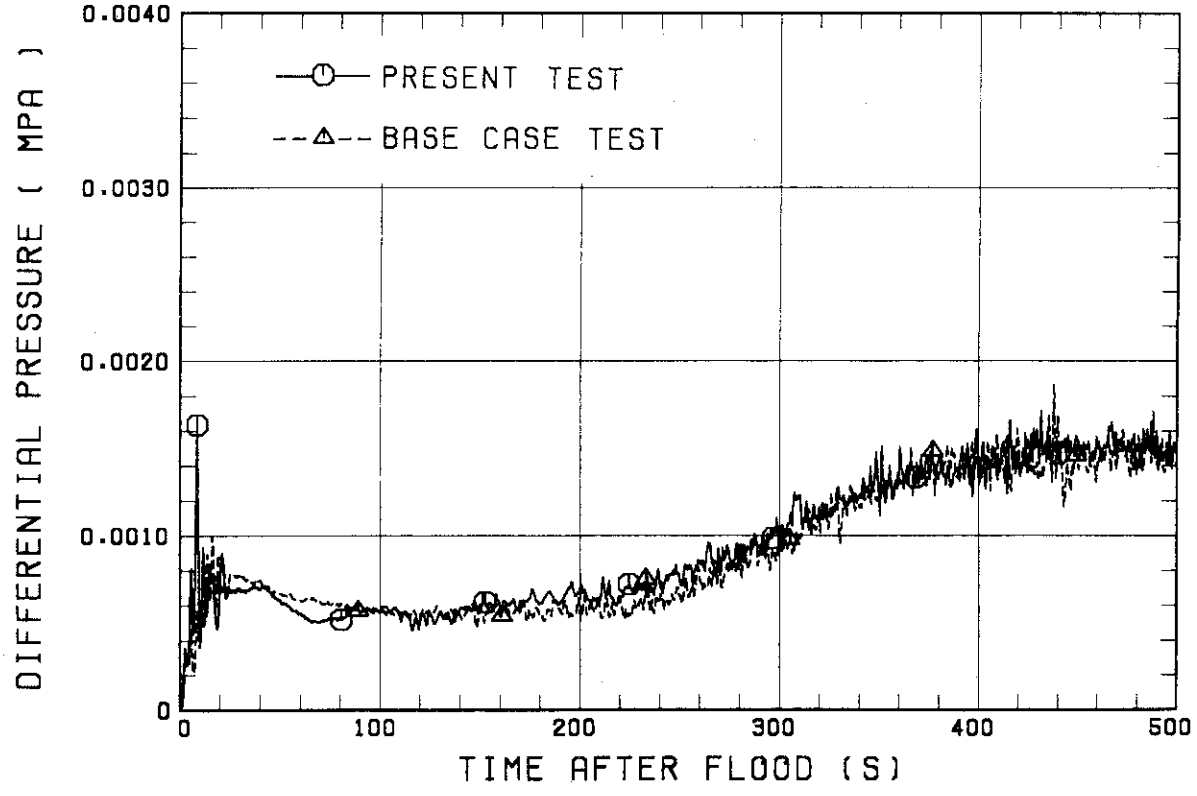

Fig. 4.9(d) Core sectional differential pressures between 1.83 and 2.44 m elevations

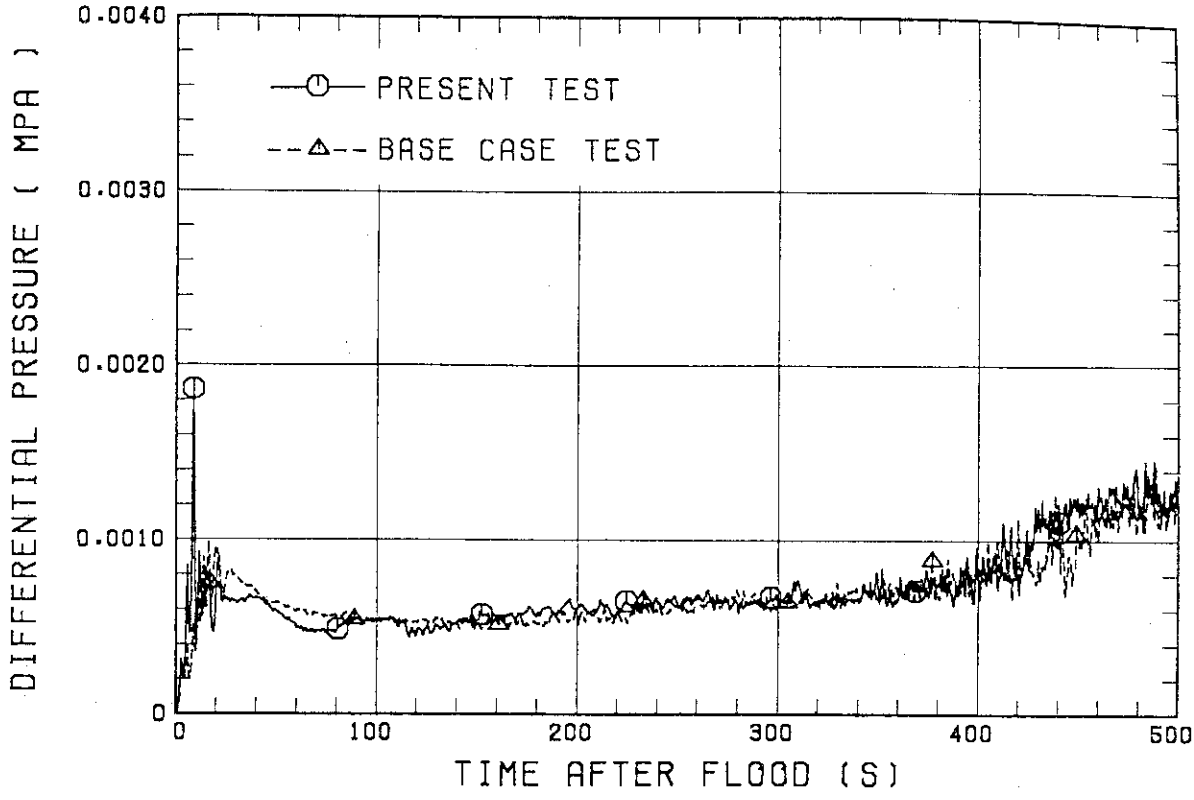

Fig. 4.9(e) Core sectional differential pressures between 2.44 and 3.05 m elevations

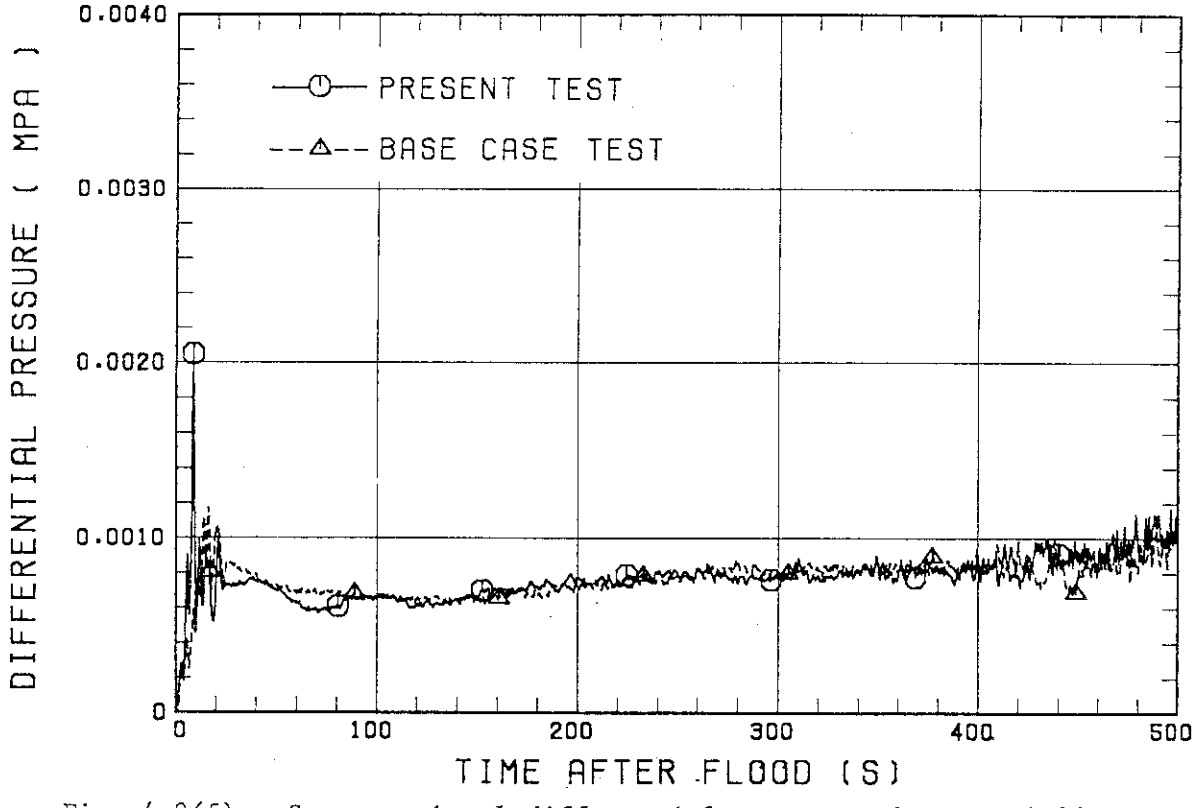

Fig. 4.9(f) Core sectional differential pressures between 3.05 and 3.66 m elevations

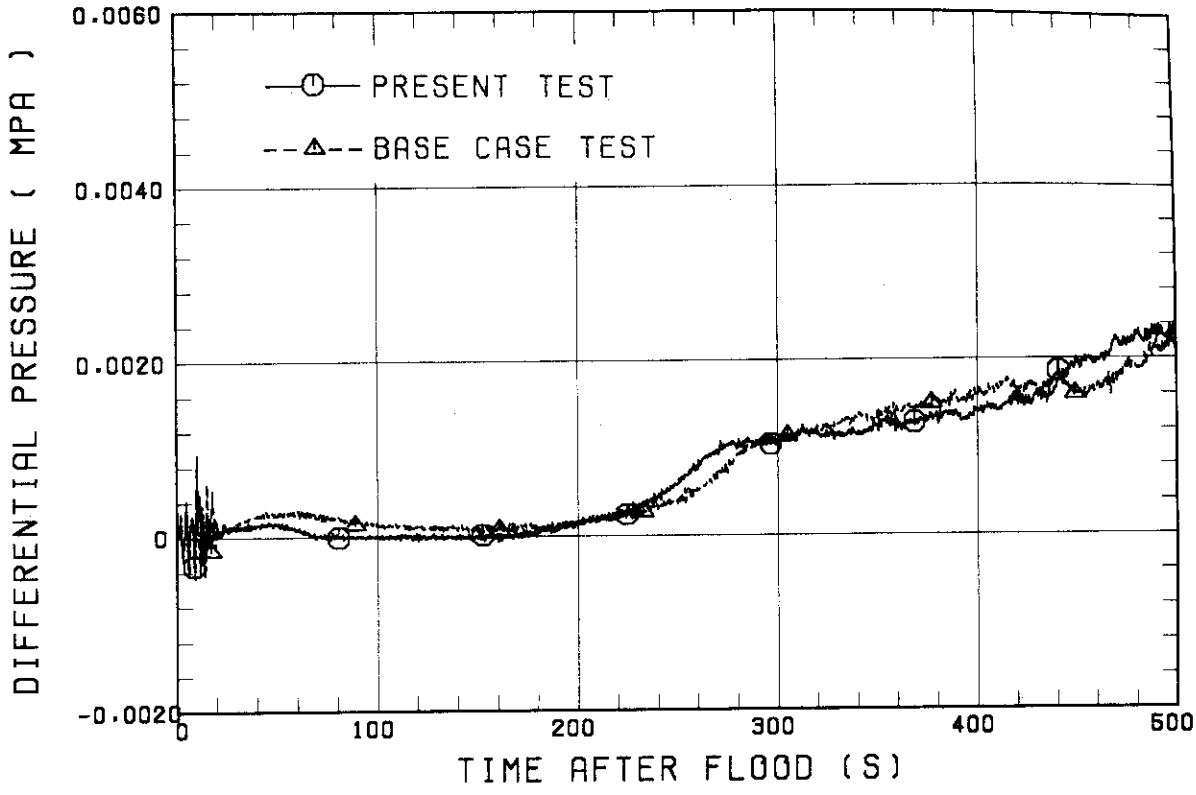

Fig. 4.10 Upper plenum differential pressures above UCSP

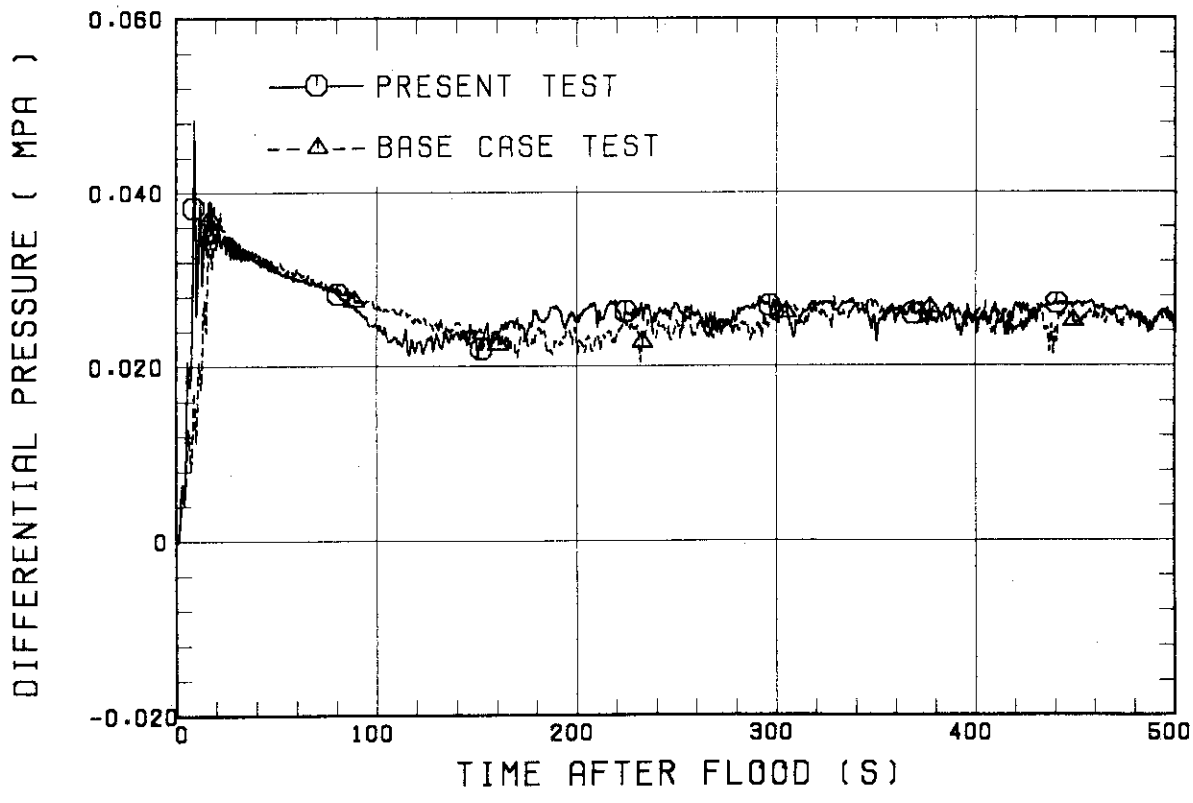

Fig. 4.11 Intact loop differential pressures

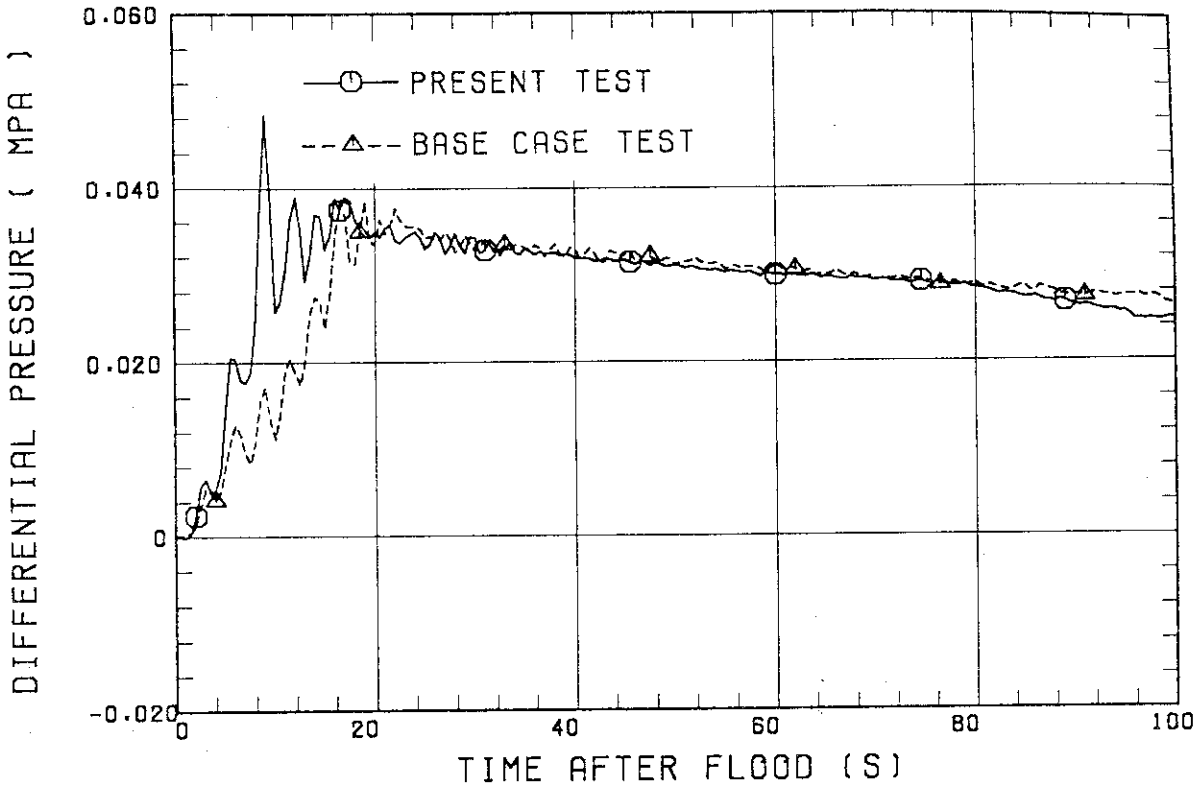

Fig. 4.12　　Intact loop differential pressures (0 - 100 s)

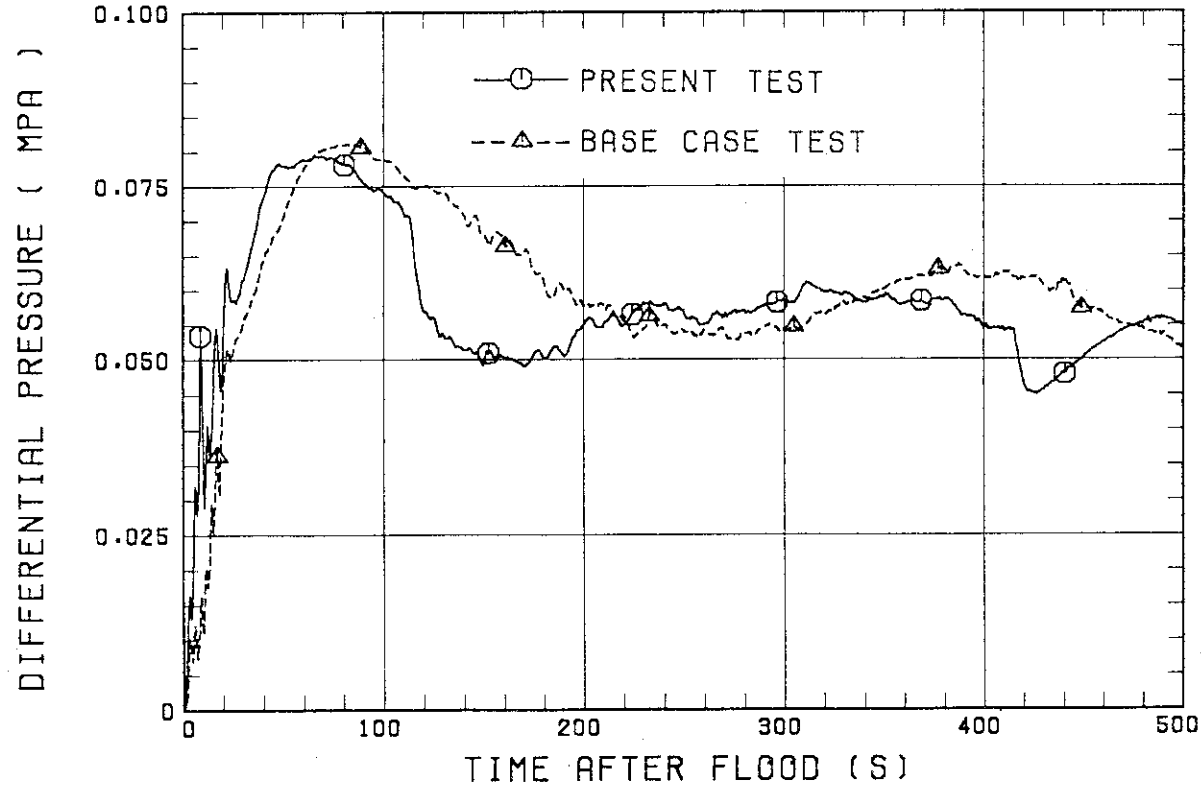

Fig. 4.13　　Broken loop differential pressures

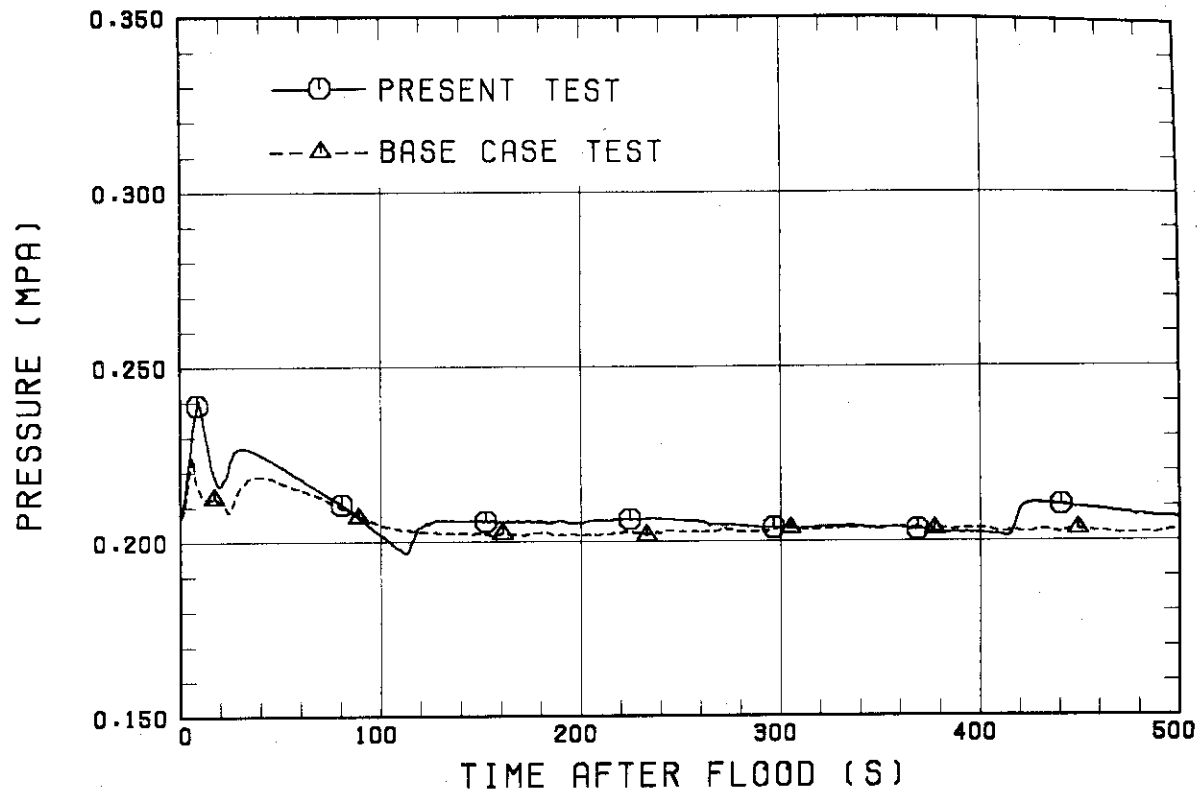

Fig. 4.14 Containment tank 2 pressures

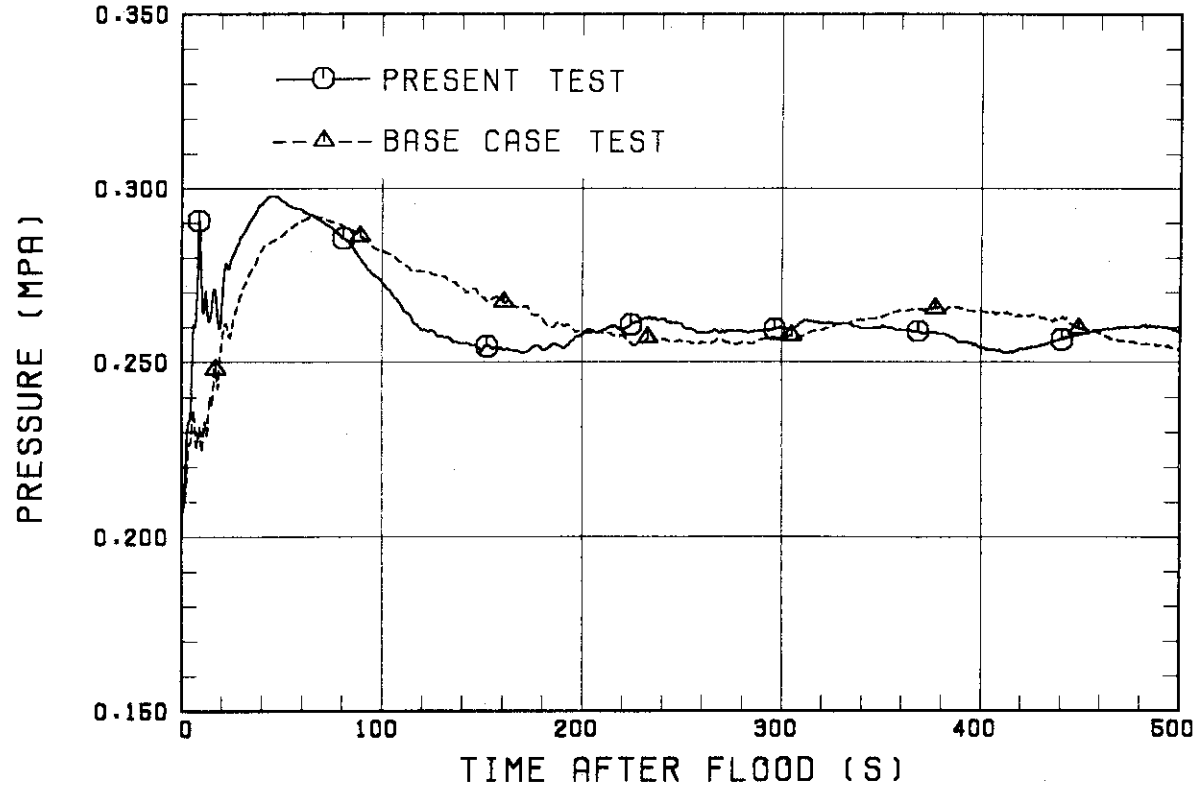

Fig. 4.15 Upper plenum pressures

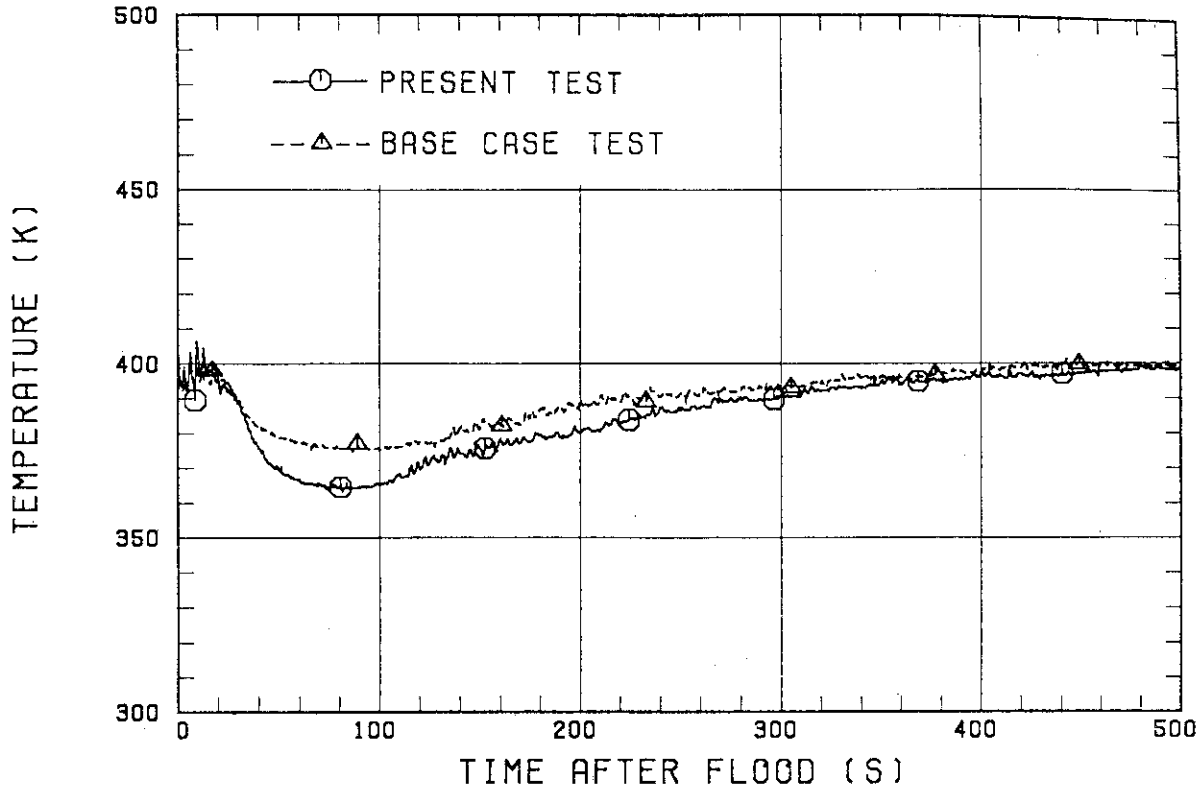

Fig. 4.16 Fluid temperatures at core inlet

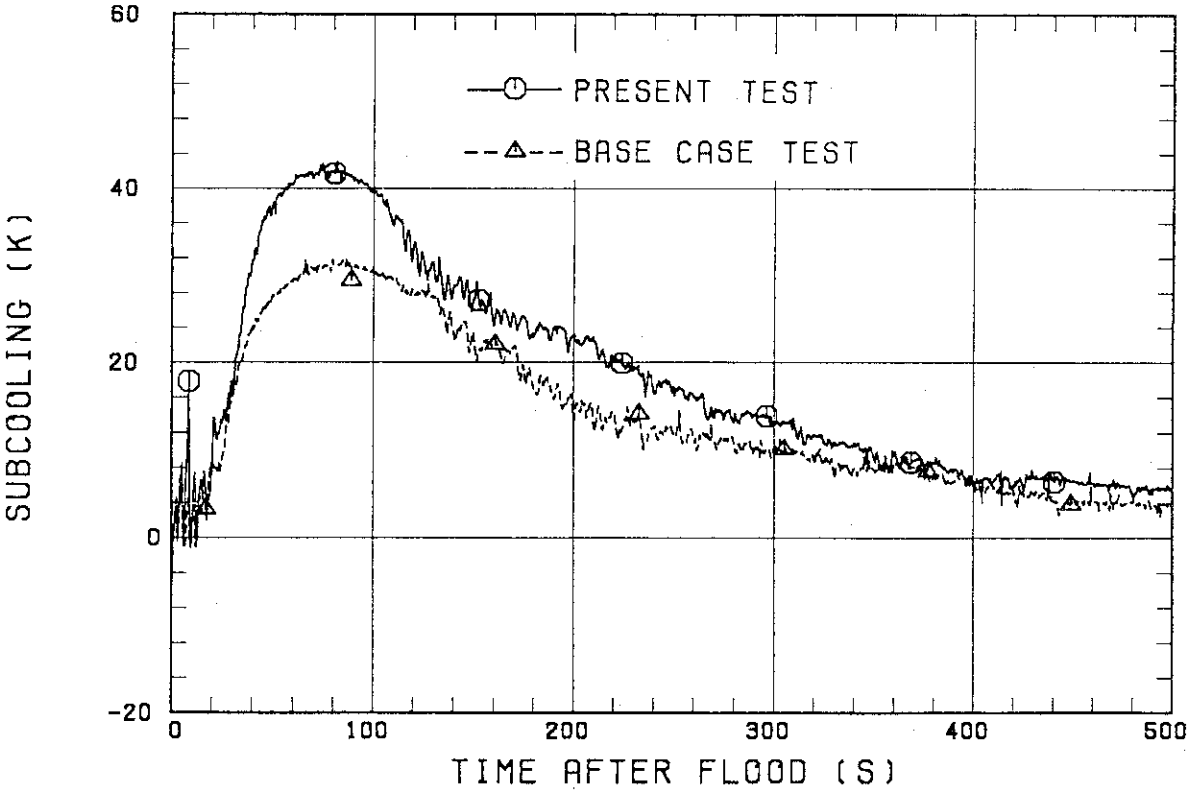

Fig. 4.17 Core inlet subcoolings

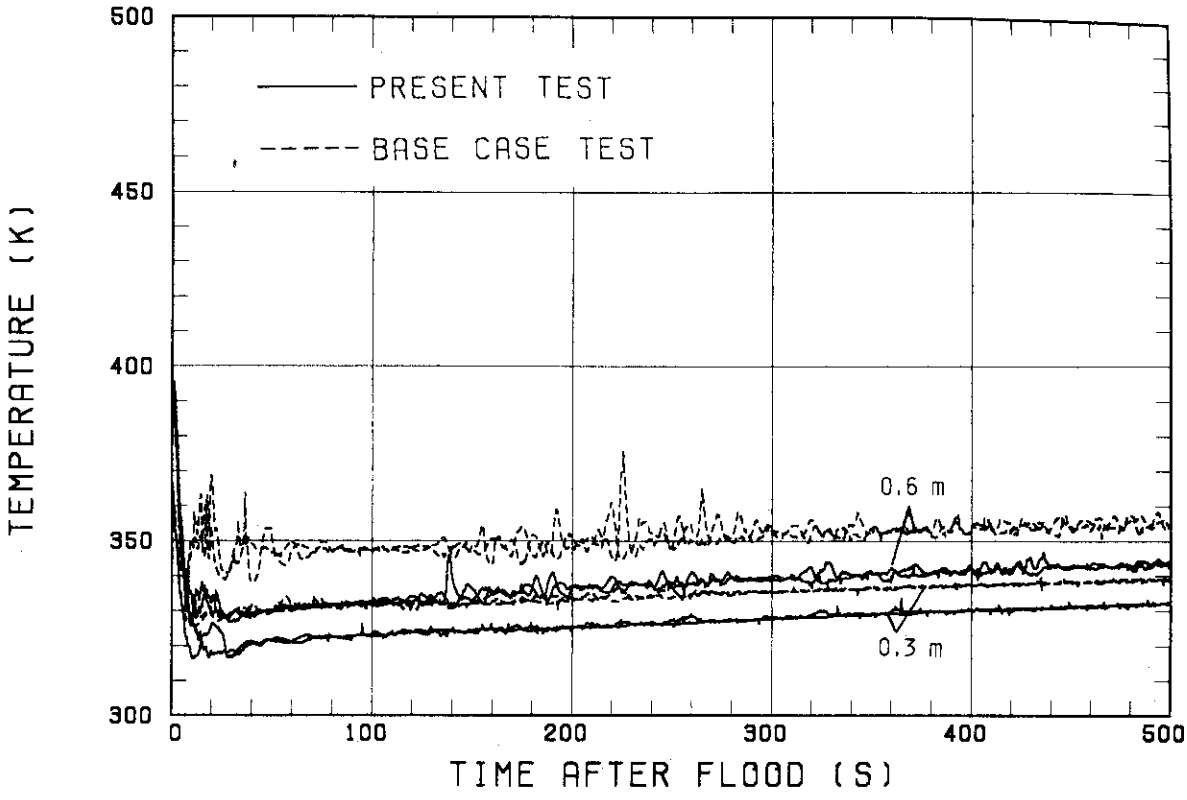

Fig. 4.18 Fluid temperatures in lower plenum

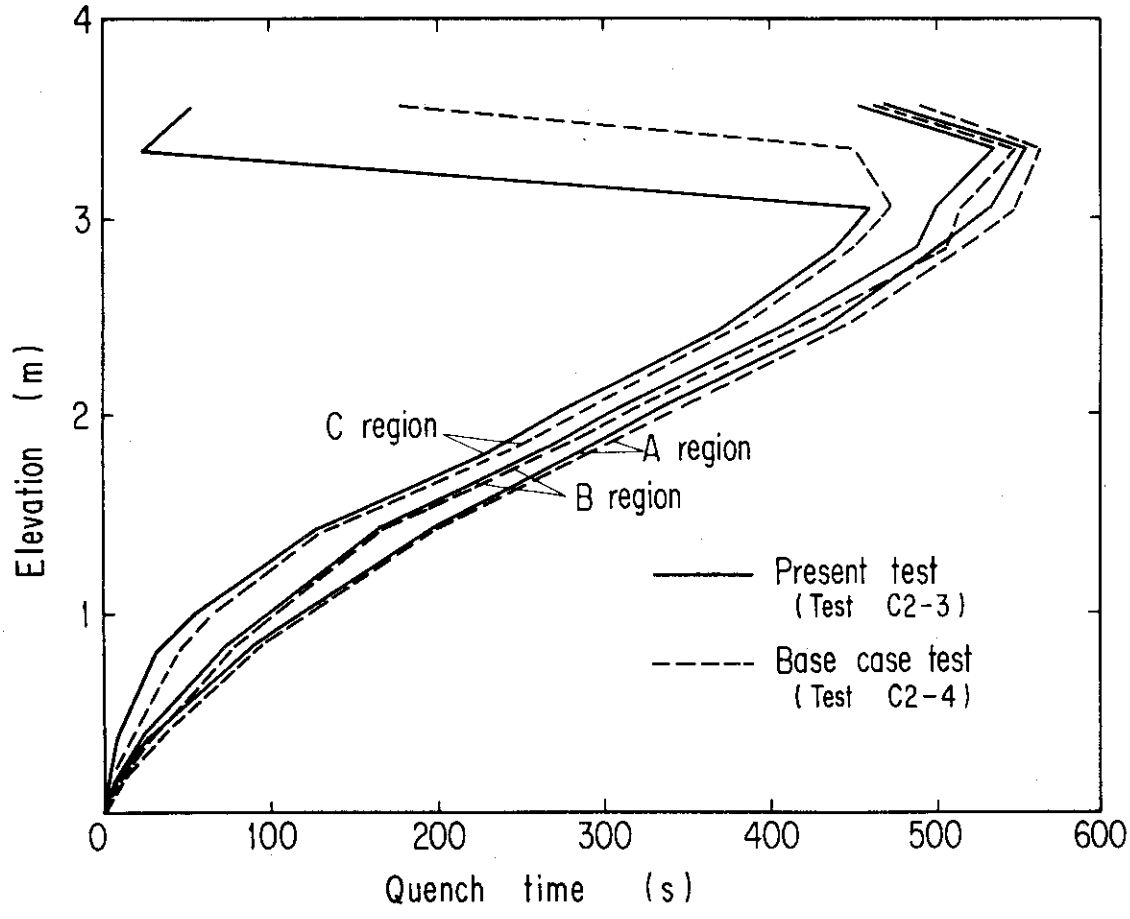

Fig. 4.19 Quench envelopes (mean values)

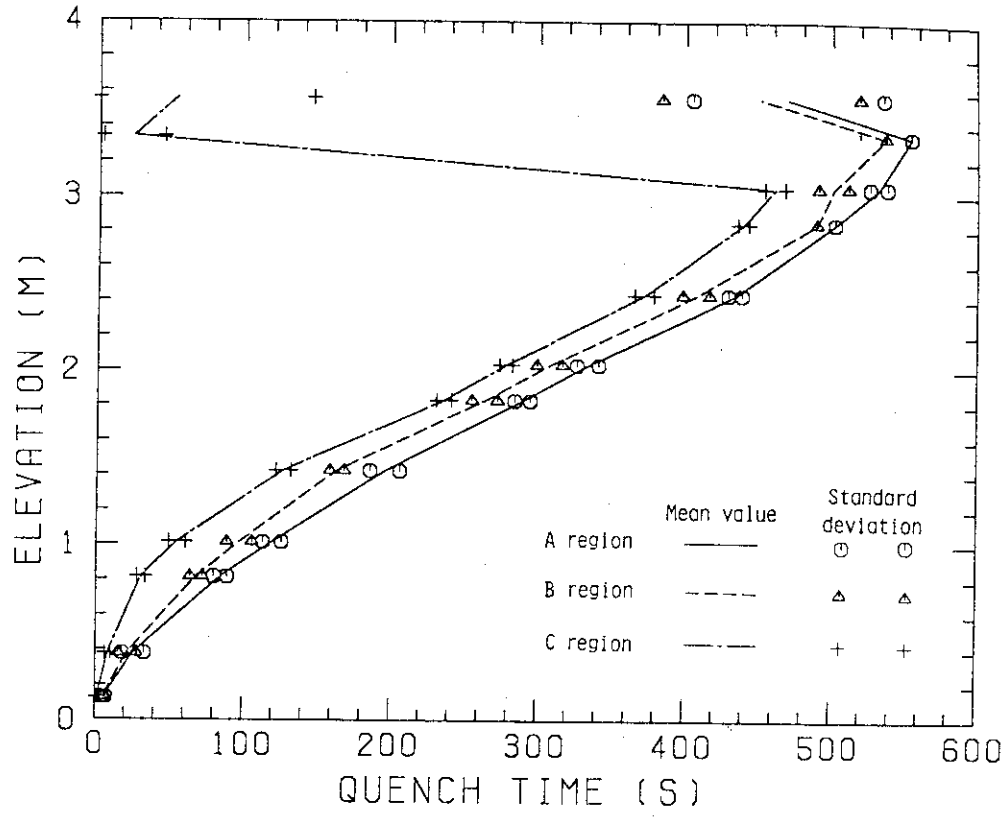

Fig. 4.20(a) Quench envelope for present test

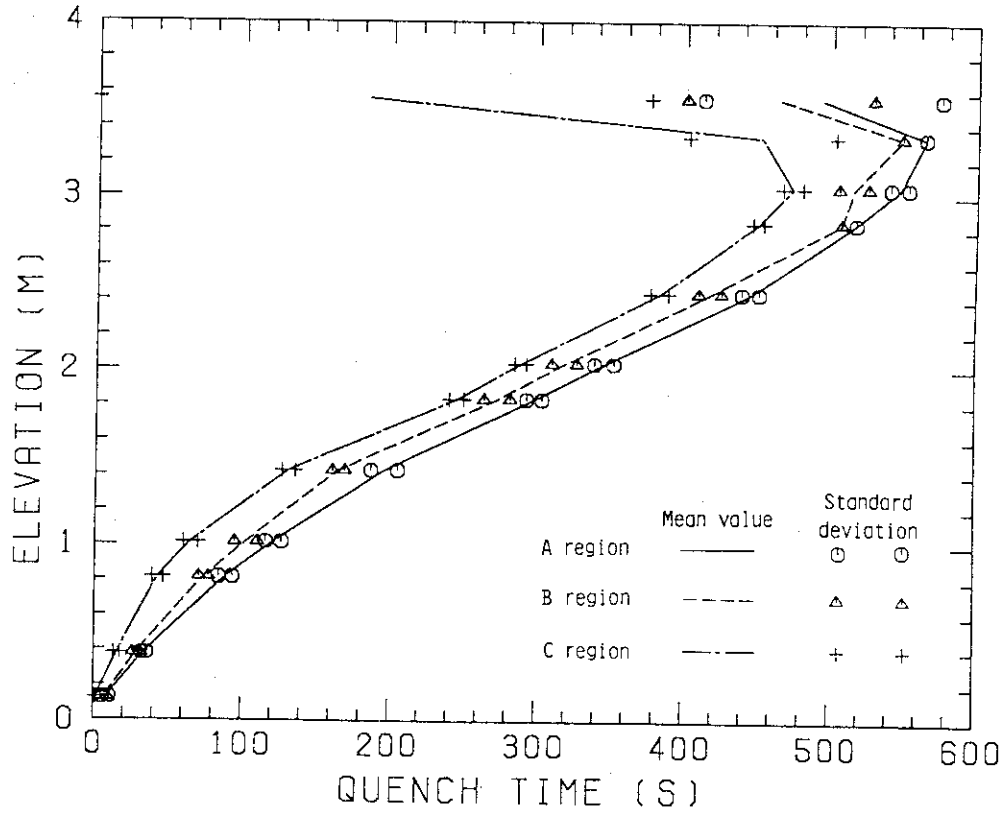

Fig. 4.20(b) Quench envelope for base case test

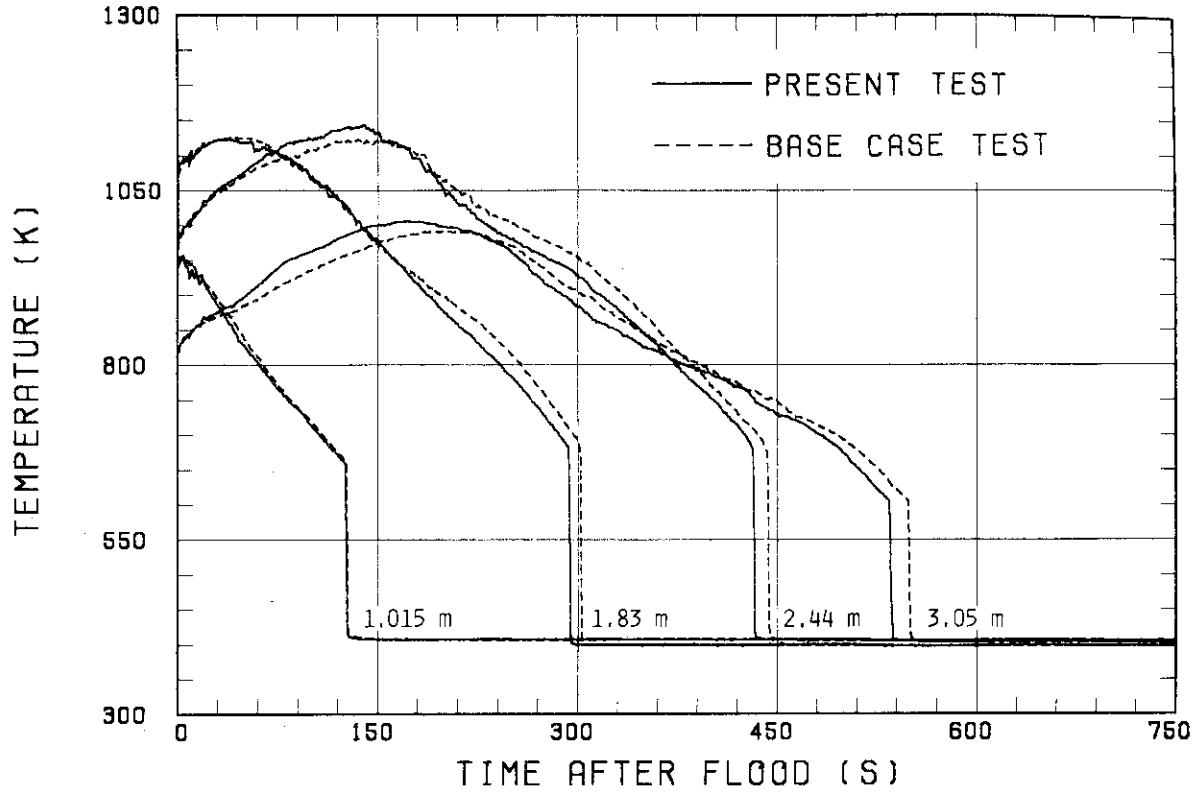

Fig. 4.21(a) Rod surface temperatures in A region

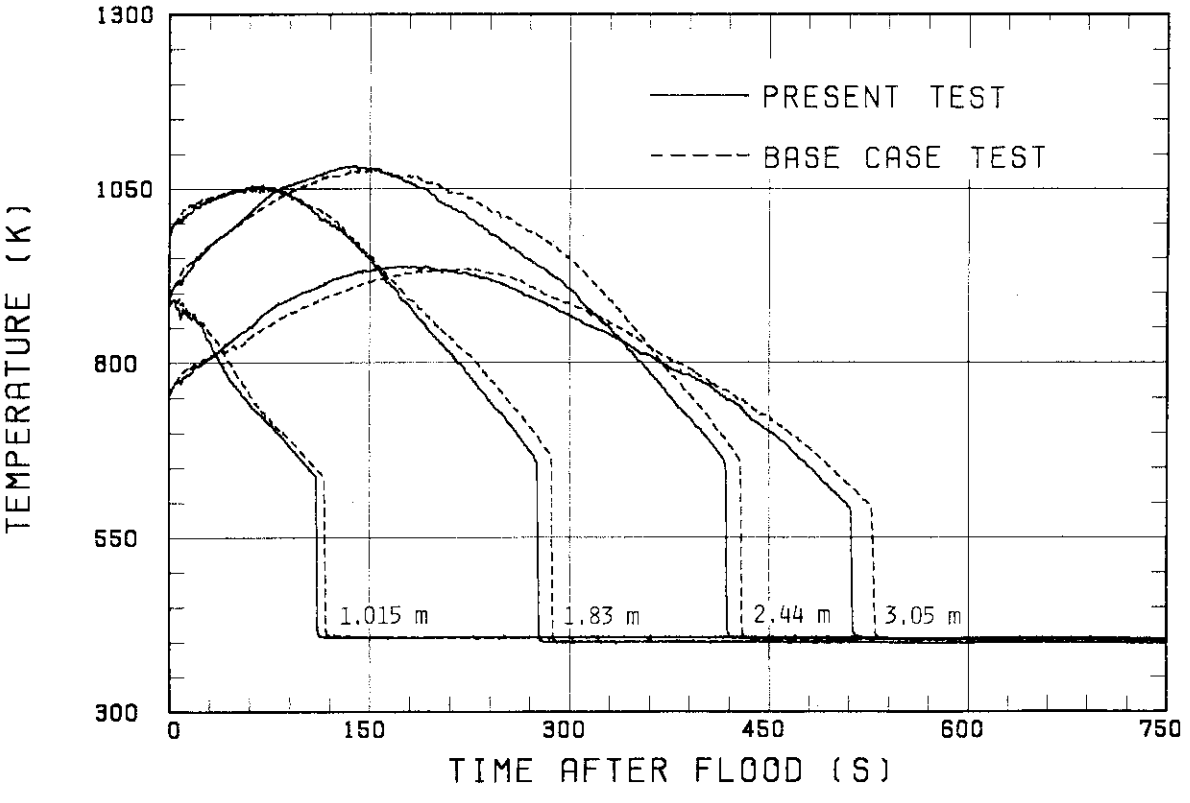

Fig. 4.21(b) Rod surface temperatures in B region

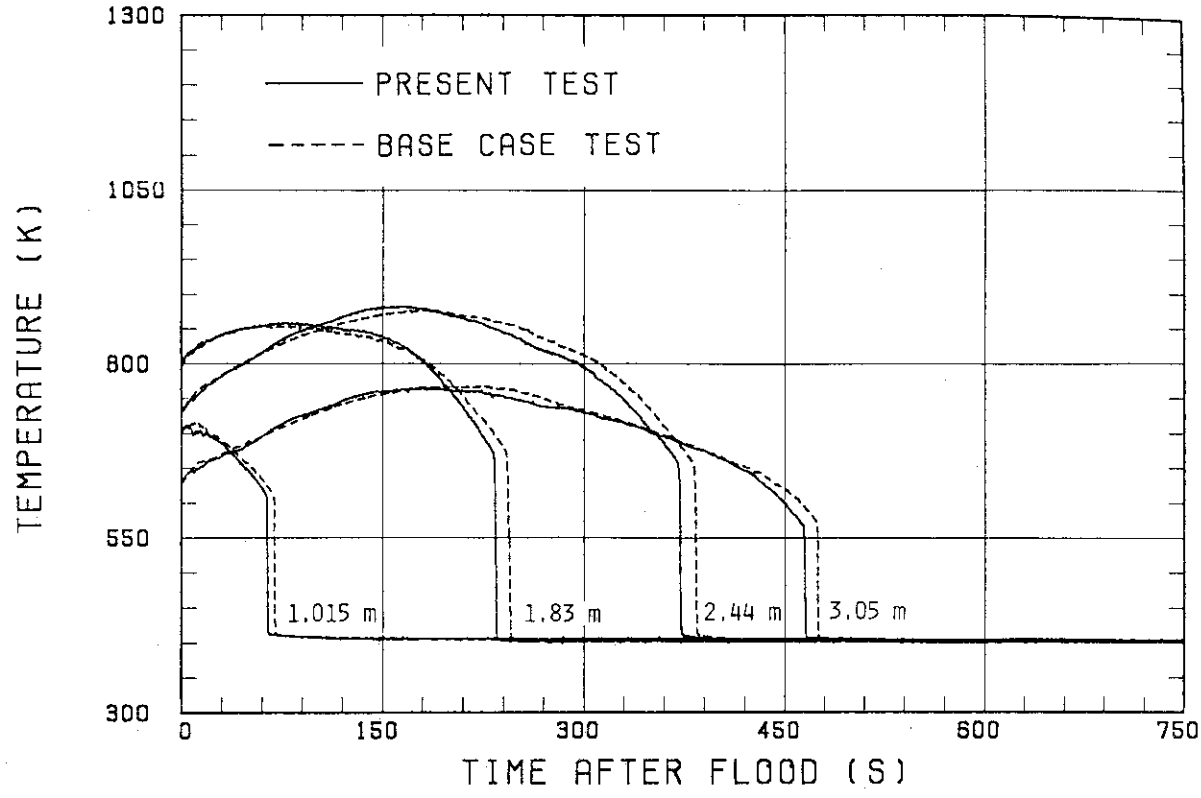

Fig. 4.21(c) Rod surface temperatures in C region

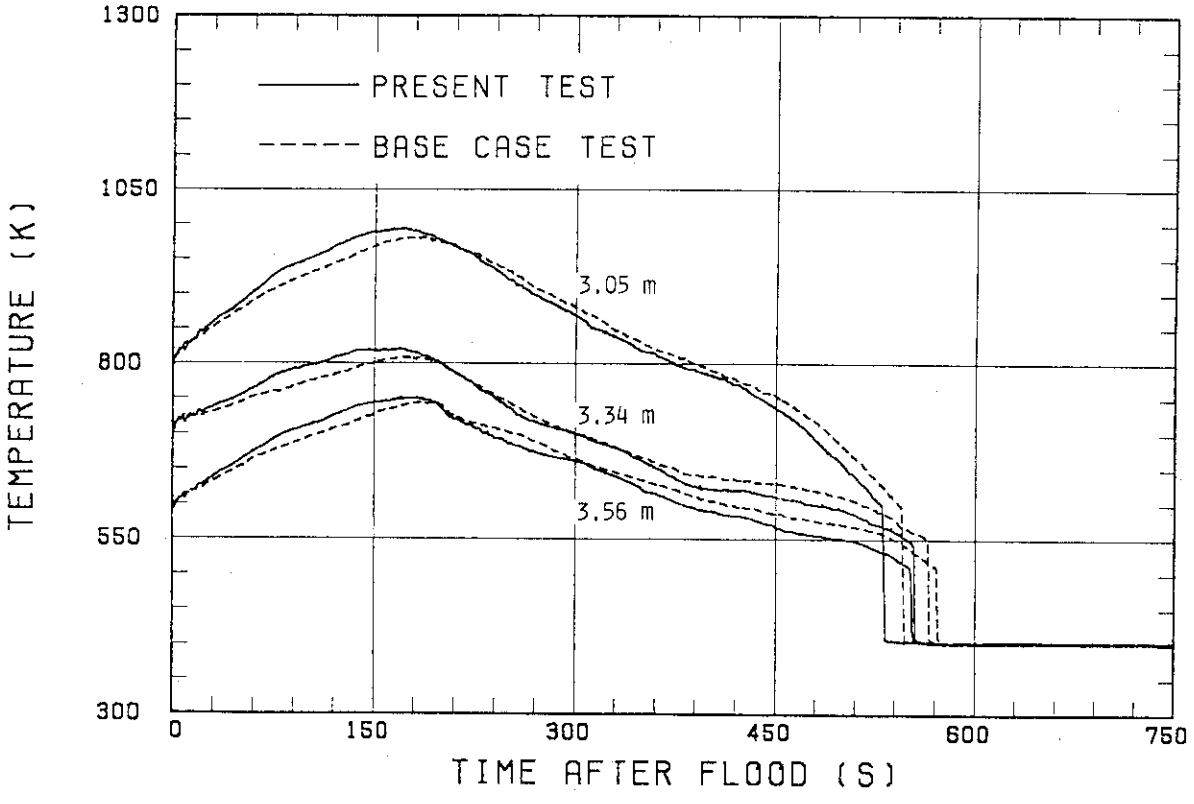

Fig. 4.22 Rod surface temperatures at top part in A region

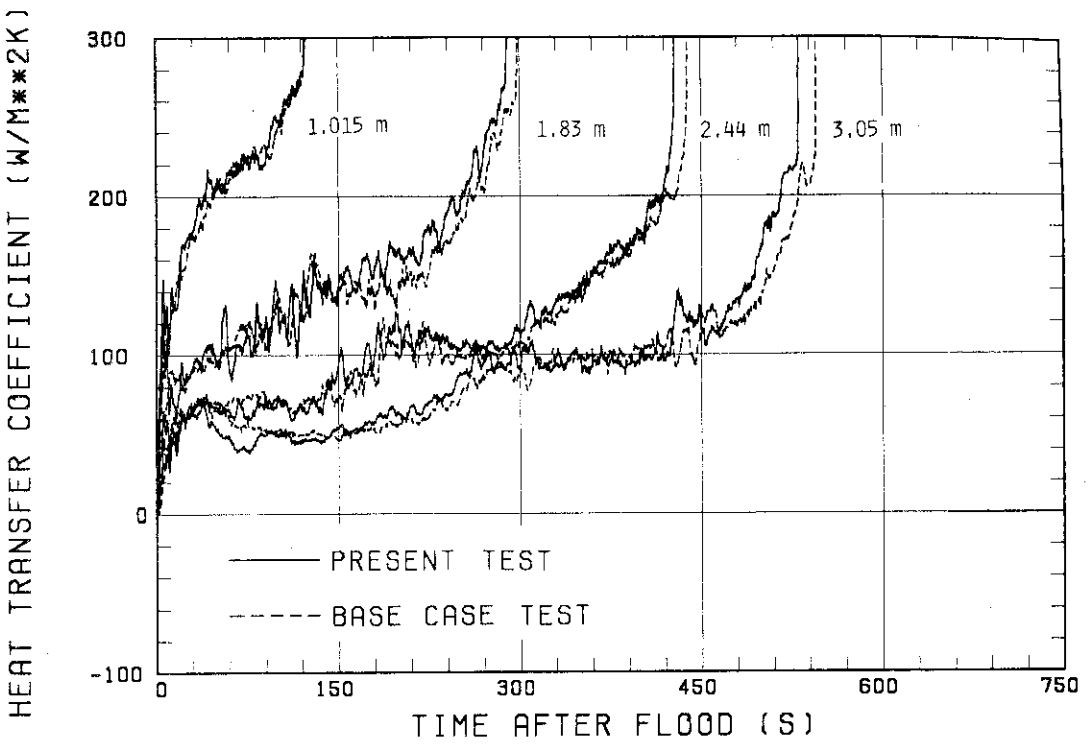

Fig. 4.23 Heat transfer coefficients in A region

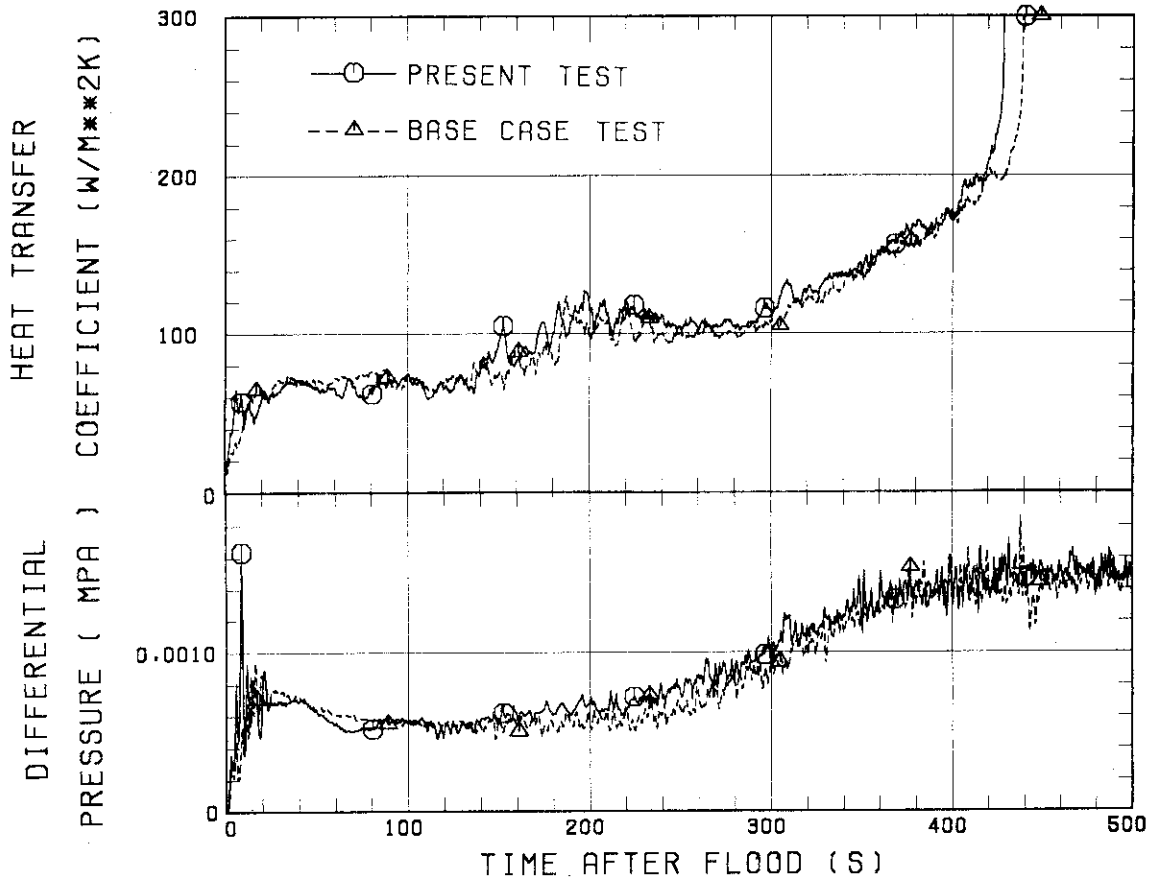

Fig. 4.24 Comparisons of heat transfer coefficients and core differential pressures

5. Conclusions

Analyzing the data of the present test and comparing these with those of the base case test, the following results are obtained:

(1) The time to fill the downcomer was about 8 s in the present test and was significantly shorter than that in the base case test (*i.e.* 16 s).

(2) The higher downcomer water accumulation velocity in the initial period is considered to result in the observed higher core flooding rate and the larger U-tube type oscillation in the initial period.

(3) The intact loop differential pressure, *i.e.* the steam binding, and the core differential pressure were also observed to increase rapidly, and hence, are considered to reduce the core flooding rate rapidly.

(4) By 20 s the core flooding rates for the present test and the base case test were observed to become identical. The larger oscillation in the present test was also observed to be damped by 30 s.

(5) After 20 s the thermo-hydrodynamic behaviors in the system of both tests were observed to be almost identical, and the effects of the initial downcomer water accumulation velocity was unnoticeable.

(6) The core cooling behaviors were observed to be almost identical in both tests through the whole transient including the initial period.

(7) Therefore, it is concluded that although the downcomer flow area of the CCTF is larger than the scaled value, with respect to this point there is no problem for applying the CCTF test results to the PWR analyses.

Acknowledgements

The authors are much indebted to Drs. K. Sato and T. Shimooke of JAERI for their guidance and encouragement for this work.

They would like to express their appreciation to the member of their analysis group, especially Messrs. H. Adachi, M. Sobajima, T. Iwamura, A. Ohnuki and Y. Abe of JAERI for valuable discussion.

They are deeply indebted to Messrs. Y. Fukaya, T. Ohyama, T. Wakabayashi, Y. Niitsuma, K. Nakajima, T. Chiba, J. Matsumoto, K. Komori and H. Sonobe of JAERI for their contribution to the test conduction.

References

1. Hirano, K. and Murao, Y.: "Large Scale Reflood Test", Nihon-Genshiryoku-Gakkai Shi (J. At. Energy Soc. Japan), 22 [10], 681 (1980) [in Japanese].
2. Murao, Y. *et al.*: "Analysis Report on CCTF Core-I Reflood Test", To be published as a JAERI-M report.
3. Okubo, T. and Murao, Y.: "Experimental Study of ECC Water Injection Rate Effects on Reflood Phase of PWR-LOCA", J. Nucl. Sci. Technol., 22 [2], 93 (1985).
4. Okubo, T. *et al.*: "Evaluation report on CCTF Core-II reflood test C2-4 (Run 62) — Investigation of reproducibility —", JAERI-M 85-026 (1985).
5. Portland General Electric Company: "Trojan Nuclear Plant Final Safety Analysis Report", Docket-50-344-38∿46 (1972).
6. Kyushyu Electric Power Company: "Genkai (No. 3 and No. 4) Safety Analysis Report" (1982).
7. Adachi, H. *et al.*: "Cold leg injection reflood test results in SCTF Core-I under constant system pressure", To be published as a JAERI-M report.
8. Sudo, Y. *et al.*: "Experimental Results of the Effective Water Head in Downcomer during Reflood Phase of a PWR LOCA (2nd Report, 50 mm Gap Size)", JAERI-M 8978 (1980).

Appendix

Appendix A

Definitions of Tag IDs

Figure List

1. Definition of Tag. ID for clad surface temperatures and heat fransfer coefficients

Notation : TEnnYlm (temperature)

HTEmmYlm (heat transfer coefficient)

nn : Bundle number (see Fig. A-1)

m : Elevation number

	Elevation (m)	Axial power factor
3	0.38	0.651
5	1.015	1.147
7	1.83	1.40
9	2.44	1.256
A	3.05	0.854

2. Definition of power zone and boundle number

See Fig. A-1

3. Definition of Tag. ID for void fraction

See Fig. A-2

4. Definition of Tag. ID for average linear power of heater rod in each power unit zone

See Fig. A-3

5. Definition of Tag. ID for differential pressure through downcomer, upper plenum, core and lower plenum

See Fig. A-4

6. Definition of Tag. ID for differential pressure through intact and broken loop and broken cold leg nozzle

See Fig. A-5

7. Definition of Tag. ID for fluid temperature in inlet and outlet plenum and secondary side of steam generator

See Fig. A-6

8. Definition of Tag. ID for ECC water injection rate, ECC water temperature and vented steam flow rate

See Fig. A-7

9. Definition of initial temperature, turnaround temperature quench temperature, temperature rise, turnaround time and quench time. (See Fig. A-8)

T_i : Initial temperature (Clad surface temperature at reflood initiation)

T_t : Turnaround temperature (Maximum clad surface temperature in each temperature history)

ΔT_r : Temperature rise ($= T_t - T_i$)

T_q : Quench temperature (Clad surface temperature at quenching)

10. Definition of quenching

See Fig. A-8

Quench time t_t is determined as

$$t_t = i \times \Delta t - \text{(reflood initiation time)}$$

In above equation, i is determined by the following criteria.

(1) Clad surface temperature is high, compared with the saturation temperature.

$$T_i > T_{sat} + \Delta T_1$$

(2) Decreasing rate of clad surface temperature is large.

$$\frac{T_{i+1} - T_i}{\Delta t} < - C_{st}$$

(3) Clad surface temperature falls around the saturation temperature.

$$T_{i + k_1} \leq T_{sat} + \Delta T_1$$

(4) If the determined i is inadequate, the value i is manually re-determined.

Δt : Data sampling period (s)

T_i : Clad surface temperature (K)

T_{sat}: Saturation temperature at the pressure in upper plenum (K)

ΔT_1 : Temperature discrepancy (K)
Default value = 50.0

C_{st} : Decreasing rate of clad surface temperature (K/S)
Default value = 25.0

k_1 : Number of referred data (-)
Default value = 6

11. Definition of Tag. ID for core inlet mass flow rate, time-integral core inlet mass flow rate and carry-over rate fraction

(1) Core inlet mass flow rate : $\dot{m}_F$
Notation : MLCRI□ (□ = N, 1 or 11)

(2) Time-intefral core inlet mass flow rate : $\int \dot{m}_F dt$
Notation : IMLCRI□ (□ = N, 1 or 11)

(3) Carry-over rate fraction : $(\dot{m}_F - \dot{m}_{CR})/\dot{m}_F$
Natation : CRF□ (□ = N, 1 or 11)

where $\dot{m}_F$: Core inlet mass flow rat (See item 12)

$\dot{m}_{CR}$: Water accumulation rate in core

Suffix	$\dot{m}_F$ base on
N	Eq.(A.1) with K=20
1	Eq.(A.1) with K=15
11	Eq.(A.2)

12. Evaluation of core inlet mass flow rate

The reflood phenomena is a relatively slow transient and a steady state condition can be applied. In a steady state condition, based on the mass balance relations of the system, the core flooding mass flow rates $\dot{m}_F$s can be written as follows:

By using the data measured at the downstream of the core inlet, $\dot{m}_F$ is derived as,

$$\dot{m}_F = \dot{m}_C + \dot{m}_U + \dot{m}_B + \Sigma \dot{m}_I \quad , \qquad (A.1)$$

where $\dot{m}_C$ and $\dot{m}_U$ are the mass accumulation rates in the core and the upper plenum respectively. The $\dot{m}_B$ and $\dot{m}_I$ are the mass flow rates in the broken loop and the intact loop, respectively.

By using the data measured at the upstream of the core inlet, $\dot{m}_F$ is derived as,

$$\dot{m}_F = \Sigma \dot{m}_{DL} - \dot{m}_D - \dot{m}_O + \dot{m}_{ECC/LP} \quad , \tag{A.2}$$

where $\dot{m}_{DL}$ and $\dot{m}_O$ are the mass flow rates of the water flowing into and overflowing from the downcomer, $\dot{m}_{ECC/LP}$ and $\dot{m}_D$ are the mass flow rate of the ECC water injected into the lower plenum and the water accumulation rate in the dowmcomer respectively.

The $\dot{m}_I$s and $\dot{m}_B$ can be obtained from the pressure drops at the pump simulators with orifices by assuming the K-factor of the orifice is constant. The values of $\dot{m}_C$, $\dot{m}_D$ and $\dot{m}_U$ can be evaluated with the differential pressure ΔP_C, ΔP_D and ΔP_U, respectively, as follows:

$$\dot{m}_n = d(\Delta P_n S_n/g)/dt \quad (n : C, D, U) \quad , \tag{A.3}$$

where g is the gravitational acceleration and S_n is the cross sectional area. The value of $\dot{m}_O$ can be obtained from the liquid level X in the Containment tank 1 as,

$$\dot{m}_O = d(X\rho_\ell S_o)/dt \quad , \tag{A.4}$$

where ρ_ℓ is the liquid density and S_o is the cross sectional area of the containment tank 1.

The value of $\dot{m}_{DL}$, $\dot{m}_{DV}$ and h, which are liquid flow rate, steam flow rate and enthalpy of two phase mixture downstream each ECC port respectively, are obtained from the following mass and energy balance relations at each ECC port under the assumption of thermal equilibrium:

$$\dot{m}_{DV} + \dot{m}_{DL} = \dot{m}_{ECC} + \dot{m}_I \quad , \tag{A.5}$$

$$(\dot{m}_{DV} + \dot{m}_{DL})i = \dot{m}_{ECC}h_{ECC} + \dot{m}_I h_I \quad , \tag{A.6}$$

$$\text{if} \quad h_g \geq h \geq h_\ell \ , \ (\dot{m}_{DV} + \dot{m}_{DL})h = \dot{m}_{DV}h_g + \dot{m}_{DL}h_\ell$$

$$\text{if} \quad h \geq h_g \quad , \ \dot{m}_{DL} = 0 \quad , \tag{A.7}$$

$$\text{if} \quad h \geq h_\ell \quad , \ \dot{m}_{DV} = 0$$

where h is enthalpy of fluid and h_ℓ and h_g are enthalpies of liquid and steam at the saturation temperature, respectively.

The fluid temperatures can be measured with thermocouples immersed in the fluid and the enthalpies h_I and h_{ECC} can be estimated.

Mass balance calculations were performed with Eqs. (A.1) and (A.2). The K-factor of the orifice in the pump simulator was evaluated in the following two ways.

The K-factor of 20 was obtained with the steam and water single phase calibration tests using the flow meter and spool piece data. The K-factor of 15 was obtained with the Pitot tube measurement in a typical reflood condition assuming the flat velocity profile in the pipings. In the differentiation, higher frequency components of the data tends to be amplified more. Therefore, in the differentiation of the differential pressure data, the smoothing procedure was used to uppress the high frequency components of the data.

In the Acc injection period, the calculated $\dot{m}_F$s with Eqs. (A.1) and (A.2) are significantly different from each other. This discrepancy may be caused by inaccuracy of the mass flow rate injected into the system and by the unaccounting of the storage of water in the cold leg pipe. The former might be introduced from the slow time response of the flow meter (time constant 1 second) and the change of the gas volume in the injection line. In this period, especially before the steam generation from the core becomes noticeable, the mass flow rate, $\dot{m}_F$, calculated with Eq. (A.1) is probably reasonable, since the calculation uses the increasing rates of the masses in the core and the upper plenum and their accuracy is good enough for our estimation.

In the LPCI injection period, the calculated $\dot{m}_F$s are slightly different from each other. Judging from the time-integral values of both $\dot{m}_F$s, their average values are nearly proportional. The discrepancy was inferred to be caused by the disregard of the bypass of steam and liquid from the upper plenum without going through the hot legs in the calculation with Eq. (A.1). And additionally the discrepancy was caused by the disregard of the steam generation in the downcomer due to the hot wall of the pressure vessel in the calculation with Eq. (A.2). It was estimated that the disregard of the downcomer steam generation causes the error of 0.25 kg/s on predicted $\dot{m}_F$. The estimation was made by comparing the results of the tests with hot and cold downcomer conditions.

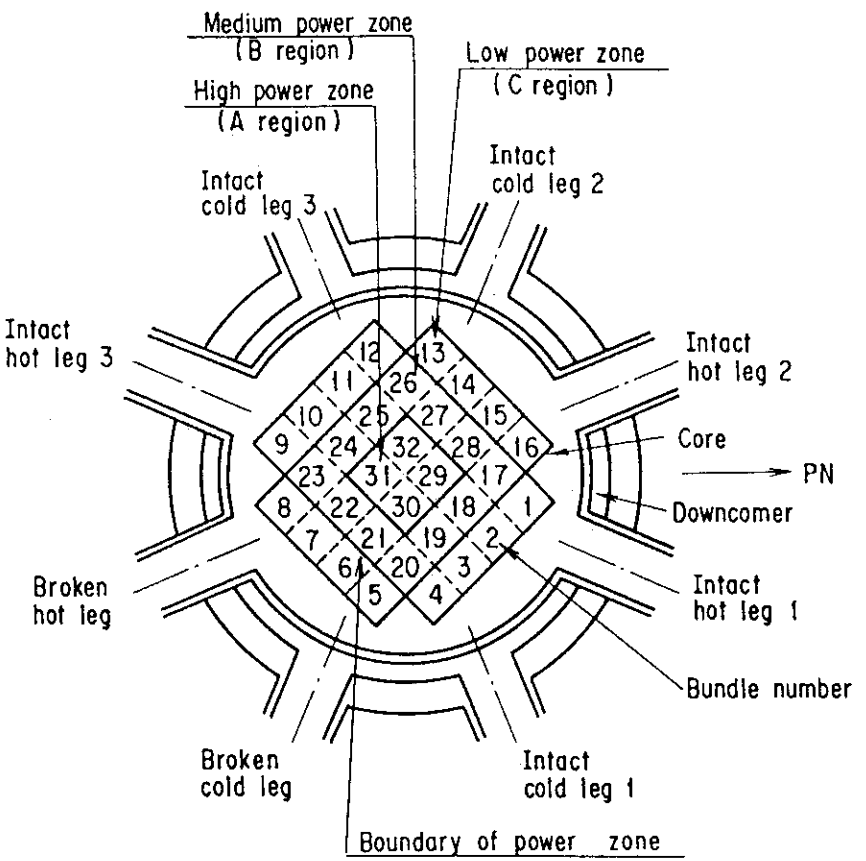

Fig. A-1 Definition of power zones and bundle numbers

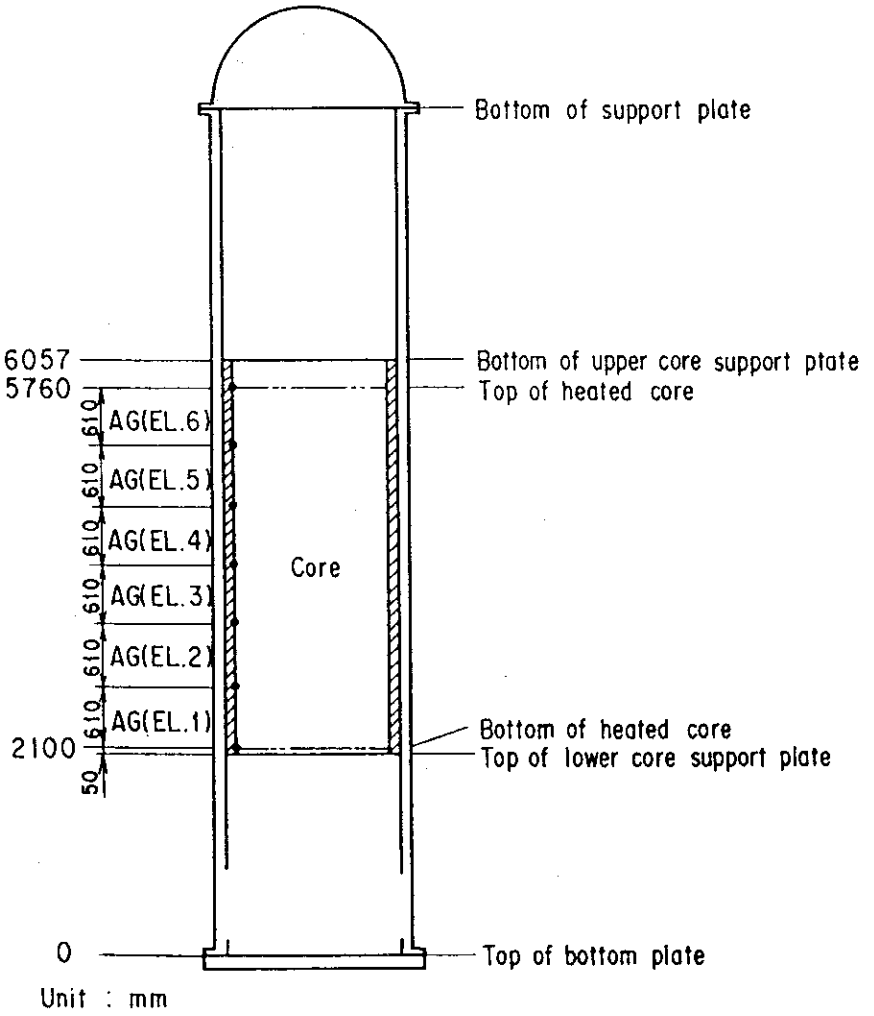

Fig. A-2 Definition of Tag ID for void fraction (AG(EL.1) ~ AG(EL.6))

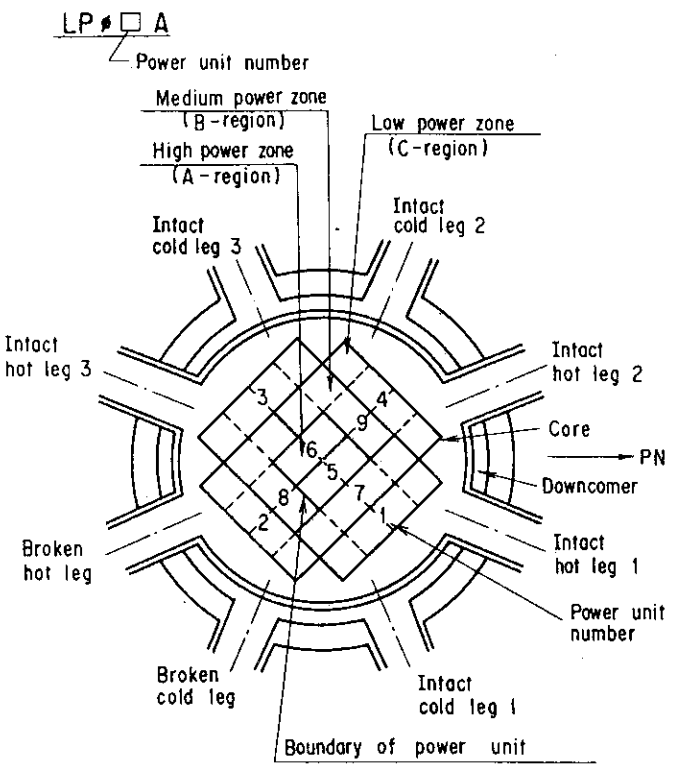

Fig. A-3 Definition of Tag. ID for average linear power of heater rod in each power unit zone
(LP01A ~ LP09A)

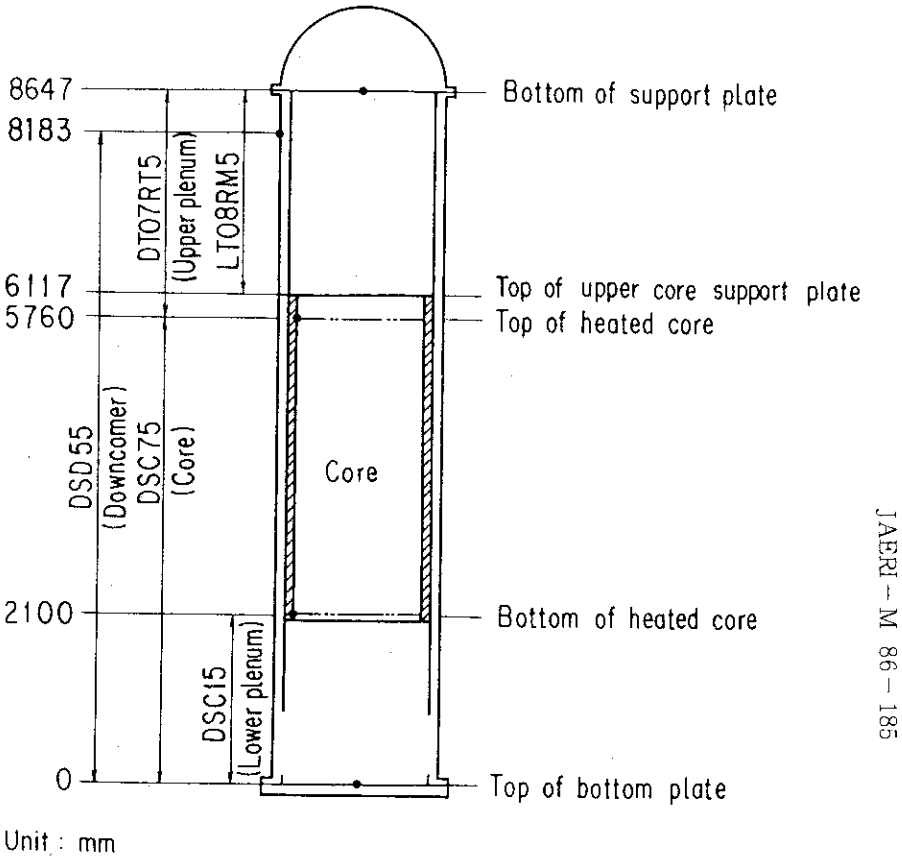

Fig. A-4 Definition of Tag. ID for differential pressure through downcomer, upper plenum, core, and lower plenum
(DSD55, DT07RT5, LT08RM5, DSC75, DSC15)

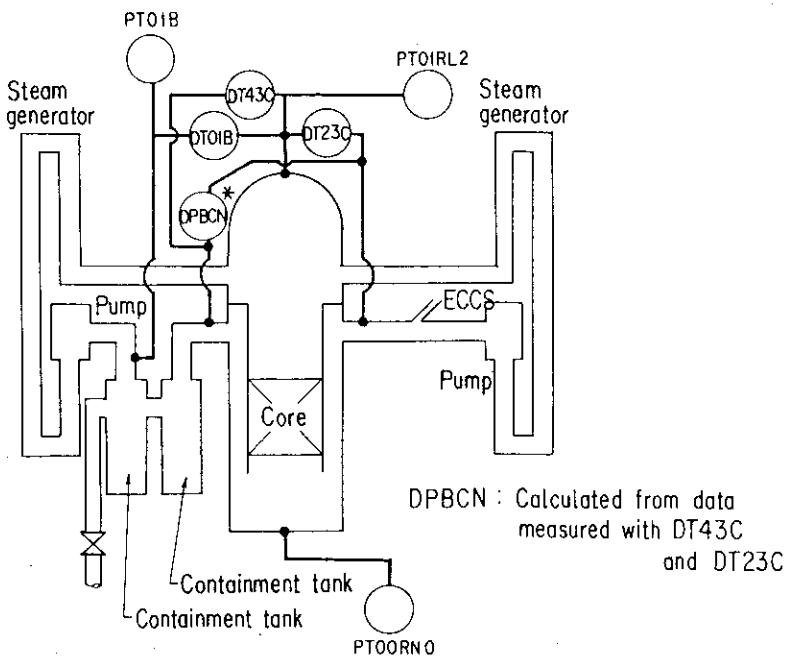

Fig. A-5 Definition of Tag. ID for pressures in upper and lower plena and contaimment tank 2 (PT01RL2, PT00RN0, PT01B) and for differential pressure through intact and broken loop and broken cold leg nozzle (DT23C, DT01B, DPBCN)

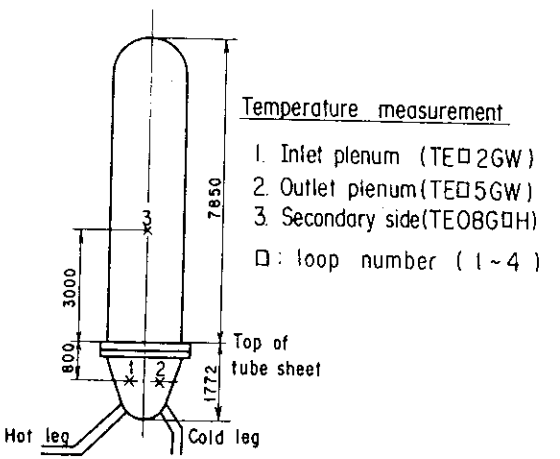

Fig. A-6 Definition of Tag. ID for fluid temperature in inlet and outlet plenum and secondary of steam generator (TE□2GW, TE□5GW, TE08G□H)

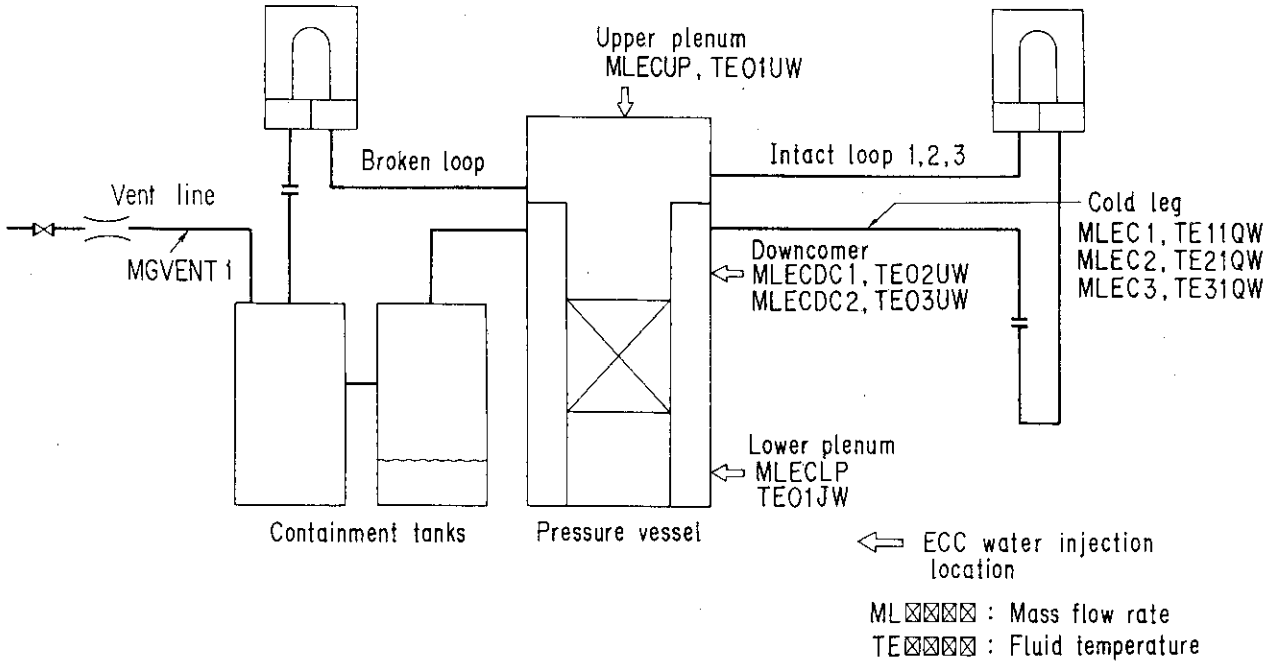

Fig. A-7 Definition of Tag. ID for ECC water injection rate, ECC water temperature and vented steam flow rate

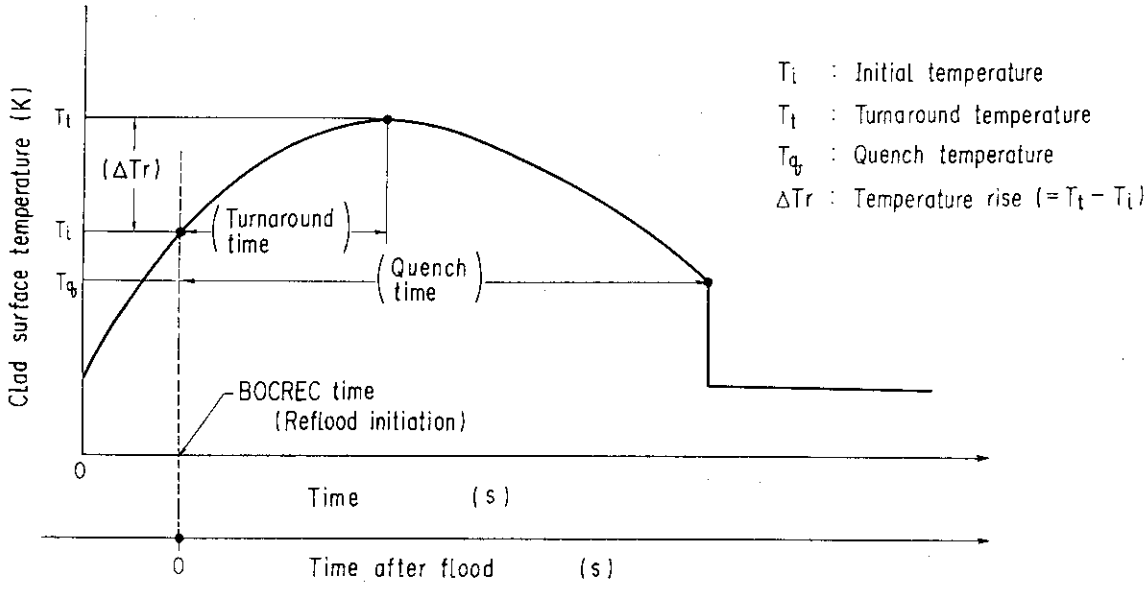

Fig. A-8 Definition of initial temperature, turnaround temperature, quench temperature, temperature rise, turnaround time and quench time

Appendix B

Selected data of CCTF Test C2-3 (Run 61)

Figure List

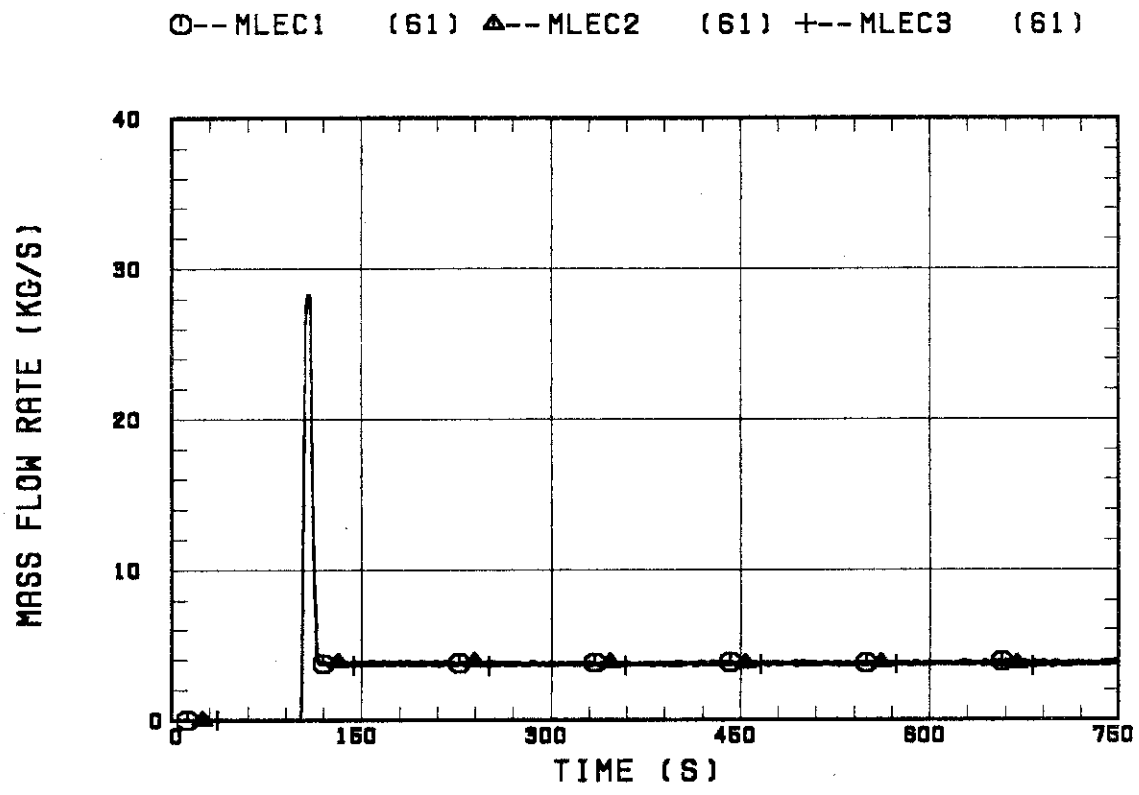

Fig. B.1 ECC water injection rates into the primary system.

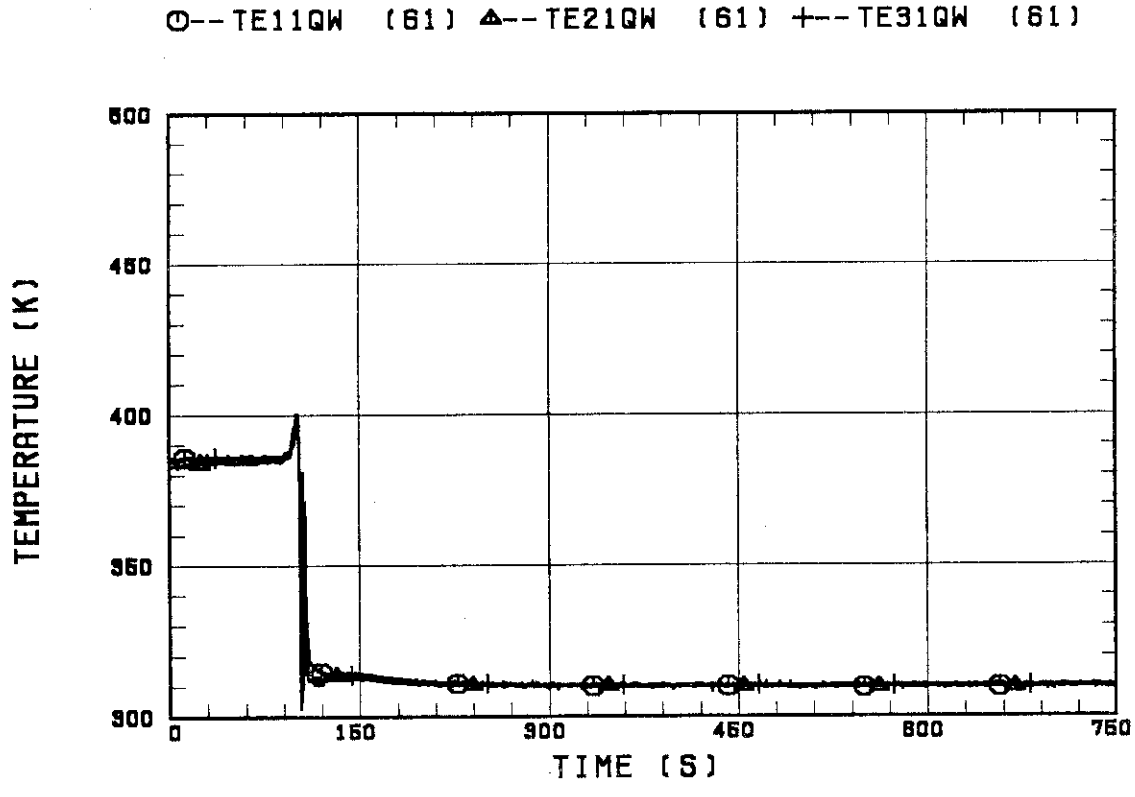

Fig. B.2 ECC water temperature.

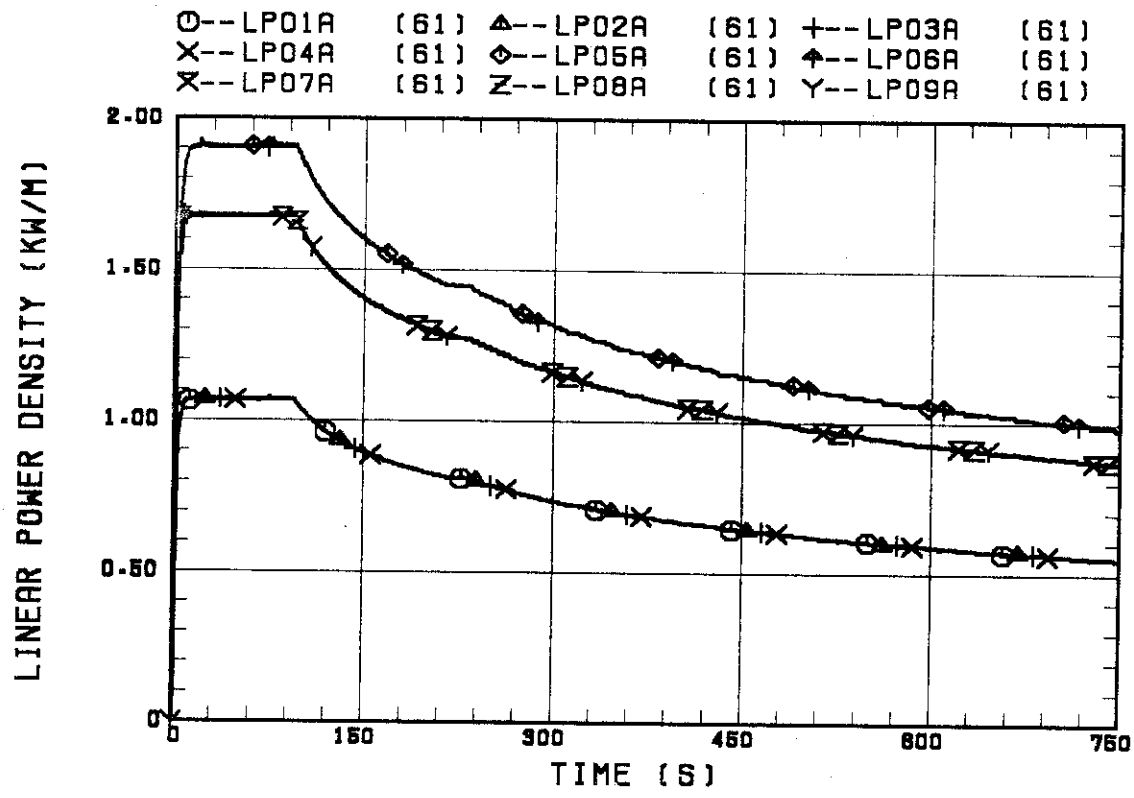

Fig. B.3 Average linear power of heater rod in each power unit zone.

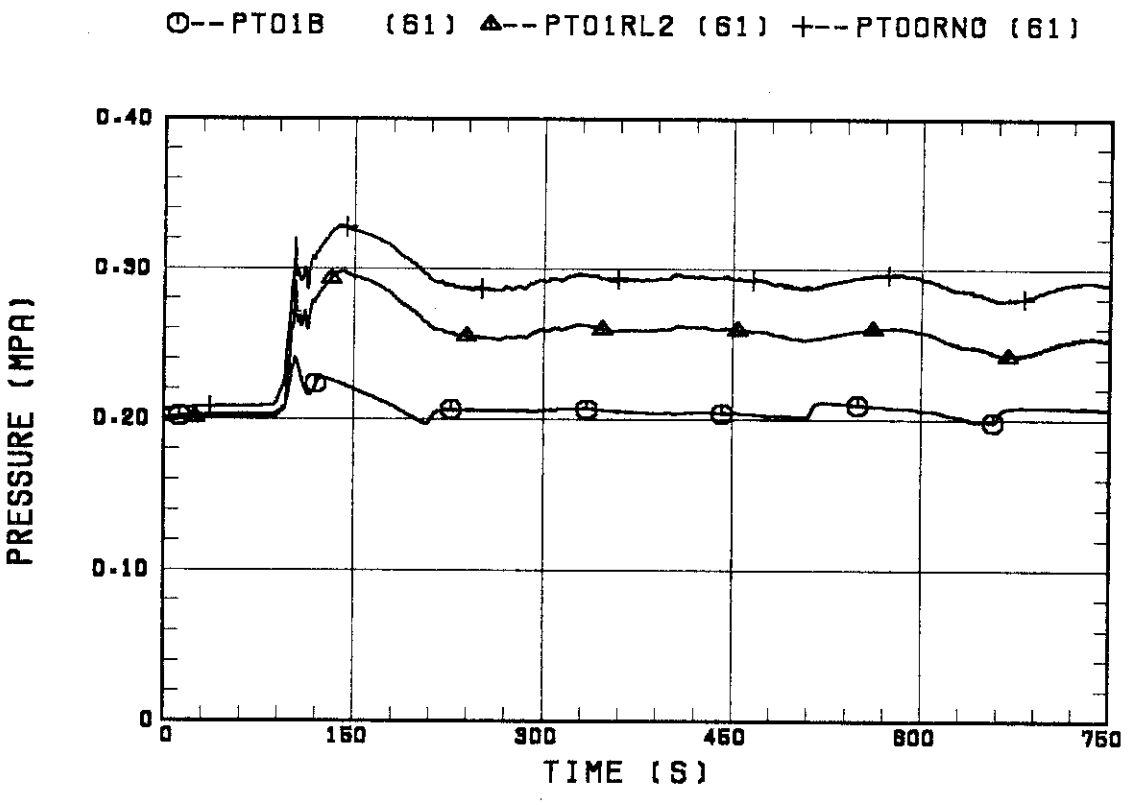

Fig. B.4 Pressure history in containment tank 2, upper plenum and lower plenum.

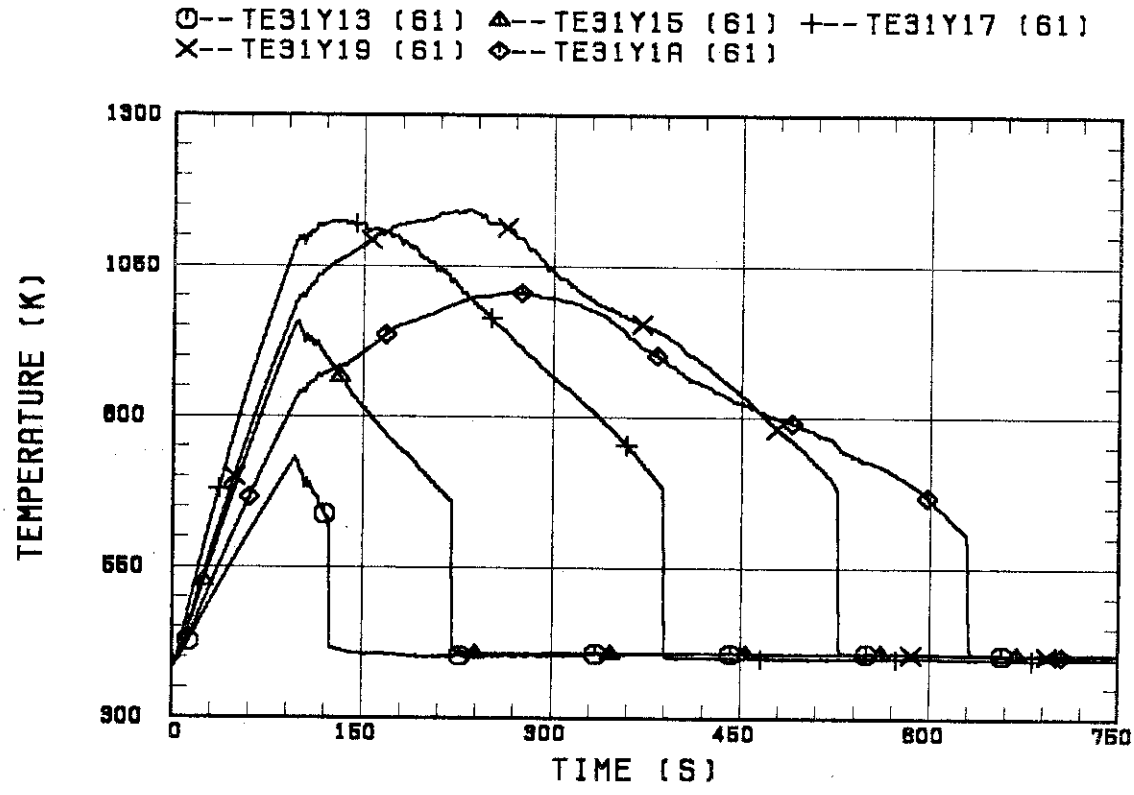

Fig. B.5 Clad surface temperature at various elevations along a heater rod in high power region (A region).

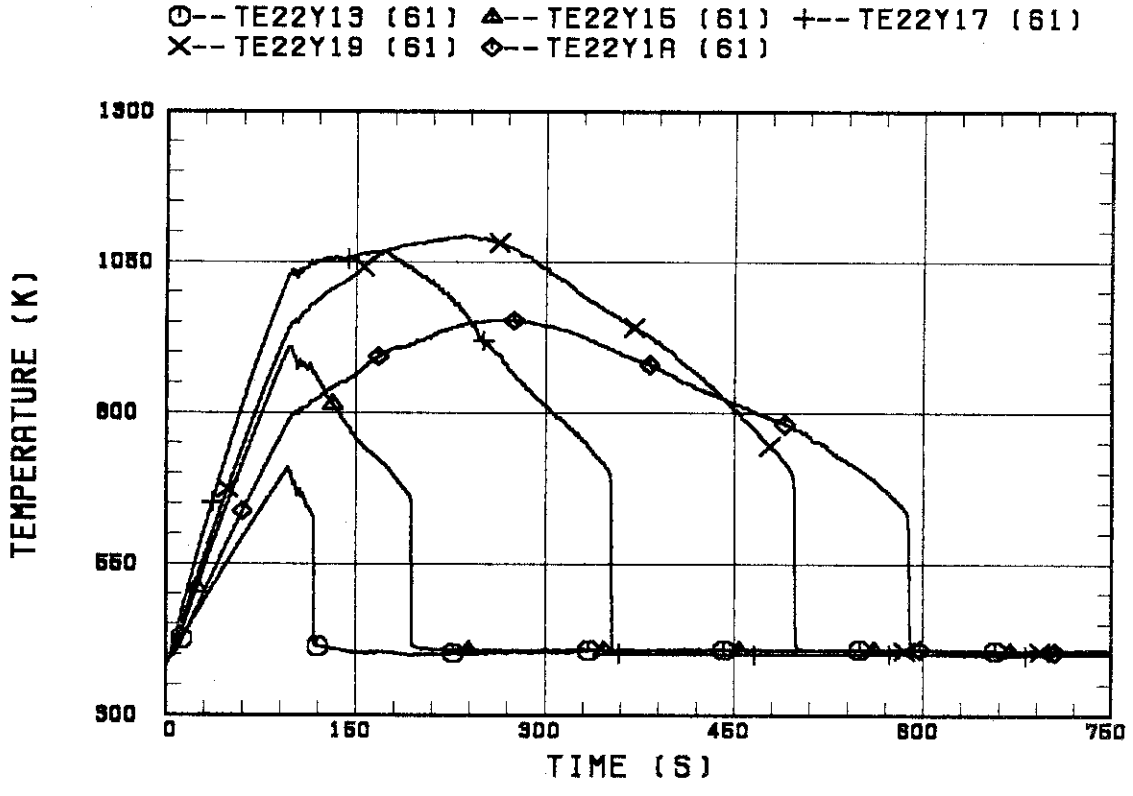

Fig. B.6 Clad surface temperature at various elevations along a heater rod in medium power region (B region).

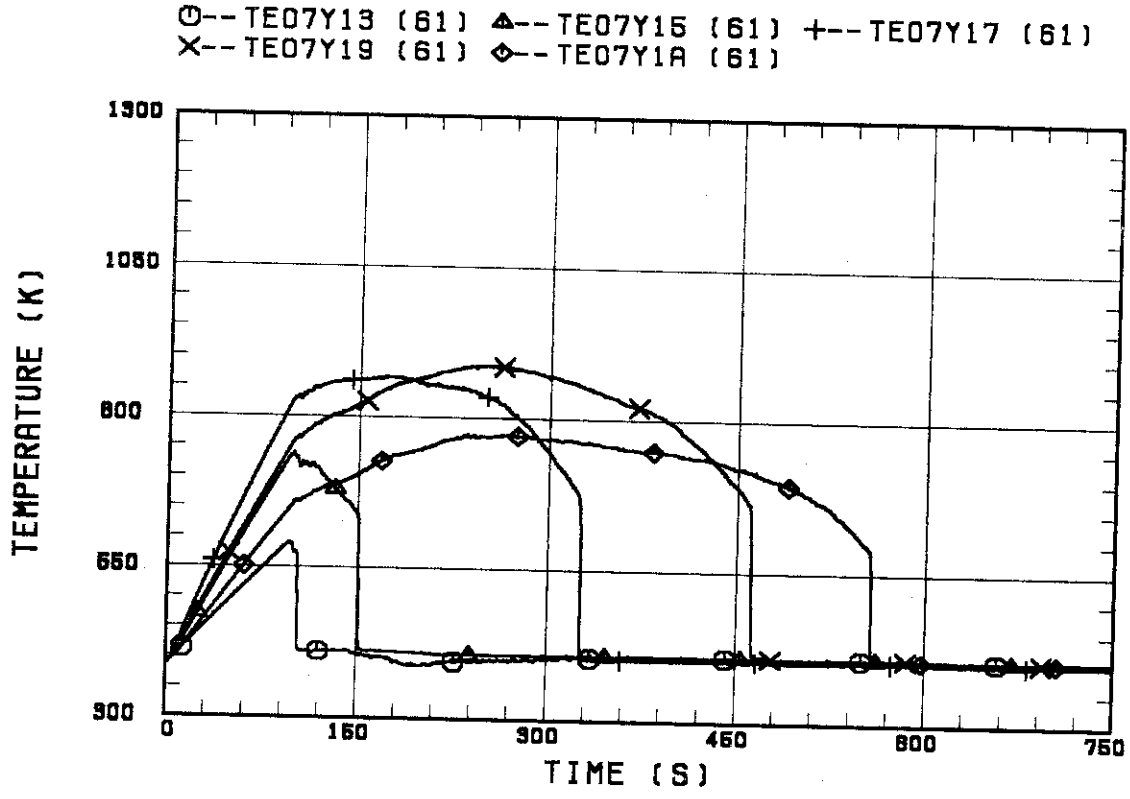

Fig. B.7 Clad surface temperature at various elevations along a heater rod in low power region (C region).

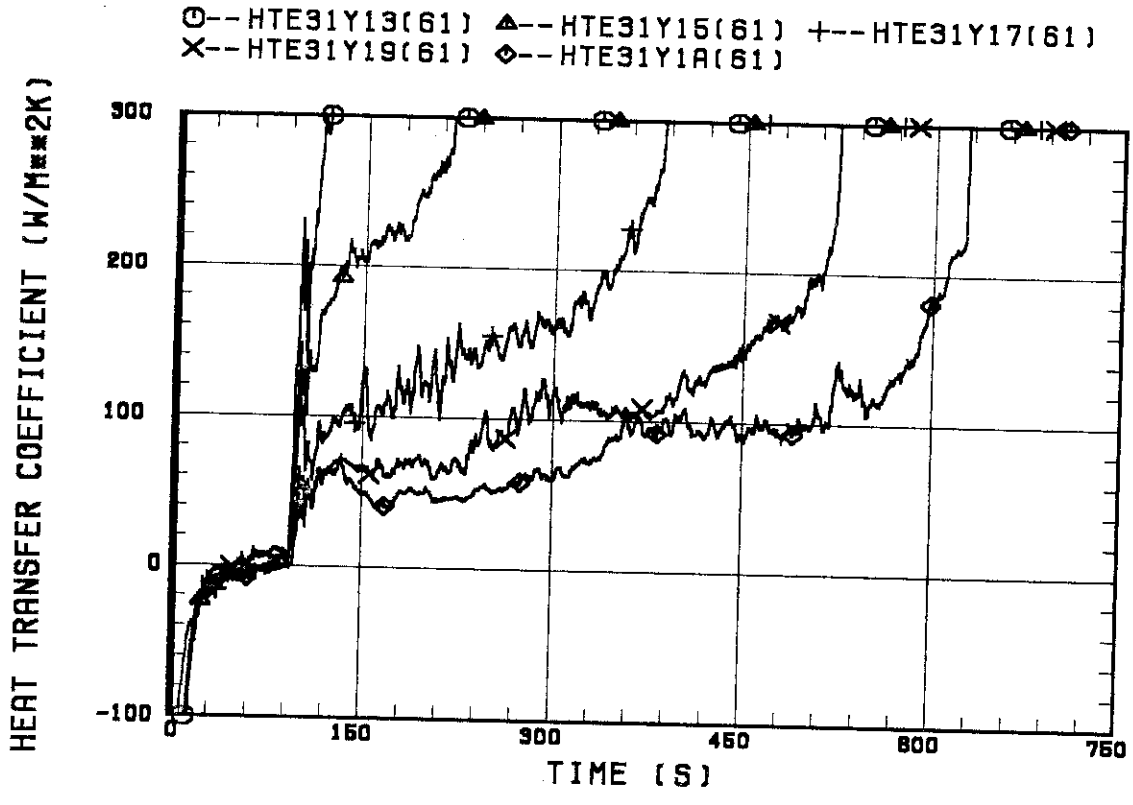

Fig. B.8 Heat transfer coefficient at various elevations along a heater rod in high power region (A region).

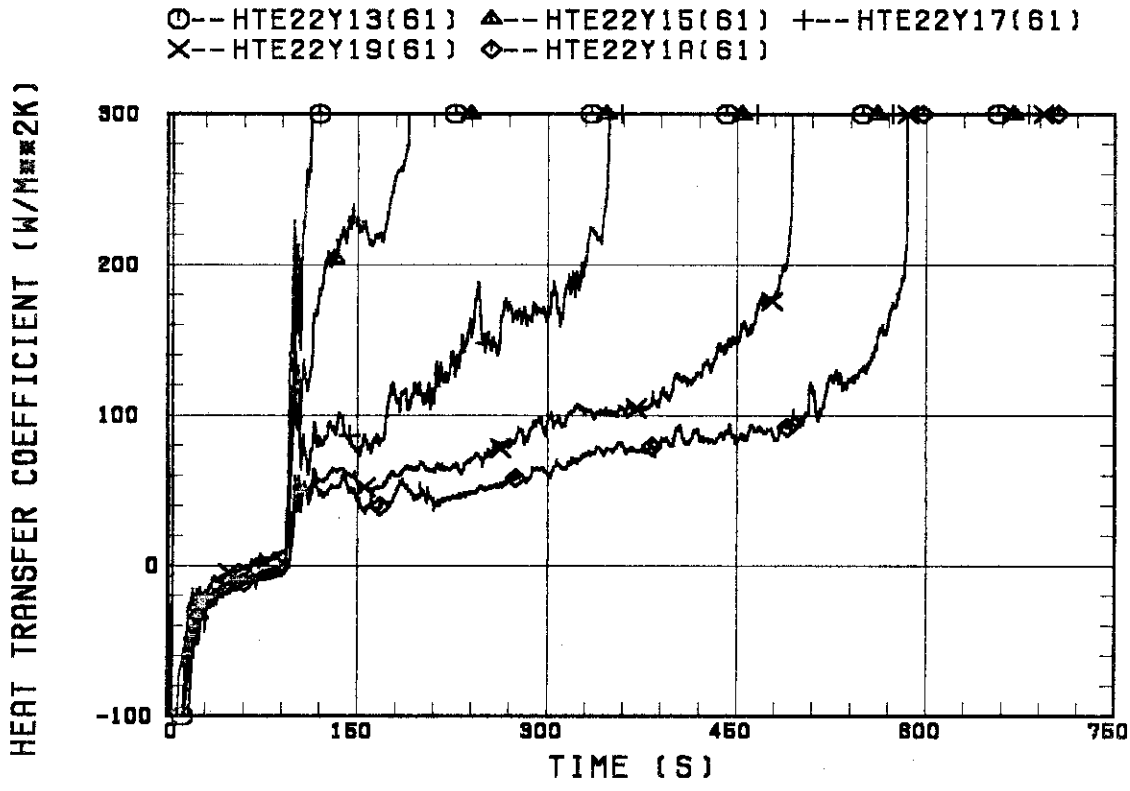

Fig. B.9 Heat transfer coefficient at various elevations along a heater rod in medium power region (B region).

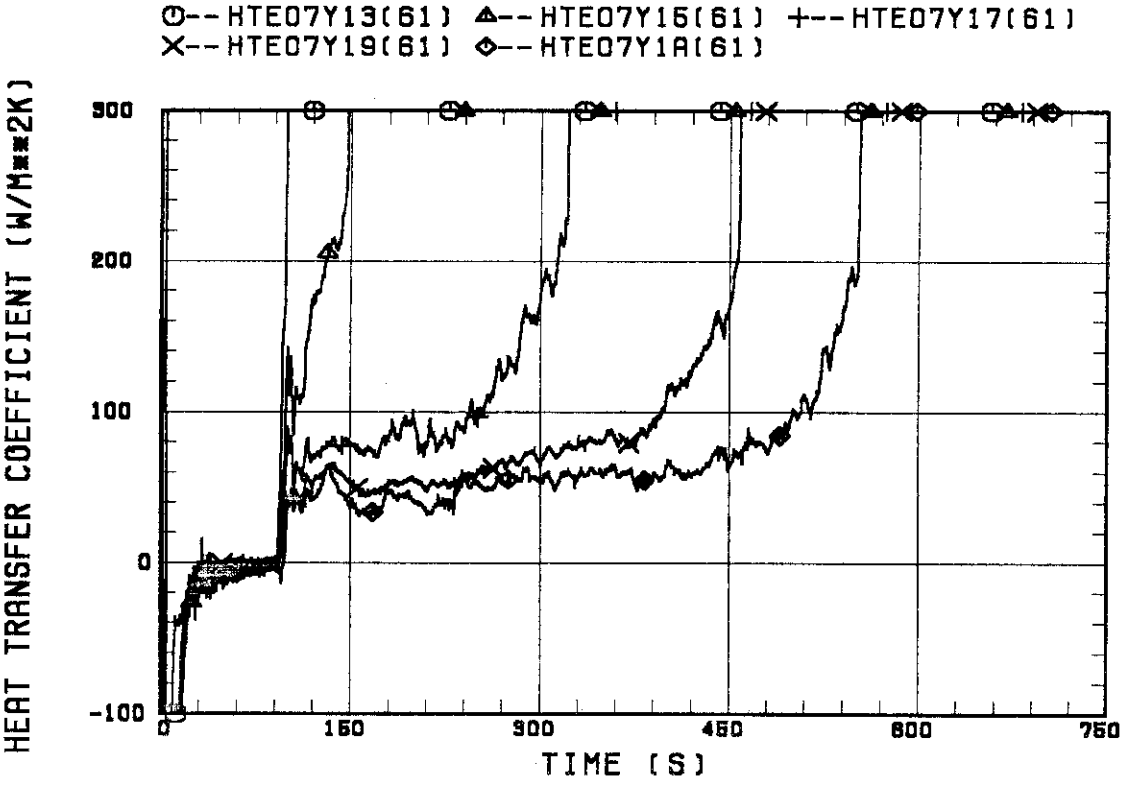

Fig. B.10 Heat transfer coefficient at various elevations along a heater rod in low power region (C region).

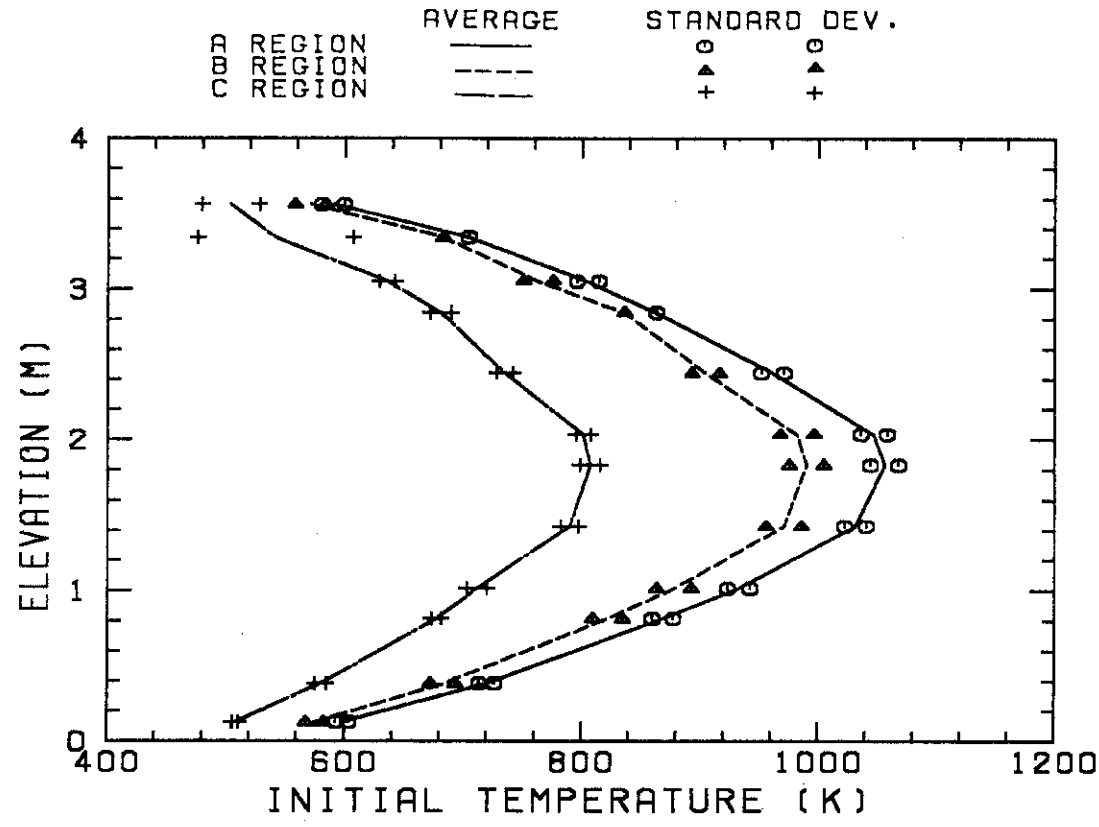

Fig. B.11 Initial clad surface temperature.

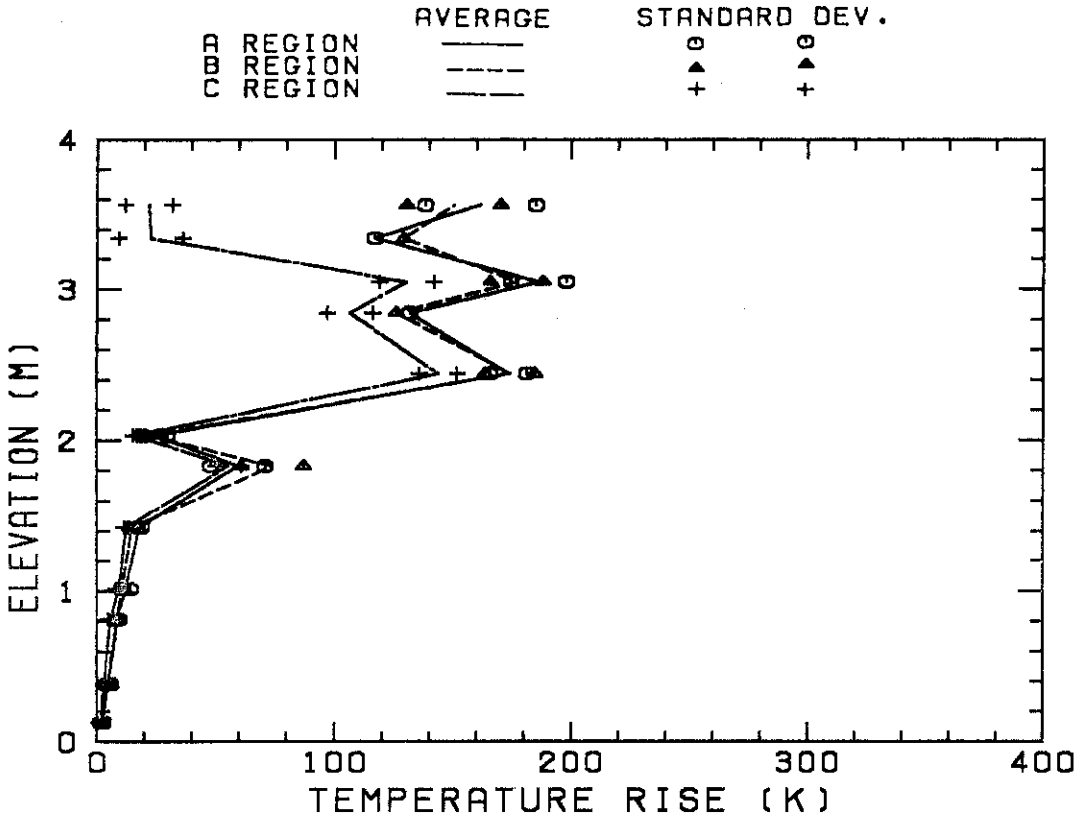

Fig. B.12 Temperature rise.

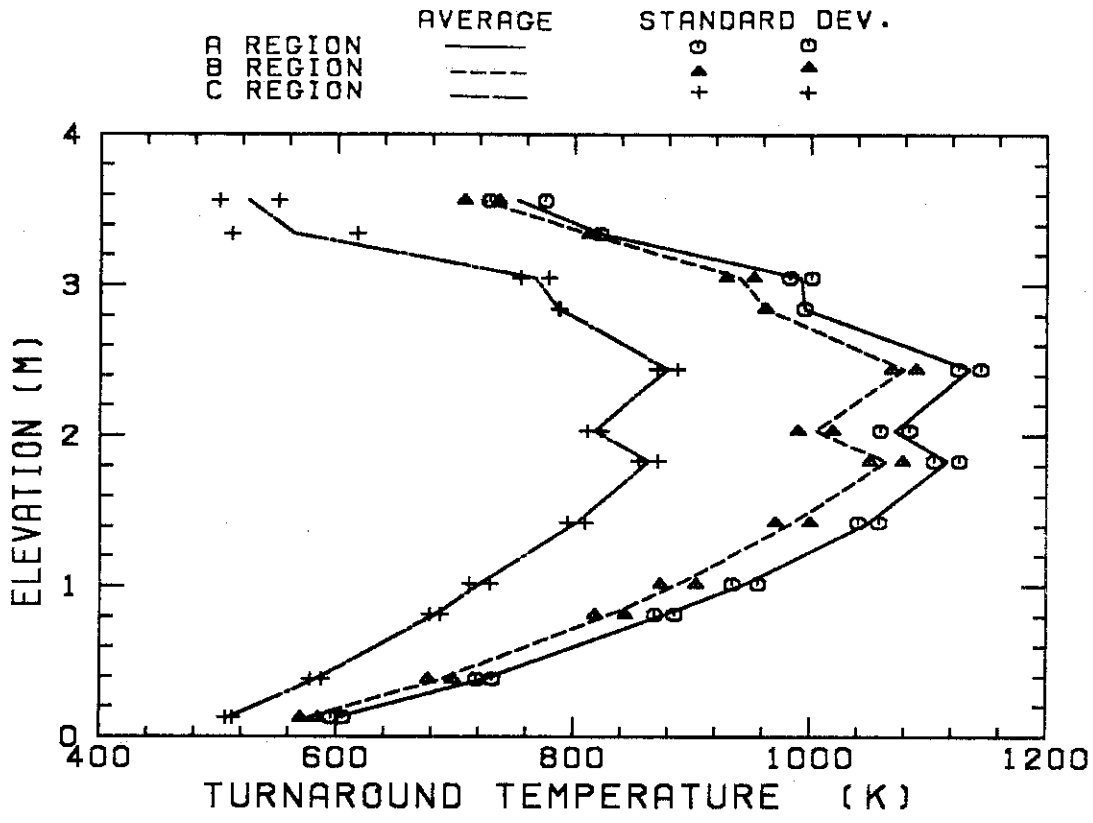

Fig. B.13 Turnaround temperature.

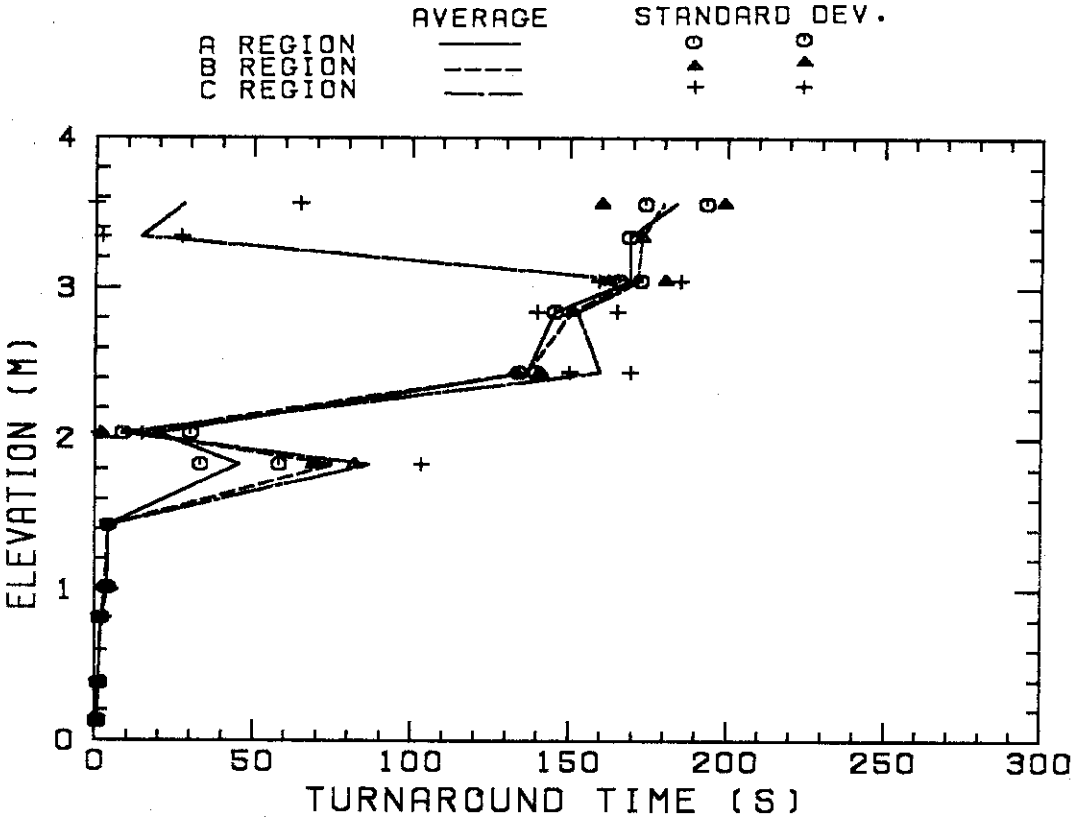

Fig. B.14 Turnaround time.

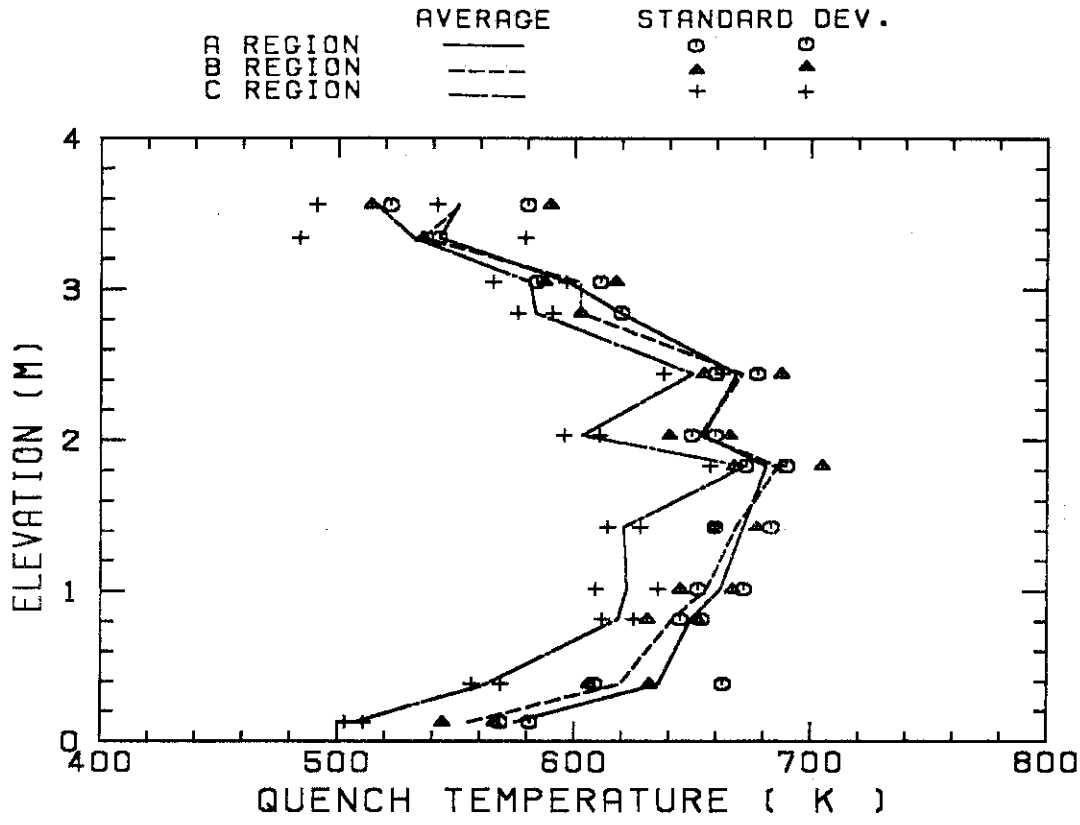

Fig. B.15 Quench temperature.

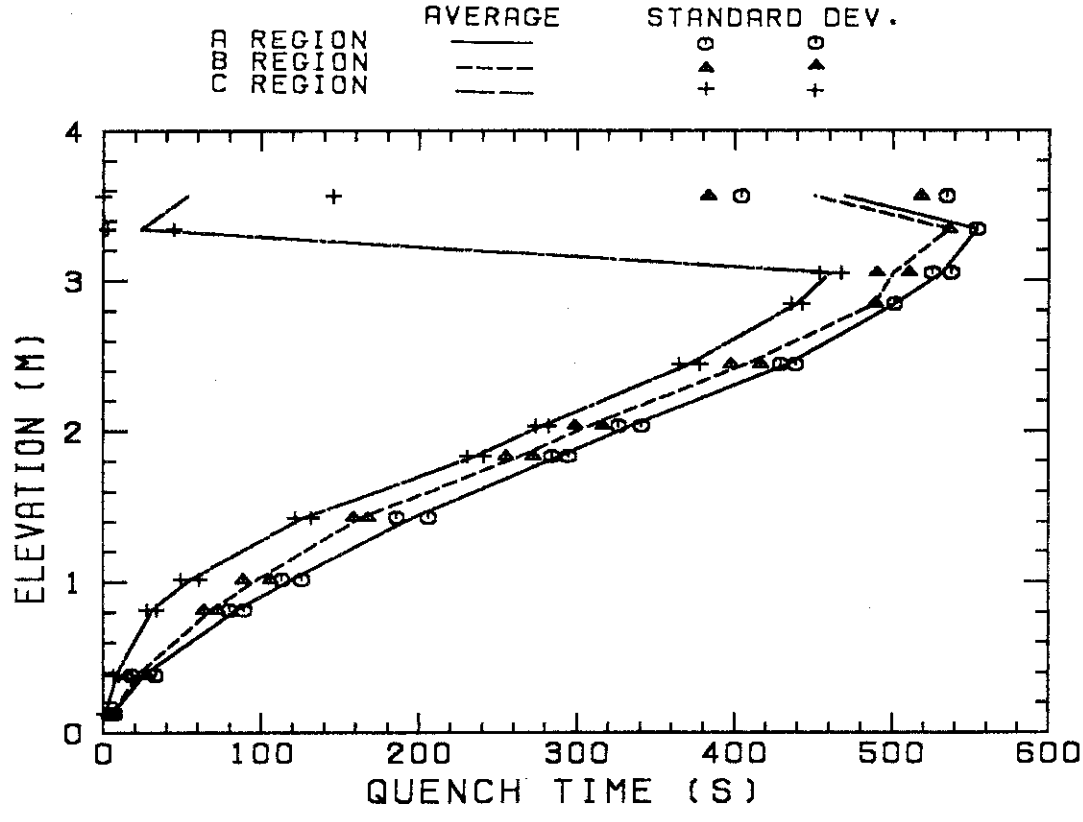

Fig. B.16 Quench time.

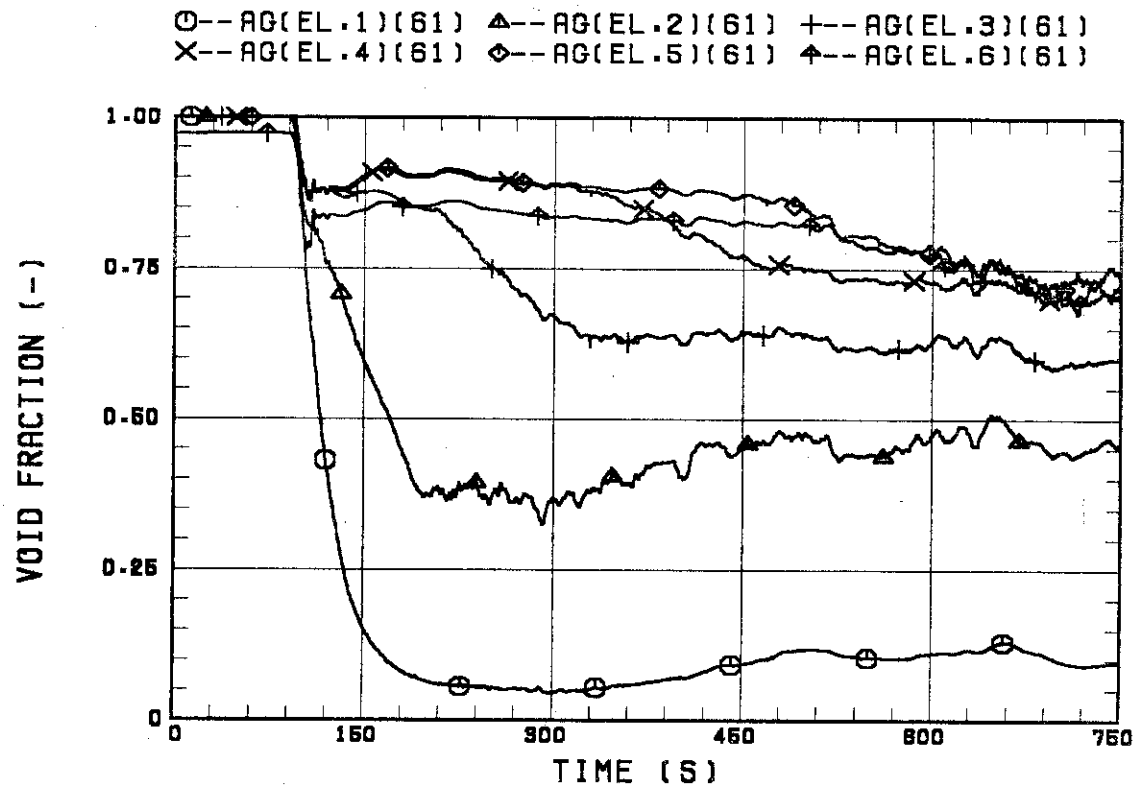

Fig. B.17 Void fraction in core.

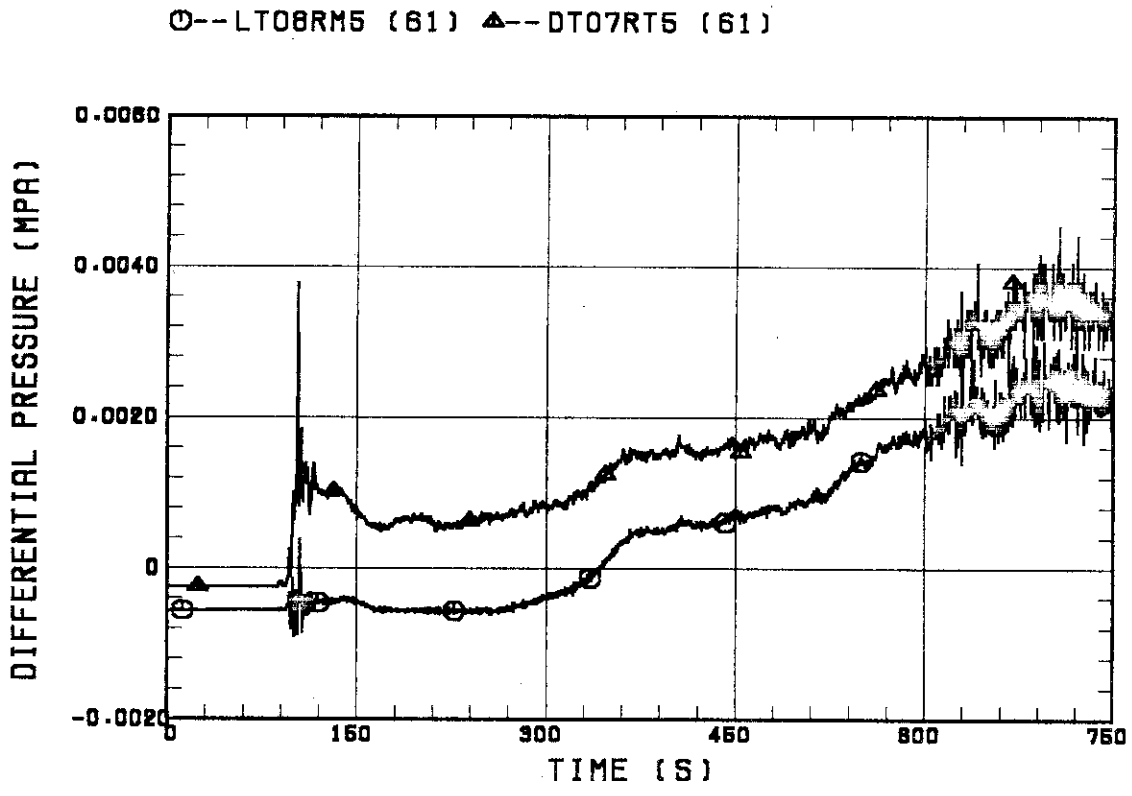

Fig. B.18 Differential pressure through upper plenum.

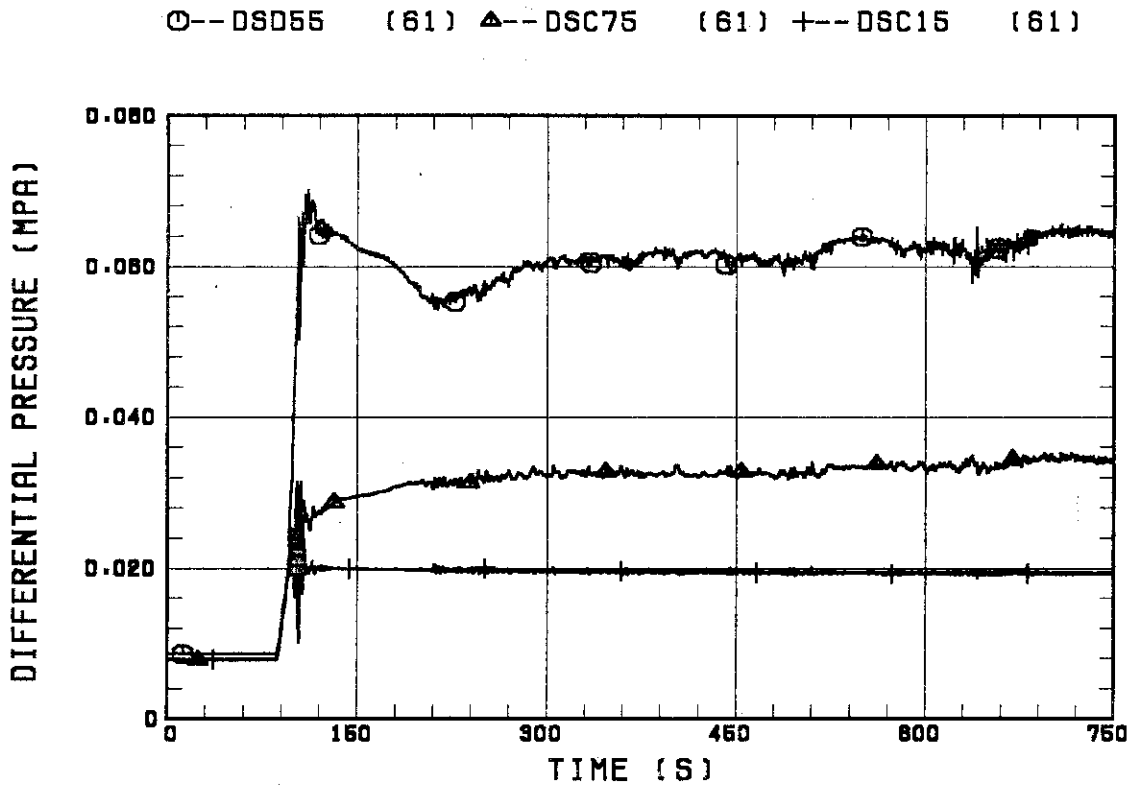

Fig. B.19 Differential pressure through downcomer, core, and lower plenum.

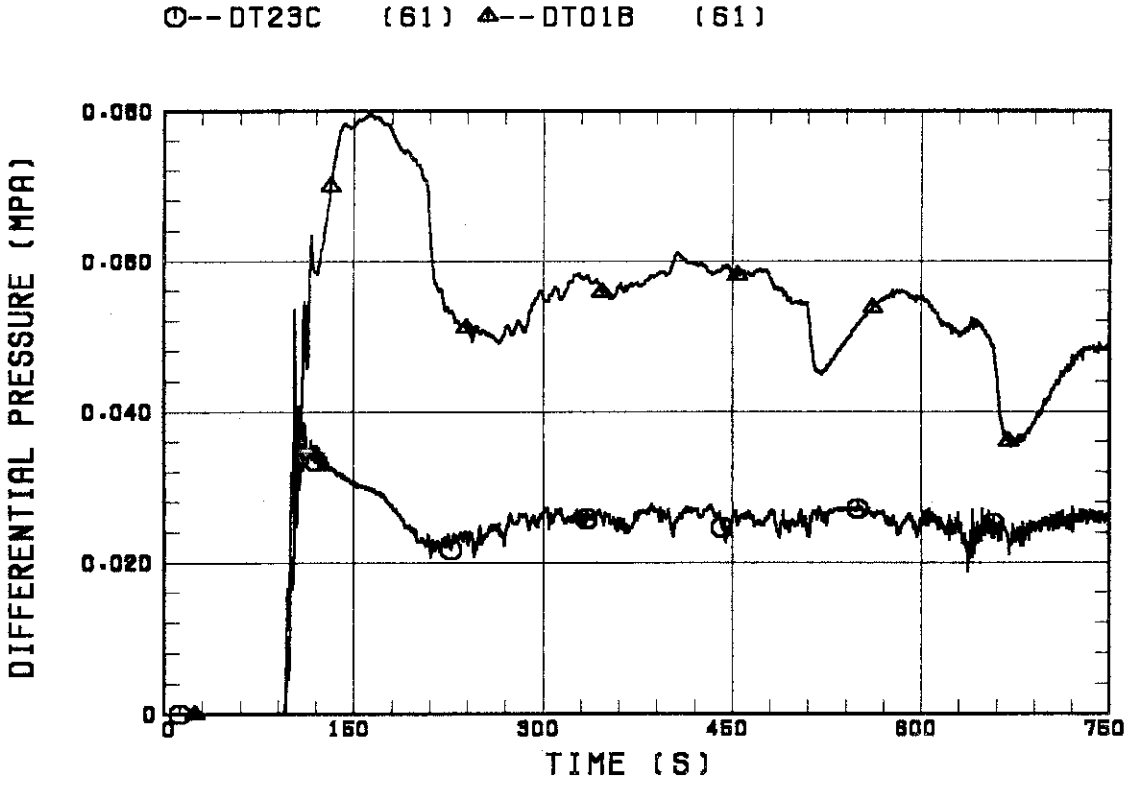

Fig. B.20 Differential pressure through intact and broken loops.

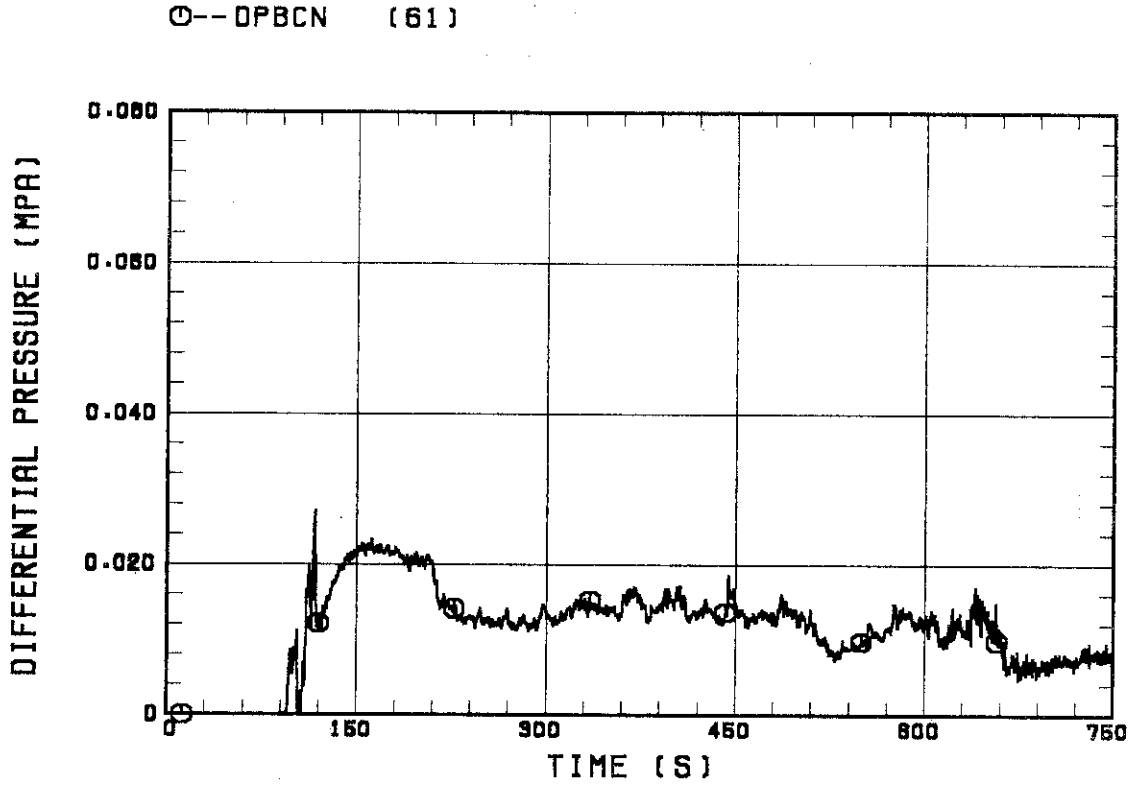

Fig. B.21 Differential pressure through broken cold leg nozzle.

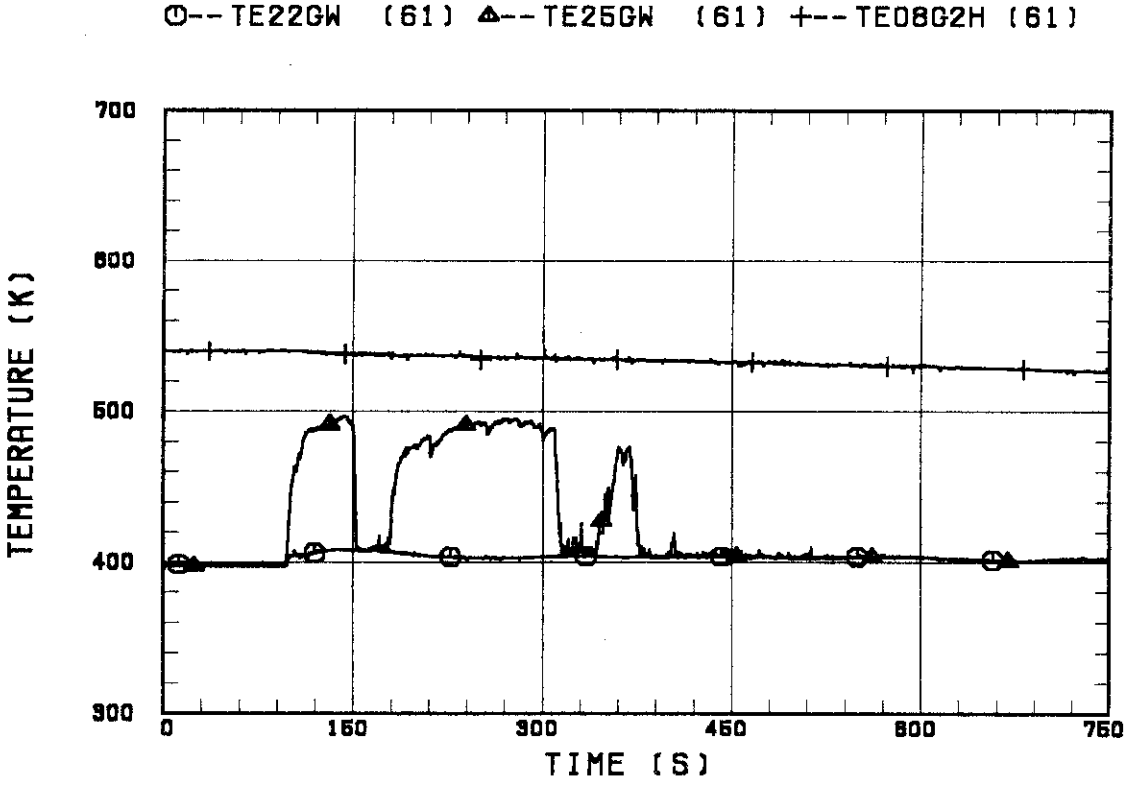

Fig. B.22 Fluid temperature in inlet plenum, outlet plenum, and secondary of steam generator 1.

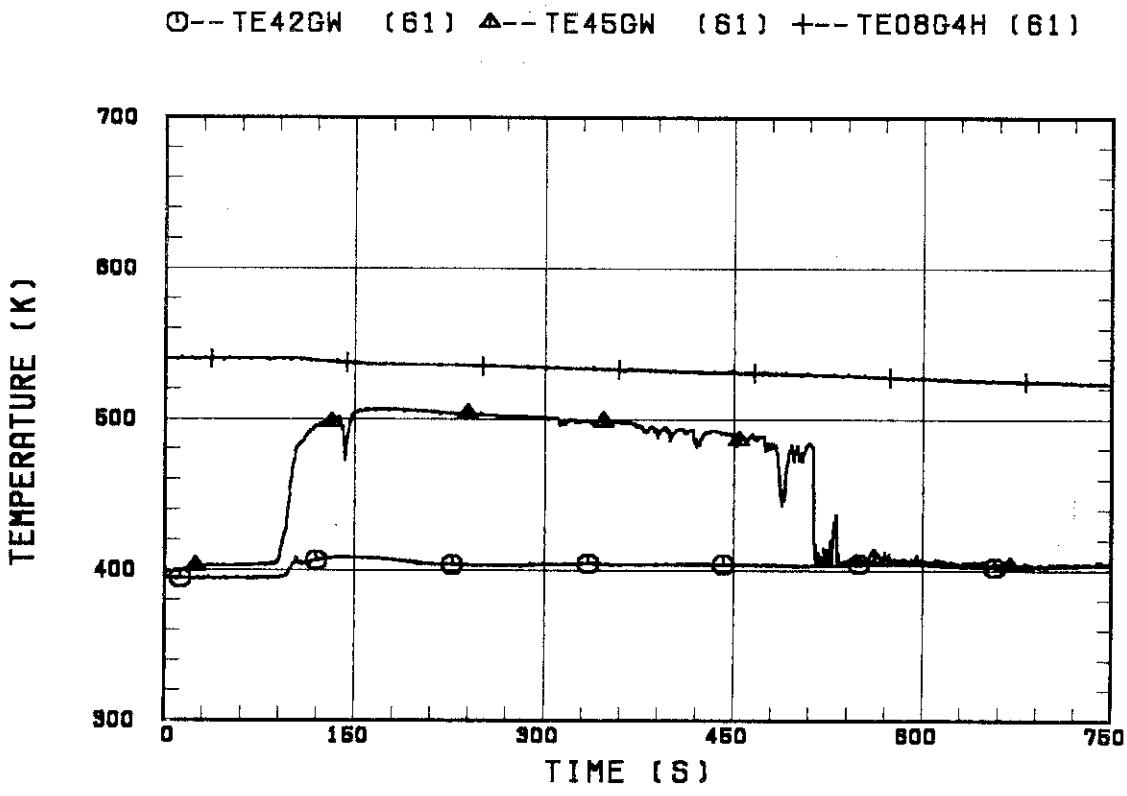

Fig. B.23 Fluid temperature in inlet plenum, outlet plenum, and secondary of steam generator 2.

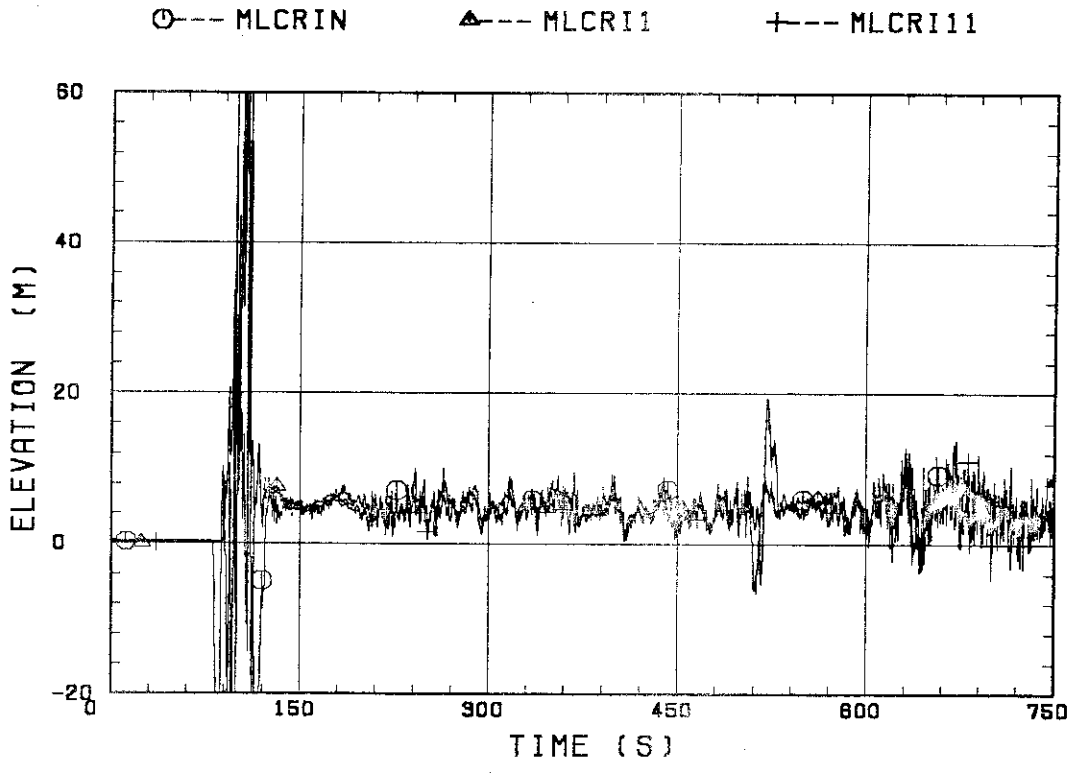

Fig. B.24 Core flooding mass flow rates evaluated with Eqs. (A.1) (A.2)

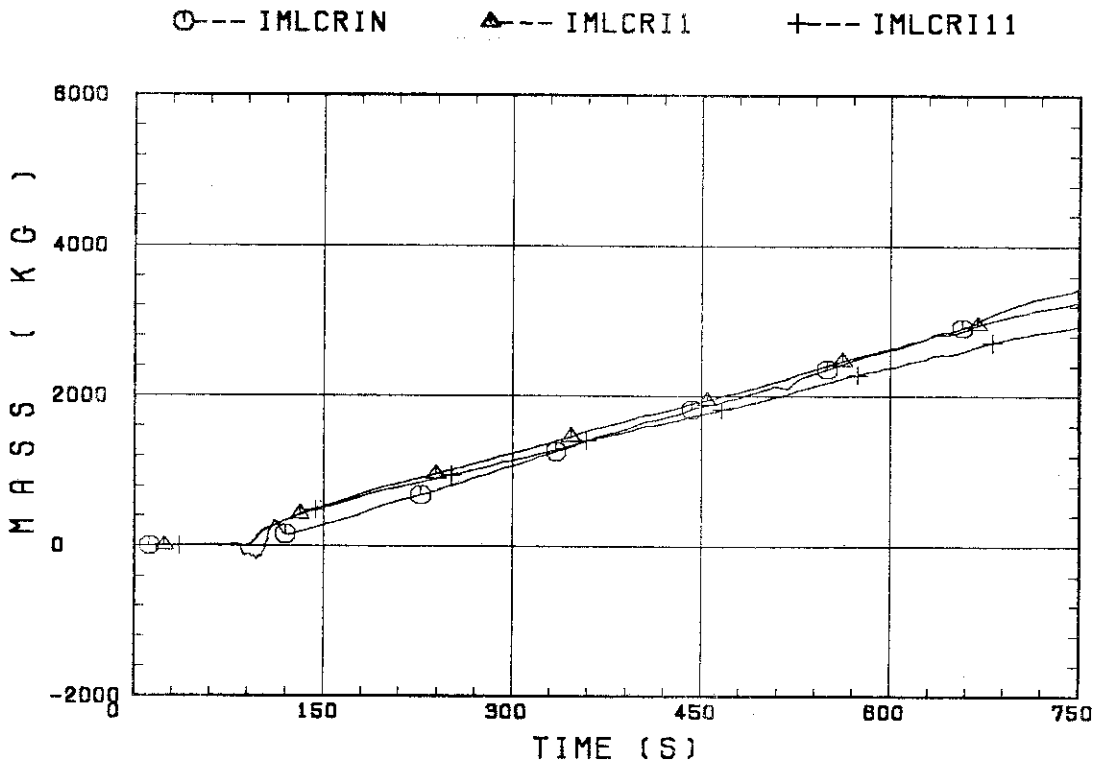

Fig. B.25 Time-integral mass flooded into core evaluated with Eqs. (A.1) and (A.2).

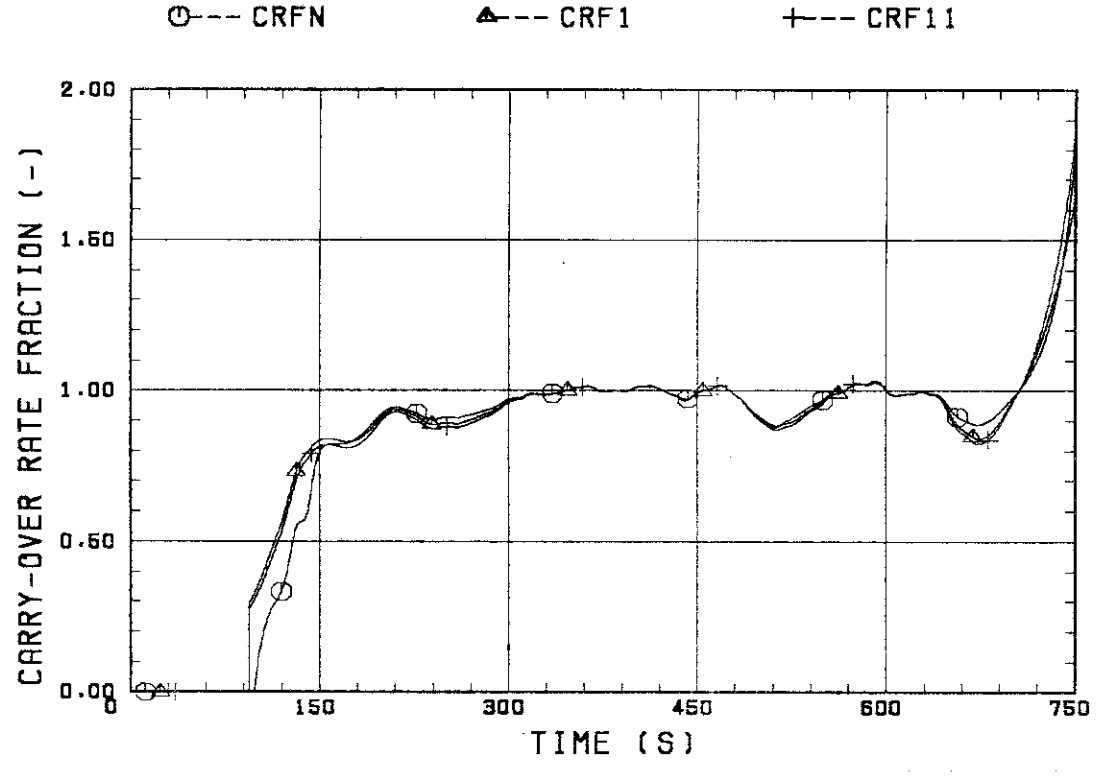

Fig. B.26 Carry-over rate fraction.

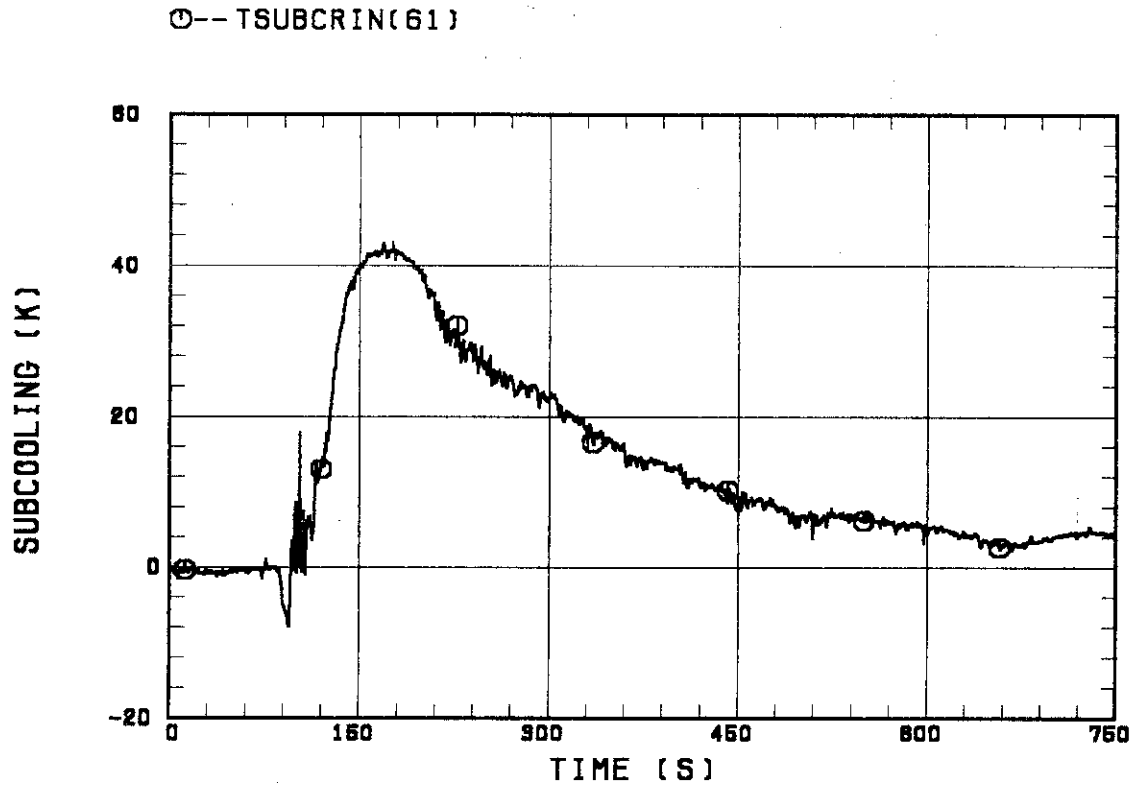

Fig. B.27 Core inlet subcooling.

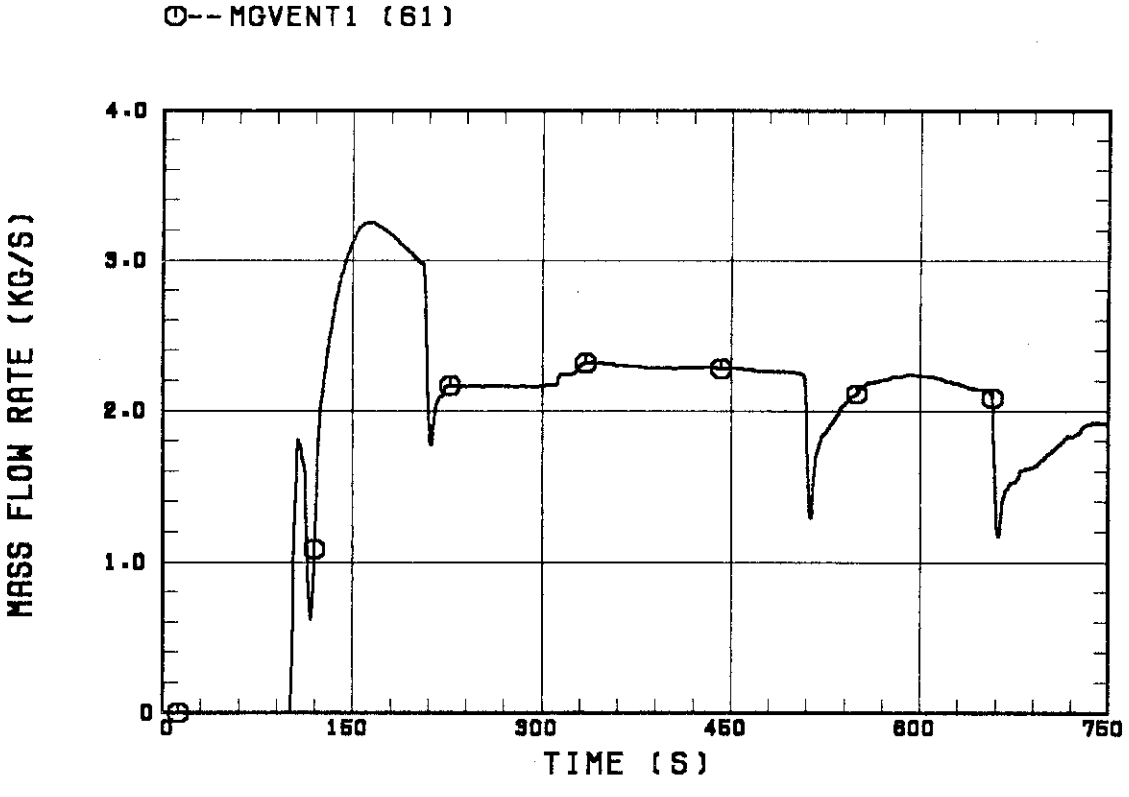

Fig. B.28 Exhausted mass flow rate from containment tank 2.